University of Alberta

Surface mass balance of Arctic glaciers: Climate influences and modeling approaches

by

Alex Sandy Gardner

A thesis submitted to the Faculty of Graduate Studies and Research
in partial fulfillment of the requirements for the degree of

Doctor of Philosophy

Department of Earth and Atmospheric Sciences

Fall 2010
Edmonton, Alberta

Examining Committee

Martin J. Sharp, Earth and Atmospheric Sciences

Andrew B.G. Bush, Earth and Atmospheric Sciences

Jeffrey L. Kavanaugh, Earth and Atmospheric Sciences

Christian Haas, Earth and Atmospheric Sciences

Faye Hicks, Civil and Environmental Engineering

Jon Ove Hagen, Department of Geosciences, University of Oslo

To Tara, my adventuress best friend and loving wife, and my son Finnley.

You both bring my life balance and color.

ABSTRACT

Land ice is losing mass to the world's oceans at an accelerated rate. The world's glaciers contain much less ice than the ice sheets but contribute equally to eustatic sea level rise and are expected to continue to do so over the coming centuries if global temperatures continue to rise. It is therefore important to characterize the mass balance of these glaciers and its relationship to climate trends and variability. In the Canadian High Arctic, analysis of long-term surface mass balance records shows a shift to more negative mass balances after 1987 and is coincident with a change in the mean location of the July circumpolar vortex, a mid-troposphere cyclonic feature known to have a strong influence on Arctic summer climate. Since 1987 the occurrence of July vortices centered in the Eastern Hemisphere have increased significantly. This change is associated with an increased frequency of tropospheric ridging over the Canadian High Arctic, higher surface air temperatures, and more negative glacier mass balance. However, regional scale mass balance modeling is needed to determine whether or not the long-term mass balance measurements in this region accurately reflect the mass balance of the entire Canadian High Arctic.

The Canadian High Arctic is characterized by high relief and complex terrain that result in steep horizontal gradients in surface mass balance, which can only be resolved if models are run at high spatial resolutions. For such runs, models often require input fields such as air temperature that are derived by downscaling of output from climate models or reanalyses. Downscaling is often performed using a specified relationship between temperature and elevation

(a lapse rate). Although a constant lapse rate is often assumed, this is not well justified by observations. To improve upon this assumption, near-surface temperature lapse rates during the summer ablation season were derived from surface measurements on 4 Arctic glaciers. Near-surface lapse rates vary systematically with free-air temperatures and are less steep than the free-air lapse rates that have often been used in mass balance modeling. Available observations were used to derive a new variable temperature downscaling method based on temperature dependent daily lapse rates. This method was implemented in a temperature index mass balance model, and results were compared with those derived from a constant linear lapse rate. Compared with other approaches, model estimates of surface mass balance fit observations much better when variable, temperature dependent lapse rates are used. To better account for glacier-climate feedbacks within mass balance models, more physically explicit representations of snow and ice processes must be used. Since absorption of shortwave radiation is often the single largest source of energy for melt, one of the most important parameters to model correctly is surface albedo. To move beyond the limitations of empirical snow and ice albedo parameterizations often used in surface mass balance models, a computationally simple, theoretically-based parameterization for snow and ice albedo was developed. Unlike previous parameterizations, it provides a single set of equations for the estimation of both snow and ice albedo. The parameterization also produces accurate results for a much wider range of snow, ice, and atmospheric conditions.

ACKNOWLEDGEMENTS

This manuscript is the product of my PhD research but I am a product of the great people that have supported and encouraged me along the way.

First and foremost, I thank my PhD supervisor Dr. Martin Sharp for giving me complete creative freedom to explore a diverse range of research areas and for spending countless hours reviewing my manuscripts in a selfless effort to develop my scientific writing abilities. You have contributed significantly to the researcher that I am today.

In my second year of my PhD I had the pleasure of being a student in Dr. John Wilson's course on atmospheric modeling. John's class eased my apprehensions of numerical modeling and provided me with a toolset that has empowered me to answer scientific questions previously out of reach.

Many friends and peers have helped and supported me during my PhD. Lindsey Nicholson was a great friend and mentor during the early years of my PhD and I hope we have the chance to work together in the future. My field partner and friend Brad Danielson can take credit for making all three of my field excursions to the Arctic an absolute joy. Ben Gready and Inka Koch gave great feedback and kept my spirits high. I greatly appreciate the friendship and support of Jamie Davis, Gabe Wolken, Angus Duncan, Gabrielle Gascon, Nick Barrand and the rest of the Arctic and Alpine Research Group.

Dr. Jeffrey Kavanaugh (University of Alberta) gave me good feedback and career advice. Dr. Brian Toon (University of Colorado – Boulder) and Stephen Warren (University of Washington) provided invaluable discussions that shaped the research contained in Chapter 5 of my thesis. I would also like to thank all members of my PhD committee for dedicating their time and providing useful feedback on the final draft of my thesis.

Financial and logistical support was provided by the Natural Sciences and Engineering Research Council of Canada, the Alberta Ingenuity Fund, the University of Alberta, Canadian Foundation for Climate and Atmospheric Sciences through the Polar Climate Stability Network, the ArcticNet a Network of Centres of Excellence, the Polar Continental Shelf Project, the Canadian Circumpolar Institute, the Northern Scientific Training Program, and the American Geophysical Union. Much of the work was conducted using the infrastructure and resources of the Academic Information and Communication Technologies of the University of Alberta.

Lastly I thank Flo, Ed, my sister, mother and father for all of their love and support.

TABLE OF CONTENTS

LIST OF TABLES

LIST OF FIGURES

CHAPTER 1 : INTRODUCTION

Motivation

The world's land ice (ice sheets, ice caps, icefields and glaciers) is in a continual state of flux, exchanging mass and energy with its surroundings. These exchanges occur over a wide range of temporal and spatial scales, from the multi-millennial growth and demise of continental ice sheets to the diurnal exchange of mass and energy between the ice surface and the atmosphere. Understanding these exchanges and the processes relevant to their quantification at the different spatial and temporal scales is necessary for the development of numerical models that can simulate the growth and decay of the world's land ice, a process that can have a large influence on the global climate, regional water resources, and sea level change. This has motivated over half a century of research focused on the quantification of the mass and energy budgets of land ice (Koerner 1970; Holmgren 1971). In recent years there has been a heightened interest in this area as the concern over anthropogenic climate change and rising sea levels has increased (Bindoff et al. 2007). As rapid changes in land ice are being observed around the globe (Kaser et al. 2006; Lemke et al. 2007; Meier et al. 2007; Chen et al. 2009; van den Broeke et al. 2009), cryosphere and climate researchers have been attempting to answer several key questions:

- *Is land ice showing accelerated rates of mass loss? If so, is the acceleration a result of anthropogenic changes in climate?*
- *How much of the observed eustatic sea level change is due to mass loss from land ice? How much can we expect it to rise in the future?*
- *What feedbacks does the land ice have on the surface energy budget in a changing climate? How important are these feedbacks when modeling the global climate system?*

Current estimates of mass loss from glaciers, ice caps, and icefields are suggest that these masses are contributing about as much to sea level rise as are the ice sheets of Antarctica and Greenland (Meier et al. 2007), which are ~2 orders of magnitude larger. There is therefore considerable interest in characterizing the mass balance of these smaller ice masses and its relationship to climate trends and variability, and to improve estimates of their mass balance. The research contained within this dissertation focuses on a series of topics that will hopefully help achieve these goals. Specifically, the dissertation focuses on two broad themes:

1. Determining whether mass loss rates in the Canadian High Arctic have accelerated in recent years and, if so, why.
2. Improving the parameterization of certain aspects of mass and energy exchanges between the atmosphere and the ice surface in an Arctic setting for improved simulation of glacier surface mass balance.

Background

Glacier Mass Balance

This dissertation is focused on the characterization and assessment of glacier surface mass balance, the change in mass of the whole glaciers arising from processes occurring in top upper ~50 m. While changes in mass due to other processes, such as iceberg calving, can also be highly significant to the overall mass balance of the glacier, this dissertation only addresses the glacier surface mass balance. Losses at the base of the glacier (e.g. by basal melting) are also neglected. The time interval over which the mass change is determined is usually the period between freeze-up at the end of one melt season (year $= i - 1$) and the last day of melt in the following melt season (year $= i$). The computed change in mass over this interval is referred to as the *annual mass balance*. The surface mass balance is the direct link between the glacier and the atmosphere. In this dissertation, the term *surface mass balance* refers to the surface mass balance averaged over the surface area of the glaciers (with units of m^{-2} yr^{-1}). Throughout this dissertation, glacier surface mass balance is often referred to as simply mass balance. In addition, the term glacier is used to refer to land ice in general (mountain glaciers, ice caps, icefields, and ice sheets) unless distinguished from ice sheets in which case it refers to mountain glaciers, ice caps and icefields. The research presented here deals exclusively with glaciers but many of the principles and methods discussed are of direct interest to researchers that study other parts of the cryosphere, particularly those interested in mass and energy exchanges between the atmosphere and lake ice, river ice, sea ice and seasonal snow cover.

Mass balance measurements can be made directly though repeat surveying of a network of stakes drilled into the glacier surface, or indirectly through repeat measurements of glacier elevation, glacier area, or the earth's gravitational field. The direct method is labor intensive and logistically expensive, and it is thus usually only possible to monitor a small fraction of the glacier's surface. Although the direct method is one of the more reliable methods of measuring surface mass balance, it is not free from errors (Cogley et al. 1996; Cogley 1999). Repeat measurements of glacier elevation are used to construct elevation models of the ice surface at discrete time intervals. Using the geodetic method, changes in ice volume over the period between the two models can then be determined by differencing the elevations. Changes in the area extent of glaciers can also be used to estimate changes in volume through area-volume scaling relationships (Chen and Ohmura 1990; Burgess and Sharp 2004; DeBeer and Sharp 2007; Barrand and Sharp 2010). Changes in volume can then be converted to changes in mass using assumptions about the density of the material lost or gained. Due to the high error-to-estimate ratios, estimates of mass change derived from volume change estimates require a large temporal interval between the datasets from which the estimates are derived (e.g. Helsen et al. 2008). The coarse temporal resolution of volume change studies limits their use for assessing climate influences on glacier mass balance. Repeated measurements of the earth's gravitational field offer a direct measure of changes in mass for a specific region, but extracting the mass change signal due to changes in land ice is complicated by other sources of mass variation (i.g. postglacial rebound, ocean tides and seasonal snow cover). Gravity measurements have a very coarse spatial resolution making this method most applicable to measuring the mass change of large ice sheets (Ramillien et al. 2006; Wouters et al. 2008; Cazenave et al. 2009; Khan et al. 2010). In addition, repeat measurements of the earth's gravitational field only date back to the early 2000s. All three geodetic methods are complicated by the fact that the derived volume/mass changes are due to changes in both iceberg calving and surface mass balance. Separating the two terms requires a separate estimation of one of the two components. Because of these limitations, studies that assess climatic influences on surface mass balance most often rely on estimates of surface mass balance based on direct measurements (Alt 1978; Alt 1979; Alt 1987; Dyurgerov and McCabe 2006) or produced using numerical models that simulate the glacier surface mass balance (Hanna et al. 2008; Ettema et al. 2009). When assessing the response of glacier mass balance to past and future changes in climate, numerical modeling is the only method available.

The numerical methods used to model the surface mass balance of ice caps, mountain glaciers and icefields have different requirements than those methods used to simulate the surface mass balance of the ice sheets. The principal difference is that models for estimating the mass balance of glaciers must compute the surface mass balance at a much higher spatial resolution than is necessary for simulations of the surface mass balance of an ice sheet. This is required to capture the steep spatial gradients in melt rates and precipitation that are associated with the high relief and complex terrain in which many glaciers and ice caps are located. The same issue arises for modeling the surface mass balance around the perimeter of the Greenland Ice Sheet, where surface slopes are steep. A range of numerical methods have been applied to estimate the surface mass balance of these topographically complex regions. Currently all global estimates of the mass balance of glaciers and ice caps involve some form of statistical scaling. Most often, mass balance records for individual glaciers are simply extrapolated over the entire region from which the measurements were obtained and to regions that either share similar climate characteristics but lack local measurements or are simply adjacent to regions with local measurements (Dyurgerov and Meier 1997; Cogley and Adams 1998; Kaser et al. 2006). Slightly more sophisticated statistical approaches estimate the sensitivities of glacier melt and accumulation to changes in temperature and precipitation, respectively, for a small number of glaciers where mass balance measurements are available, and extrapolate these estimates to the world's remaining glaciers (Zuo and Oerlemans 1997; Oerlemans and Reichert 2000; Raper and Braithwaite 2006; Hock et al. 2009). If the climate sensitivities are well known, estimates of glacier response to changes in temperature and precipitation can be made. All of these statistical approaches rely on a small number of temporally and spatially heterogeneous glacier mass balance records that may not necessarily be representative of regional values. For this reason, it is desirable to move towards global mass balance assessments that use physically based models to simulate the surface mass balance for a horizontal grid covering entire regions. In addition, long-term simulations of glacier surface mass balance need to take into account changes in both glacier coverage and topography.

Two primary classes of models are used to simulate the surface mass balance for a horizontal grid: the energy balance approach which resolves the major energy fluxes to and from the glacier surface (Greuell and Konzelmann 1994; Bougamont and Bamber 2005), and the simplified temperature-index approach, which parameterizes the energy balance as a linear function of positive degree day sums (Braithwaite 1995; Hock 2003). Both classes of model are run with varying degrees of complexity, but it can generally be said that energy balance models provide a better physical representation of the melt process at the expense of requiring a large number of meteorological variables as input while the temperature-index approach is more empirically based but requires fewer inputs. Since both methods accept precipitation (the major source of accumulation) as input, these approaches can be viewed as methods for modeling ablation. While the temperature-index approach is often seen as inferior to the energy balance approach because the energy balance approach offers a better physical representation of ablation processes, it is important to consider the physical justification behind the temperature-index approach.

The energy balance approach requires a large number of meteorological inputs (e.g. wind speed, air temperature, long- and short-wave radiation, relative humidity, and atmospheric pressure) that must be either extrapolated and/or interpolated from point location measurements to the individual grid cells of the ablation model or prescribed from global and regional climate model or climate reanalysis fields. Meteorological measurements are often temporally and spatially sparse, collected far from the location for which the ablation modeling is being conducted, and at locations such as airports and settlements that have significantly different boundary layer characteristics than the snow/ice surface being modeled. Extrapolation and/or interpolation of the meteorological fields often requires more resources than developing the ablation model itself, and can introduce significant uncertainties and errors into ablation simulations.

The temperature-index approach effectively lumps the effects of the individual energy components into a single degree-day factor, and only requires mean daily temperatures as input. Mean daily temperatures is likely the most common and precise meteorological measurement made in the high latitude and high altitude environments where glaciers exist. The temperature-index method is physically justified by the large contribution of incoming long-wave radiation to overall the surface energy balance, and by the strong correlations between temperature, net short-wave radiation and the sensible heat flux (Ohmura 2001). Incoming long-wave radiation is largely governed by the thermal structure of the atmosphere (with the atmosphere closest to the surface having the most influence), and is well predicted by near-surface temperatures (Konzelmann et al. 1994). The main limitation of the temperature index method is that it does not allow for investigation of the physical processes governing changes in ablation rates. Since it lumps the influence of all energy balance terms into a single coefficient (the "degree day factor"), its application requires that coefficient values are taken from previous temperature-index studies of glaciers with similar energy balance characteristics or for the model to be calibrated using in-situ measurements. The validity of the coefficients will also be limited to the climatic range for which they were developed - that is, the temperature-index method may or may not be appropriate for modeling long-term changes in ablation rates resulting from substantial changes in climate (Van de Wal 1996).

The meteorological variables required to determine the energy balance are resolved within global and regional climate models along with the energy balance itself. The sophistication with which the energy balance over glacier surfaces is resolved varies greatly between models. Those models that explicitly resolve surface energy and mass balance for glacier surfaces at a sufficient spatial resolution to adequately capture gradients in surface mass balance are able to model glacier ablation in a coupled ice-atmosphere framework (Box et al. 2004; Fettweis et al. 2005; Fettweis 2007; Ettema et al. 2009; Vizcaino et al. 2010). This approach is ideal for assessing glacier ablation because it accounts for feedbacks that occur between the climate and the glacier surface (i.g. temperature-albedo feedback). Global and regional mass balance studies are, however, limited in their temporal coverage and spatial resolution by their computational requirements. This makes climate modeling well suited for simulation of the Antarctic Ice Sheets and the interior of the Greenland Ice Sheet where gradients in surface mass balance are generally low. The regional climate modeling approach is also well suited for the assessment of individual glaciers and ice caps. For large areas with high relief and complex terrain such as the Canadian Arctic islands, the Antarctic Peninsula and the margin of the Greenland Ice Sheet it is computationally challenging to run global or regional climate models at high enough resolution to adequately model gradients in surface mass balance. Modeling the mass balance of regions with these characteristics often requires the application of a non-coupled approach, where a surface mass balance model is forced with a meteorological dataset that has been upscaled/downscaled to the resolution of the model grid. This has been done using downscaled climate model output (i.e. Thompson and Pollard 1997; Glover 1999), downscaled climate reanalysis output (i.e. Hanna et al. 2005) and interpolated/extrapolated point location measurements (i.e. Mair et al. 2005). This approach is much less computationally intensive, and makes possible high spatial resolution mass balance modeling of large regions and long temporal periods. It, however, lacks any representation of climate-glacier feedbacks.

The Canadian High Arctic and challenges to modeling its surface mass balance

The Canadian High Arctic (Figure 1.1) is a region of global importance as it contains the largest volume of land ice on Earth after Greenland and Antarctica (Radić et al. 2010), making it a potentially significant contributor to sea level change. The entire region is considered to be a "polar desert", where annual precipitation is often < 200 mm with minimal inter-annual variability (Serreze and Barry, 2005). Surface air temperatures over glaciers in this region exceed the freezing temperature only during two to three months of the year. Because of this, variability in summer (June, July, August) mass balance (in which surface melt dominates over accumulation) accounts for ~95% of the inter-annual variation in annual mass balance. This indicates that summer melt is the governing factor in the variability of the annual mass balance (Koerner 2002). This important characteristic of Canadian High Arctic glaciers tsuggests that, at the scale of whole ice masses, the climate patterns and respective energy exchange processes that control summer melt largely control the variability in the annual mass balance.

The first measurements of the surface mass balance of a Canadian High Arctic glacier were collected in 1957 on a small glacier located on northern Ellesmere Island (Hattersley-Smith et al. 1961). Since this time more than a dozen glaciers in this region have been the subject of surface mass balance studies, and four of these glaciers have records spanning more than 40 years (e.g. Koerner 2002). Inter-annual changes in surface mass balance of this region have been shown to be highly correlated with changes in summer surface air temperatures (Hattersley-Smith et al. 1961; Bradley 1975; Bradley and England 1978; Blatter and Kappenberger 1988; Braun et al. 2004). This strong correlation has led to the development of several mass balance models that simulate surface melt as an empirical function of the near-surface air temperature (Arendt and Sharp 1999; Mair et al. 2005; Shepherd et al. 2007). Continuous records of surface air temperature in the Canadian High Arctic began with the construction of five manned weather stations by the Canadian and United States governments between 1947 and 1950. Of these five stations, three (Alert, Eureka and Resolute;

Figure 1.1) have remained in continuous operation since they were established. In addition to these long-term records, several multi-year field campaigns have collected sub-daily measurements of near-surface air temperatures over glacier ice using automatic weather stations (Blatter and Kappenberger 1988; Arendt and Sharp 1999; Boon et al. 2003; Braun et al. 2004; Koerner 2005; Mueller and Vincent 2006; Marshall et al. 2007). Thanks to the foresight of the late Roy Koerner and Claude Labine, who pioneered the use of automatic weather stations on Canada's Arctic Glaciers, some of these records span more than 20 years. These records of glacier surface mass balance and near-surface temperatures represent one of the highest concentrations of long-term measurements of glacier mass balance and surface temperatures in the Arctic. Combined with datasets collected during shorter field campaigns, they offer a unique opportunity to assess the multi-decadal influences of climate on the regional surface mass balance and to investigate the regional scale processes controlling glacier melt.

Since records of Canadian High Arctic glacier surface mass balance first began, only Alt (1987) has attempted to explain the variability in the regional mass balance in terms of synoptic climate forcing. Building on previous studies of synoptic climate controls on the mass balance of the Devon Island (Alt 1978) and Meighen Ice Caps (Alt 1979), Alt (1987) identified the synoptic conditions associated with extreme mass balance years. Using records of surface mass balance and near-surface temperature combined with surface and upper air synoptic charts, Alt (1987) was able to link inter-annual changes in the shape and position of the summer Arctic circumpolar vortex to annual changes in summer mass balance conditions for the period 1960 to 1976. The arctic circumpolar vortex is a mid-tropospheric feature which consists of a cyclonic system with strong winds rotating counter-clockwise about the cold polar air mass in its center, and is widely recognized as the dominant factor in Arctic summer atmospheric circulation (Maxwell 1980). Since the late 1980s glaciers in the Canadian High Arctic have experienced a sharp reduction in glacier mass balance. In the work presented in Chapter 2, the relationships recognized by Alt (1987) are reexamined to see whether they can explain this marked change.

The early work by Alt (1987) and the results presented in Chapter 2 provide a qualitative insight into the influence of synoptic climate on the surface mass balance of Canadian High Arctic glaciers, but do not allow for a quantitative assessment of the impact of changes in climate on the regional mass balance in this topographically complex region. One way to do this is to simulate the surface mass balance using a glacier mass balance model that is forced with meteorological fields and run at a high enough spatial resolution to accurately resolve surface mass balance gradients.

Climate reanalysis projects, which assimilate meteorological observations into a climate model framework to produce temporally and spatially continuous meteorological fields, produce datasets that are ideal for (1) investigating the influence of synoptic climate patterns on the regional surface mass balance of Canadian High Arctic glaciers (see Chapter 2) and (2) as input into regional scale models designed to simulate glacier surface mass balance (see Chapter 4). Climate reanalysis projects that include the Canadian High Arctic in their domains have produced datasets with horizontal resolutions of up to 32 km by 32 km (Kalnay et al. 1996; Kistler et al. 2001; Mesinger et al. 2006). However, even at this resolution the reanalysis fields must still be downscaled for input into mass balance models. Downscaling must be done at a fine enough resolution (~1km by 1km) to capture that large spatial gradients in surface mass balance that result from the region's high relief and complex terrain.

Whether using the energy balance approach or the temperature-index method to model glacier melt, model results are highly sensitive to input near-surface air temperature. Downscaling of temperature fields is most often performed either by running a regional climate model at the desired resolution forced at its boundaries with output from a climate reanalysis (or global climate model), or by computing near-surface temperatures from reanalysis fields using a digital elevation model of the glacier surface and an assumed air temperature lapse rate (decrease in air temperature with increasing surface elevation). Regional climate modeling at high spatial resolution requires extensive computational resources, so this approach is best suited for downscaling temperature fields for short time periods, either to relatively small ice masses or to larger ice masses with low spatial gradients in melt rates. For large and topographically complex regions like the Canadian High Arctic, running a regional climate model for multiple years at a resolution required for modeling glacier melt is computationally challenging, leaving statistical temperature downscaling as an attractive alternative.

When using the statistical approach to downscale near-surface air temperatures to model topography, the lapse rate is often taken to be the moist adiabatic lapse rate (MALR = 6 to 7°C km^{-1}; Glover 1999; Flowers and Clarke 2002; Thomas et al. 2003; Arnold et al. 2006; Bassford et al. 2006; Bassford et al. 2006; de Woul et al. 2006; Otto-Bliesner et al. 2006; Raper and Braithwaite 2006). However, temperature lapse rates measured close to glacier surfaces can differ substantially from this value (Greuell and Böhm 1998; Braun and Hock 2004; Hanna et al. 2005; Marshall et al. 2007). Through analysis of near-surface temperatures measured over a Canadian High Arctic icefield, Marshall and others (2007) found that near-surface temperature lapse rates (change in near-surface temperature with elevation following the glacier surface) were systematically less steep than the MALR, and that daily changes in lapse rates were associated with changes in synoptic weather patterns. In the summer, lapse rates were closer to the MALR when there was enhanced cyclonic activity, but were considerably lower than the MALR (< 2°C km^{-1}) when anticyclonic circulation prevailed. Neglecting to account for these observed deviations from the MALR likely results in large errors in downscaled temperature fields and in the melt estimates generated by mass balance models that use these temperatures as input (Greuell and Böhm 1998). In Chapter 3 efforts are made to derive a method for prescribing near-surface air temperature lapse rates that minimizes errors in near-surface temperatures when downscaling coarse resolution temperature fields over glacier surfaces. Building on the findings of Chapter 3, Chapter 4 examines the implications of using near-surface temperature fields that have been downscaled using the method outlined in Chapter 3 as input into glacier surface mass balance models. Model results are compared with results produced using temperature fields that have been downscaled using a constant lapse rate – either the MALR or the observed summer mean near surface lapse rate - and the results of the different approaches are evaluated against mass balance observations.

The energy balance approach to modeling surface melt requires individual energy flux components to be resolved. When using this approach as the basis for a mass balance model, it is as important to correctly model the surface albedo (reflectance) as it is to correctly estimate the surface air temperature. This is because, under most atmospheric conditions, absorption of shortwave radiation is the single largest energy source for melting snow and ice. The amount of shortwave radiation absorbed is dependent on both the incident radiation and the surface albedo, both of which are highly variable in space and time. It is therefore critical to incorporate the temporal variability of snow and ice albedo into numerical models of the surface energy balance. Despite the strong influence of snow and ice albedo on climate, surface energy balance, and melt rates, there is little consensus as to which albedo parameterizations are most appropriate for large scale modeling. This motivated the development of a computationally simple, theoretically-based parameterization for snow and ice albedo that can accurately reproduce broadband albedos under a wide range of snow, ice, and atmospheric conditions. Results of this work are presented in Chapter 5.

Reducing errors in downscaled near-surface temperatures and improving the parameterization of snow and ice albedo are two of the major obstacles that must be overcome before meaningful simulations of the regional surface mass balance of Canadian High Arctic glaciers can be performed. With this in mind, this is the major focus of the research presented in this dissertation.

Progression of papers

This dissertation is composed of four published papers. The first paper (Chapter 2) characterizes the regional glacier surface mass balance of the Canadian High Arctic and its relation to synoptic climate over the past 50 years. In particular, this research characterizes the inter-annual variability in the July circumpolar vortex and defines its relationship to both inter-annual and longer-term changes in the mass balance of glaciers in the Canadian High Arctic. This work was published in the *Journal of Climate* in 2007 and was co-authored with Martin Sharp (University of Alberta).

The second paper (Chapter 3) focuses on improving the downscaling of near-surface temperatures over glacier surfaces. It represents one of the largest datasets of near-surface air temperatures measured along altitudinal transects over glacier surfaces. Through extensive analysis of this dataset, a clear relationship between lower troposphere temperatures and near-surface temperature lapse rates is established. This work was published in the *Journal of Climate* in 2009 and is co-authored with Martin Sharp, the late Roy Koerner (formally with the Geological Survey of Canada), Claude Labine (Campbell Scientific Canada Limited), Sarah Boon (University of Lethbridge), Shawn Marshall (University of Calgary), David Burgess (Geological Survey of Canada), and David Lewis (University of Alberta).

The third paper (Chapter 4) assesses the implications of modeling temporal lapse rate variability when downscaled temperatures are used to force glacier surface mass balance models. This is done by forcing a temperature-index model designed to simulate the surface mass balance of the Devon Island Ice Cap (Figure 1.1) with temperatures downscaled using the method proposed in Chapter 3 and comparing the results with those produced using temperatures downscaled using (1) the mean measured ablation season lapse rate and (2) a constant MALR. Surface mass-balance estimates are determined for the years 1980–2006 and are evaluated against 23 years (1980–2003) of surface mass balance measurements from the northwest sector of the ice cap made by the late Roy Koerner. This paper was published in the *Annals of Glaciology* in 2009 and is co-authored with Martin Sharp.

The fourth and final paper (Chapter 5) details the development of a computationally simple and theoretically-based parameterization for snow and ice albedo that can accurately reproduce broadband albedos under a wide range of snow, ice, and atmospheric conditions. The parameterization is developed by fitting equations to broadband albedo estimates generated using a plane-parallel, discrete ordinates radiative transfer model of snow and ice that is coupled to a similar model of the atmosphere. This work was published in the *Journal of Geophysical Research – Earth Surface* in 2010 and is co-authored with Martin Sharp. The last three papers of this dissertation are part of a larger effort to develop a regional model to simulate the surface mass balance of Canadian High Arctic glaciers over the past 60 years and, more generally, to improve regional scale models of glacier surface mass balance.

References

Alt, B. T., 1978: Synoptic climate controls of mass-balance variations on Devon Island Ice-Cap. *Arctic and Alpine Research*, **10,** 61-80.

______, 1979: Investigation of summer synoptic climate controls on the mass balance of Meighen Ice Cap. *Atmosphere-Ocean*, **17,** 181-199.

______, 1987: Developing synoptic analogs for extreme mass balance conditions on Queen Elizabeth Island ice caps. *Journal of Climate and Applied Meteorology*, **26,** 1605-1623.

Arnold, N. S., W. G. Rees, A. J. Hodson, and J. Kohler, 2006: Topographic controls on the surface energy balance of a High Arctic valley glacier. *Journal of Geophysical Research-Earth Surface*, **111,** doi:10.1029/2005JF000426.

Barrand, N. E. and M. J. Sharp, 2010: Sustained rapid shrinkage of Yukon glaciers since the 1957-1958 International Geophysical Year. *Geophysical Research Letters*, **37,** L07501.

Bassford, R. P., M. J. Siegert, and J. A. Dowdeswell, 2006: Quantifying the mass balance of ice caps on Severnaya Zemlya, Russian High Arctic. II: Modeling the flow of the Vavilov Ice Cap under the present climate. *Arctic Antarctic and Alpine Research*, **38,** 13-20.

Bassford, R. P., M. J. Siegert, J. A. Dowdeswell, J. Oerlemans, A. F. Glazovsky, and Y. Y. Macheret, 2006: Quantifying the mass balance of ice caps on Severnaya Zemlya, Russian High Arctic. I: Climate and mass balance of tle Vavilov Ice Cap. *Arctic Antarctic and Alpine Research*, **38,** 1-12.

Bindoff, N. L., J. Willebrand, V. Artale, A. Cazenave, J. Gregory, S. Gulev, K. Hanawa, C. Le Quéré, et al., 2007: Observations: Oceanic climate change and sea level. *Climate Change 2007: The Physical Science Basis. Contribution of Working Group I to the Fourth Assessment Report of the Intergovernmental Panel on Climate Change*, Cambridge University Press, 384-432.

Blatter, H. and G. Kappenberger, 1988: Mass balance and thermal regime of Laika Ice Cap, Coburg Island, NWT, Canada. *Journal of Glaciology*, **34,** 102-110.

Bougamont, M. and J. L. Bamber, 2005: A surface mass balance model for the Greenland Ice Sheet. *Journal of Geophysical Research-Earth Surface*, **110,** doi:10.1029/2005JF000348.

Box, J. E., D. H. Bromwich, and L. S. Bai, 2004: Greenland Ice Sheet surface mass balance 1991-2000: Application of Polar MM5 mesoscale model and in situ data. *Journal of Geophysical Research-Atmospheres*, **109,** doi:10.1029/2003JD004451.

Bradley, R., 1975: Equilibrium-line altitudes, mass balance, and July freezing-level heights in the Canadian High Arctic. *Journal of Glaciology*, **14,** 267-274.

Bradley, R. S. and J. England, 1978: Recent climatic fluctuations of the Canadian High Arctic and their significance for glaciology. *Arctic and Alpine Research*, **10,** 715-731.

Braithwaite, R. J., 1995: Positive degree-day factors for ablation on the Greenland Ice Sheet studied by energy-balance modeling. *Journal of Glaciology*, **41,** 153-160.

Braun, C., D. R. Hardy, R. S. Bradley, and V. Sahanatien, 2004: Surface mass balance of the Ward Hunt Ice Rise and Ward Hunt Ice Shelf, Ellesmere Island, Nunavut, Canada. *Journal of Geophysical Research-Atmospheres*, **109,** doi:10.1029/2004JD004560.

Braun, M. and R. Hock, 2004: Spatially distributed surface energy balance and ablation modelling on the ice cap of King George Island (Antarctica). *Global and Planetary Change*, **42,** 45-58.

Burgess, D. O. and M. J. Sharp, 2004: Recent changes in areal extent of the Devon Ice Cap, Nunavut, Canada. *Arctic Antarctic and Alpine Research*, **36,** 261-271.

Cazenave, A., K. Dominh, S. Guinehut, E. Berthier, W. Llovel, G. Ramillien, M. Ablain, and G. Larnicol, 2009: Sea level budget over 2003-2008: A reevaluation from GRACE space gravimetry, satellite altimetry and Argo. *Global and Planetary Change*, **65,** 83-88.

Chen, J. and A. Ohmura, 1990: Estimation of Alpine glacier water resources and their change since the 1870s. *IAHS Publication*, **193,** 127-135.

Chen, J. L., C. R. Wilson, D. Blankenship, and B. D. Tapley, 2009: Accelerated Antarctic ice loss from satellite gravity measurements. *Nature Geoscience*, **2,** 859-862.

Cogley, J. G. and W. P. Adams, 1998: Mass balance of glaciers other than the ice sheets. *Journal of Glaciology*, **44,** 315-325.

de Woul, M., R. Hock, M. Braun, T. Thorsteinsson, T. Johannesson, and S. Halldorsdottir, 2006: Firn layer impact on glacial runoff: A case study at Hofsjoekull, Iceland. *Hydrological Processes*, **20,** 2171-2185.

DeBeer, C. M. and M. J. Sharp, 2007: Recent changes in glacier area and volume within the southern Canadian Cordillera. *Annals of Glaciology*, **46,** 215-221.

Dyurgerov, M. and G. J. McCabe, 2006: Associations between accelerated glacier mass wastage and increased summer temperature in coastal regions. *Arctic Antarctic and Alpine Research*, **38,** 190-197.

Dyurgerov, M. and M. F. Meier, 1997: Year-to-year fluctuations of global mass balance of small glaciers and their contribution to sea-level changes. *Arctic and Alpine Research*, **29,** 392-402.

Ettema, J., M. R. van den Broeke, E. van Meijgaard, W. J. van de Berg, J. L. Bamber, J. E. Box, and R. C. Bales, 2009: Higher surface mass balance of the Greenland ice sheet revealed by high-resolution climate modeling. *Geophysical Research Letters*, **36**.

Fettweis, X., 2007: Reconstruction of the 1979-2006 Greenland ice sheet surface mass balance using the regional climate model MAR. *The Cryosphere*, **1,** 21-40.

Fettweis, X., H. Gallee, F. Lefebre, and J. P. van Ypersele, 2005: Greenland surface mass balance simulated by a regional climate model and comparison with satellite-derived data in 1990-1991. *Climate Dynamics*, **24,** 623-640.

Flowers, G. E. and G. K. C. Clarke, 2002: A multicomponent coupled model of glacier hydrology - 2. Application to Trapridge Glacier, Yukon, Canada. *Journal of Geophysical Research-Solid Earth*, **107,** doi:10.1029/2001JB001124.

Glover, R. W., 1999: Influence of spatial resolution and treatment of orography on GCM estimates of the surface mass balance of the Greenland Ice Sheet. *Journal of Climate*, **12,** 551-563.

Greuell, W. and R. Böhm, 1998: 2 m temperatures along melting mid-latitude glaciers, and implications for the sensitivity of the mass balance to variations in temperature. *Journal of Glaciology*, **44,** 9-20.

Greuell, W. and T. Konzelmann, 1994: Numerical modeling of the energy balance and the englacial temperature of the Greenland Ice Sheet: Calculations for the ETH-Camp Location (West Greenland, 1155 m a.s.l.). *Global and Planetary Change*, **9,** 91-114.

Hanna, E., P. Huybrechts, I. Janssens, J. Cappelen, K. Steffen, and A. Stephens, 2005: Runoff and mass balance of the Greenland Ice Sheet: 1958-2003. *Journal of Geophysical Research-Atmospheres*, **110,** doi:10.1029/2004JD005641.

Hanna, E., P. Huybrechts, K. Steffen, J. Cappelen, R. Huff, C. Shuman, T. Irvine-Fynn, S. Wise, et al., 2008: Increased runoff from melt from the Greenland Ice Sheet: A response to global warming. *Journal of Climate*, **21,** 331-341.

Hattersley-Smith, G., J. R. Lotz, and R. B. Sagar, 1961: The ablation season on Gilman Glacier, Northern Ellesmere Island. *1960 General Assembly of Helsinki*, Helsinki, Finland, International Association of Scientific Hydrology, 152-168.

Helsen, M. M., M. R. van den Broeke, R. S. W. van de Wal, W. J. van de Berg, E. van Meijgaard, C. H. Davis, Y. Li, and I. Goodwin, 2008: Elevation Changes in Antarctica Mainly Determined by Accumulation Variability. *Science*, **320,** 1626-1629.

Hock, R., 2003: Temperature index melt modelling in mountain areas. *Journal of Hydrology*, **282,** 104-115.

Hock, R., M. de Woul, Radi, Valentina, and M. Dyurgerov, 2009: Mountain glaciers and ice caps around Antarctica make a large sea level rise contribution. *Geophysical Research Letters*, **36,** L07501.

Holmgren, B., 1971: *Climate and energy exchange on a sub-polar ice cap in summer, Arctic Institute of North America Devon Island Expedition 1961–1963, Part A-F*. Department of Meteorology, Uppsala University, Uppsala, Sweden, 403 pp.

Kalnay, E., M. Kanamitsu, R. Kistler, W. Collins, D. Deaven, L. Gandin, M. Iredell, S. Saha, et al., 1996: The NCEP/NCAR 40-year reanalysis project. *Bulletin of the American Meteorological Society*, **77,** 437-471.

Kaser, G., J. G. Cogley, M. B. Dyurgerov, M. F. Meier, and A. Ohmura, 2006: Mass balance of glaciers and ice caps: Consensus estimates for 1961-2004. *Geophysical Research Letters*, **33,** doi:10.1029/2006GL027511.

Khan, S. A., J. Wahr, M. Bevis, I. Velicogna, and E. Kendrick, 2010: Spread of ice mass loss into northwest Greenland observed by GRACE and GPS. *Geophysical Research Letters*, **37,** L06501.

Kistler, R., E. Kalnay, W. Collins, S. Saha, G. White, J. Woollen, M. Chelliah, W. Ebisuzaki, et al., 2001: The NCEP-NCAR 50-year reanalysis: Monthly means CD-ROM and documentation. *Bulletin of the American Meteorological Society*, **82,** 247-267.

Koerner, R. M., 1970: The mass balance of the Devon Island Ice Cap, Northwest Territories, Canada, 1961-66. *Journal of Glaciology*, **9,** 325-336.

______, 2002: Glaciers of the Arctic Islands. Glaciers of the High Arctic Islands USGS Professional Paper 1386-J-1, J111-J146 pp.

Konzelmann, T., R. S. W. Vandewal, W. Greuell, R. Bintanja, E. A. C. Henneken, and A. Abeouchi, 1994: Parameterization of global and longwave incoming radiation for the Greenland Ice Sheet. *Global and Planetary Change*, **9,** 143-164.

Lemke, P., J. Ren, R. Alley, I. Allison, J. Carrasco, G. Flato, Y. Fujii, G. Kaser, et al., 2007: Observations: changes in snow, ice and frozen ground. *Climate Change 2007: The Physical Science Basis. Contribution of Working Group I to the Fourth Assessment Report of the Intergovernmental Panel on Climate Change*, S. Solomon, D. Qin, M. Manning, Z. Chen, M. Marquis, K. B. Averyt, M. Tignor, and H. L. Miller, Eds., Cambridge University Press, 337-383.

Mair, D., D. Burgess, and M. Sharp, 2005: Thirty-seven year mass balance of Devon Ice Cap, Nunavut, Canada, determined by shallow ice coring and melt modeling. *Journal of Geophysical Research-Earth Surface*, **110,** doi:10.1029/2003JF000099.

Marshall, S. J., M. J. Sharp, D. O. Burgess, and F. S. Anslow, 2007: Surface temperature lapse rate variability on the Prince of Wales Icefield, Ellesmere Island, Canada: Implications for regional-scale downscaling of temperature. *International Journal of Climatology*, **27,** 385-398.

Maxwell, J. B., 1980: *The Climate of the Canadian Arctic Islands and Adjacent Waters* Vol. 1, *Climatological Studies*, Environment Canada, Department of supply services, 532 pp.

Meier, M. F., M. B. Dyurgerov, U. K. Rick, S. O'Neel, W. T. Pfeffer, R. S. Anderson, S. P. Anderson, and A. F. Glazovsky, 2007: Glaciers dominate eustatic sea-level rise in the 21st century. *Science*, **317,** 1064-1067.

Mesinger, F., G. DiMego, E. Kalnay, K. Mitchell, P. C. Shafran, W. Ebisuzaki, D. Jovic, J. Woollen, et al., 2006: North American Regional Reanalysis. *Bulletin of the American Meteorological Society*, **87,** 343-360.

Oerlemans, J. and B. K. Reichert, 2000: Relating glacier mass balance to meteorological data by using a seasonal sensitivity characteristic. *Journal of Glaciology*, **46,** 1-6.

Ohmura, A., 2001: Physical basis for the temperature-based melt-index method. *Journal of Applied Meteorology*, **40,** 753-761.

Otto-Bliesner, B. L., S. J. Marsha, J. T. Overpeck, G. H. Miller, and A. X. Hu, 2006: Simulating arctic climate warmth and icefield retreat in the Last Interglaciation. *Science*, **311,** 1751-1753.

Radić, Valentina, and R. Hock, 2010: Regional and global volumes of glaciers derived from statistical upscaling of glacier inventory data. *Journal of Geophysical Research*, **115,** F01010.

Ramillien, G., A. Lombard, A. Cazenave, E. R. Ivins, M. Llubes, F. Remy, and R. Biancale, 2006: Interannual variations of the mass balance of the Antarctica and Greenland ice sheets from GRACE. *Global and Planetary Change*, **53,** 198-208.

Raper, S. C. B. and R. J. Braithwaite, 2006: Low sea level rise projections from mountain glaciers and icecaps under global warming. *Nature*, **439,** 311-313.

Thomas, R. H., W. Abdalati, E. Frederick, W. B. Krabill, S. Manizade, and K. Steffen, 2003: Investigation of surface melting and dynamic thinning on Jakobshavn Isbrae, Greenland. *Journal of Glaciology*, **49,** 231-239.

Thompson, S. L. and D. Pollard, 1997: Greenland and Antarctic mass balances for present and doubled atmospheric CO2 from the GENESIS version-2 global climate model. *Journal of Climate*, **10,** 871-900.

Van de Wal, R., 1996: Mass-balance modelling of the Greenland ice sheet: a comparison of an energy-balance model and a degree-day model. *Annals of Glaciology*, **23,** 36-45.

van den Broeke, M., J. Bamber, J. Ettema, E. Rignot, E. Schrama, W. J. van de Berg, E. van Meijgaard, I. Velicogna, et al., 2009: Partitioning recent Greenland mass loss. *Science*, **326,** 984-986.

Vizcaino, M., U. Mikolajewicz, J. Jungclaus, and G. Schurgers, 2010: Climate modification by future ice sheet changes and consequences for ice sheet mass balance. *Climate Dynamics*, **34,** 301-324.

Wouters, B., D. Chambers, and E. J. O. Schrama, 2008: GRACE observes small-scale mass loss in Greenland. *Geophysical Research Letters*, **35,** 5.

Zuo, Z. and J. Oerlemans, 1997: Contribution of glacier melt to sea-level rise since AD 1865: A regionally differentiated calculation. *Climate Dynamics*, **13,** 835-845.

Figures

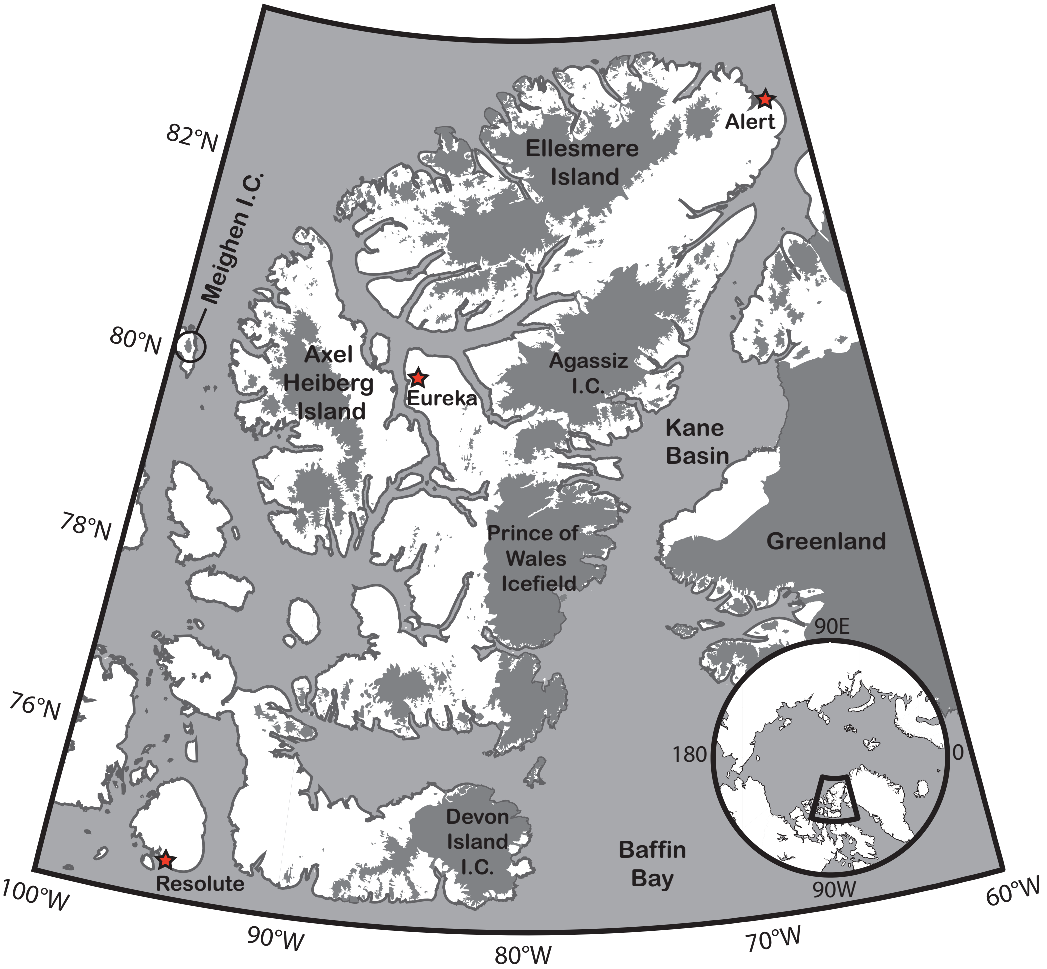

Figure 1.1: Canadian High Arctic

CHAPTER 2 : INFLUENCE OF THE ARCTIC CIRCUMPOLAR VORTEX ON THE MASS BALANCE OF CANADIAN HIGH ARCTIC GLACIERS*

Introduction

Global climate models consistently predict that climate warming associated with increasing atmospheric concentrations of greenhouse gases will be largest in northern high latitudes (Houghton et al. 2001; Jóhannessen et al. 2004). The response of Arctic glaciers, ice caps, and ice sheets to this warming may therefore be a significant influence on the eustatic component of global sea level rise. In the long term, changes in the volume the Greenland Ice Sheet are likely to have the greatest impact on sea level, but in the short term (next century or so) contributions from ice caps and glaciers may be more significant (Meier 1984; Houghton et al. 2001; Raper and Braithwaite 2006). There is therefore considerable interest in characterizing the mass balance of these smaller ice masses and their relationship to climate trends and variability (Cogley et al. 1996 Dowdeswell et al. 1997; Dyurgerov and Meier 1997; Dyurgerov and Meier 2000; McCabe et al. 2000; Braithwaite and Raper 2002; Hagen et al. 2003; Dyurgerov et al. 2005; Dyurgerov and McCabe 2006).

In this paper, ~ 40-year records of the surface mass balance of four ice masses in the Canadian high Arctic (>75°N) and their relationship to regional temperature trends and Arctic atmospheric circulation changes are analyzed. The Canadian high Arctic is a region of particular importance for this type of study as it contains the largest area of land ice in the world outside Greenland and Antarctica, and has the highest density of long-term glacier mass balance records in the Arctic.

The records used come from four ice masses in the Queen Elizabeth

---

* Previously published material: Gardner, A. S. and M. Sharp, 2007: Influence of the Arctic Circumpolar Vortex on the mass balance of Canadian High Arctic glaciers. *Journal of Climate*, **20**, 4586–4598.

Islands (QEI): Devon Island Ice Cap, Meighen Ice Cap, Melville Island South Ice Cap (Koerner 2002; Dyurgerov and Meier 2005) and White Glacier, Axel Heiberg Island (Cogley et al. 1996; Dyurgerov and Meier 2005) (Figure 2.1). All four glaciers are located in the “polar desert” climatic region, where annual precipitation is often <200 mm with minimal inter-annual variability. Surface air temperatures (SATs) over glaciers in this region only exceed the freezing temperature during two to three months of the year. For the four glaciers examined, variability in summer (June-August) mass balance accounts for 93-98% of the variation in annual mass balance. This indicates that summer melt has a dominant influence on variability in both the summer and annual mass balances. This allows variability in annual mass balance to be used as a measure of summer climate influences on glaciers and ice caps in the Canadian high Arctic.

Previous studies of glacier mass balance in the Canadian high Arctic (Meier 1984; Alt 1987; Dowdeswell et al. 1997; Dyurgerov and Meier 1999; Braun et al. 2004; Dyurgerov and McCabe 2006) have documented trends in mass balance, but only Alt (1987) has attempted to explain the variability in annual mass balance in terms of synoptic scale climatic forcing. Building on previous studies of synoptic climate controls on the mass balance of the Devon Island (Alt 1978) and Meighen Ice Caps (Alt 1979), Alt (1987) identified the synoptic conditions associated with extreme mass balance years on three ice masses in the QEI: Meighen Ice Cap, Devon Island Ice Cap, and White Glacier. By examining surface and upper air synoptic charts and climatic parameters over a 16-year period (1960-1976), Alt identified 3 sets of synoptic conditions associated with extreme mass balance years:

i. High melt conditions, associated with the intrusion of a ridge from the south into the QEI at all levels in the troposphere,
ii. Melt suppression conditions, associated with the maintenance of a deep cold trough across Ellesmere Island, and

iii. Summer snow accumulation conditions, which occur when cold polar lows track south and southeast across the QEI from the Arctic Ocean.

These three situations were related to differences in the position and shape of the July 500-mbar circumpolar vortex (Alt 1987). This mid-tropospheric feature consists of a cyclonic system with strong winds rotating counter-clockwise about the cold polar air mass in its center, and is widely recognized as the dominant factor in Arctic summer atmospheric circulation (Maxwell 1980). Unlike the stratospheric circumpolar vortex, which breaks down in summer, the tropospheric vortex, although weaker in summer, is present year-round (Serreze and Barry 2005). On a daily time scale, the July 500-mbar circumpolar vortex can split into several centers, spawning smaller cyclones that often move in a westerly direction around the pole. On a monthly time scale, the July mean polar vortex is most often characterized by a single, well defined annular geopotential low with its center located between 80°N and 90°N or by two weaker cyclonic systems with one system located near the pole and the other located over Baffin Bay.

Glaciers in the Canadian high Arctic have experienced a sharp reduction in mass balance since the late 1980s (Dyurgerov and McCabe 2006). In the work presented here, we investigate whether the relationships recognized by Alt (1987) can be used to explain this marked change in regional glacier surface mass balance. In particular, this research aims to characterize the inter-annual variability in the July 500-mbar circumpolar vortex and to define its relationship to both inter-annual and longer-term changes in the mass balance of glaciers in the Canadian high Arctic.

Methods

Long term (1963-2003) mass balance records for the four target ice masses in the Canadian high Arctic were obtained from syntheses of global glacier mass balance (Dyurgerov 2002; Dyurgerov and Meier 2005). Missing mass balance records for White Glacier and the Devon Island Ice Cap from 2002 and 2003 were obtained from the World Glacier Monitoring Service (IAHS/UNESCO 2005) and R.M. Koerner (2006, personal communication) respectively. Glacier mass balance measurements are made by monitoring a network of stakes drilled into the glacier ice and firn in both the accumulation and ablation areas. Measurements are made in spring, before the onset of summer melt. In the ablation area, the measurements required include the change in stake height, and the depth and density of the snow pack overlying glacier ice. In the accumulation area, snow depth is measured to the dense melt surface formed at the end of the previous summer and, in addition to measurements of stake height and snow density, it is necessary to estimate the fraction of summer melt retained by refreezing within the snow pack and underlying firn. This is accomplished by measuring ice accumulation in buried collection trays, and average snow densities. Cogley (1996) estimated the error in annual glacier mass balance measured at each stake on the White Glacier to be ± 200 mm water equivalent. This single stake error can be used as a conservative estimate of the error in whole glacier mass balance estimates for all monitored glaciers in the Canadian high Arctic (Cogley and Adams 1998). These measurements document the surface mass balance and do not account for mass loss due to glacier calving or basal melt, which may be significant in some cases (Burgess et al. 2005). For a more detailed description of the physical characteristics and methods used to determine the surface mass balance of each of the four glaciers, see Koerner (1996; 2002) and Cogley et al. (1996).

Non-rotated Principal Components Analysis (PCA) was used to extract the primary modes of variance from standardized time series of the four mass balance records. Time series were standardized by subtracting the mean of the series from each value and dividing the resulting values by the standard deviation of the series. Because this study is concerned with long-term changes in mass balance, the individual mass balance records were not detrended prior to PCA (Venegas 2001). To select modes for further analysis, the Kaiser Criterion (Kaiser 1960) was used, which excludes any factors with an eigenvalue of less than one, thereby excluding any factors that explain less variance than a single original variable. As the first principal component (PC1) explains 53% of the variance in the original four mass balance time series and is the only component with an eigenvalue greater than one, all other principal components were excluded.

A sequential algorithm developed for the detection of climate regime shifts from empirical data (Rodionov 2004) was used to determine whether and when any significant shifts in the mean of the PC1 anomalies occurred. Unlike commonly used confirmatory statistical methods for identifying climate regime shifts such as those employed by Mantua et al. (1997), which require an *a priori* hypothesis about the timing of the shift, this method allows automatic detection of discontinuities in the time series. Another advantage of this method is that it can detect regime shifts towards the end of a time series, which is not the case for other automatic detection methods. Only regime shifts detected using a cut-off length of 20 years and having a probability level $p \leq 0.05$ were considered. A Huber parameter (Huber 1964) of two was used to reduce the weighting of outliers that deviate by more than two standard deviations from the expected mean value of a new regime when calculating the regime shift. The red noise component of the time series to which this technique was applied was removed prior to applying the regime shift detection algorithm by "pre-whitening" the time series (Rodionov 2006). The autoregressive parameter used in the pre-whitening procedure was calculated using the method of Inverse Proportionality with 4 corrections (IPN4) with a sub-sample size of 10 (Rodionov 2006). Using these criteria, only one regime shift was detected.

The magnitude of glacier ablation, and thus the annual surface mass balance of glaciers in the Canadian high Arctic, depends on the energy balance at the glacier surface. Quantifying the historical net surface energy balance for this data sparse region is extremely difficult. For this reason, the relationship between glacier mass balance and near surface air temperatures (a commonly used proxy for the surface energy balance) was examined to investigate surface climate-glacier interactions. Surface air temperature (SAT) records were obtained for local Environment Canada meteorological stations (available at www.climate.weatheroffice.ec.gc.ca). Since only three meteorological stations in the Canadian high Arctic (Alert, Eureka and Resolute Bay; Figure 2.1) have continuous SAT records over the period of study (1963-2003), gridded 850-mbar air temperatures from the National Centers for Environmental Prediction (NCEP) and National Center for Atmospheric Research (NCAR) climate reanalysis (Kalnay et al. 1996; Kistler et al. 2001; available at www.cdc.noaa.gov) were also utilized. These were used to provide a more location independent measure of regional scale temperature and to investigate the spatial pattern of temperature changes. The 850-mbar pressure level (≈ 2 km above sea level) NCEP/NCAR reanalyzed atmospheric temperatures were used in place of reanalyzed SATs because they are less affected by the spectrally defined topography used in the climate reanalysis (Kalnay et al. 1996). This topography is too coarsely resolved to capture the complex orography of the Canadian high Arctic. An additional reason for selecting the 850-mbar pressure level was to reduce possible SAT biases due to erroneously defined snow cover within the NCEP/NCAR reanalysis model (Kanamitsu et al. 2002). SAT measurements from the three meteorological stations located in the region of interest were compared with mean monthly 850-mbar NCEP/NCAR air temperatures from the respective overlying grid cells to determine the degree of agreement between the records.

Both regional glacier mass balance and air temperatures were examined in relation to inter-annual variations in the position and strength of the circumpolar vortex. The location and standardized magnitude of the absolute minimum July NCEP/NCAR 500-mbar geopotential height north of the equator were used to characterize the center location and strength of the circumpolar vortex. The time series of minimum July 500-mbar geopotential height was standardized and inverted to provide a relative index of vortex strength. Years with positive strength indices have relatively low absolute minimum July 500-mbar geopotential heights with strong cyclonic circulation and were classified as years with a strong July vortex. In contrast, years with negative strength indices have relatively high absolute minimum July 500-mbar geopotential heights with weak cyclonic circulation and were referred to as years with a weak July vortex. We then investigated the relationships between the strength and position of the circumpolar vortex and the regional glacier mass balance.

To study the causes of the reduction in regional glacier mass balance in the late 1980s, differences between the NCEP/NCAR reanalysis fields for 850-mbar temperature and 500-mbar geopotential height for the years prior to and after 1987 were examined.

All correlation values presented in this paper are expressed in terms of r, Pearson's product-moment coefficient of correlation. The significance of the correlations was determined using a two-tailed Student's t-test with the null hypothesis that the time series are uncorrelated ($r = 0$). All r-values quoted are significant at the 0.05 level.

Results

Glacier Mass Balance

The four annual surface mass balance records, spanning the 41 years from 1963 to 2003, are not well correlated with each other ($r = 0.23$-0.52) but they nevertheless display strong underlying similarities. The first principal component (PC1) of these records has an eigenvalue of 2.13, and accounts for 53% of the variance across the four time series (Table 2.1). The loadings of the four mass balance time series on PC1 are similar in magnitude and sign, ranging between 0.64 and 0.81, suggesting that PC1 identifies a regional climatic influence on glacier mass balance. The standardized PC1 was therefore taken as a measure of the regional mass balance history of Canadian high Arctic glaciers for the period 1963-2003 and is hereafter referred to as the *regional glacier mass balance*. Individual standardized glacier mass balance records are compared with PC1 in Figure 2.2. Over the period 1961-2003, PC1 has a weak but significant linear trend toward more negative regional glacier mass balance anomalies ($r^2 = 0.27$).

Applying the regime shifts detection algorithm outlined in the methods section, only one regime shift was detected in the regional glacier mass balance signal. This occurred between 1986 and 1987 (Figure 2.3), in agreement with the findings of Dyurgerov and McCabe (2006). This method of regime shift detection is most sensitive to the user-defined variables of cut-off length and probability level. To determine the robustness of the identified regime shift, similar analyses were conducted using other cut-off lengths. For all cut-off lengths between 12 and 30 years, a 1986-87 regime shift in the mean of the regional glacier mass balance signal was detected. A significant difference in mean between the periods 1963-86 and 1987-2003 is also found when using the traditional 2-tailed Student's t-test method assuming unequal variance. The 24-year period prior to 1987 contains only 4 years with negative mass balance anomalies and has a mean standardized regional glacier mass balance anomaly of 0.46 with no linear trend. In contrast, the 17-year period after 1987 includes 12 years with negative mass balance anomalies, and has a mean standardized anomaly of -0.66. While there are too few points to identify a significant trend in the later 17 year period, there is a tendency towards increasingly negative anomalies towards the end of the series, with 4 of the 5 most negative mass balance anomaly years in the entire 41 year period occurring during the last 6 years of record (Figure 2.3).

Air Temperature

Inter-annual variability in Canadian high Arctic annual glacier mass balance is governed almost entirely by variation in summer glacier surface melt, which occurs mainly in the month of July (Wang et al. 2005). For this reason, only the relationships between regional annual mass balance, and summer air temperatures were investigated. Average June, July, August and summer (June to August) SATs for Alert, Eureka, and Resolute Bay were correlated with the regional glacier mass balance signal. Of the 12 SAT series, only June, July and summer SATs from Eureka and Resolute Bay are significantly correlated with the regional glacier mass balance. On average, July SATs from Eureka and Resolute Bay account for 56, 44, and 26 % more variance in the regional glacier mass balance than mean August, June and summer SATs respectively. In addition, when average July SATs from Eureka or Resolute Bay were used to model regional glacier mass balance, there were no significant correlations between the linear regression residuals and any June, August or summer SAT series. This strong relationship between Canadian high Arctic glacier mass balance and mean July temperature has long been recognized (Bradley and England 1978; Dowdeswell 1995). Since the majority of the variance in the Canadian high Arctic regional glacier mass balance signal is captured in the July SATs from Eureka and Resolute Bay, and there is minimal correlation with the SATs from the neighboring months, we focus solely on July atmospheric variables in the remainder of this analysis.

The average July SATs from Eureka and Resolute Bay are highly correlated ($r = 0.85$); however, no significant correlation exist between these two records and July SATs from Alert. This suggests that northern Ellesmere Island SATs may be influenced by different synoptic conditions than those that affect the more southern parts of the Canadian Arctic Archipelago. The implications of this for the glacier mass balance of the region will be discussed in the conclusion section of the manuscript.

The average July SATs from both Eureka and Resolute Bay were correlated with the 850-mbar temperatures in the 2.5° by 2.5° degree reanalysis grid cell located directly over each station. Reanalysis 850-mbar air temperatures and station SATs are reasonably well correlated ($r = 0.65$-0.87). To estimate how well variability in station derived SATs is captured by the NCEP/NCAR 850-mbar air temperatures, these temperatures (averaged over the region of interest: 75-80°N, 75-115°W) were correlated with the average Eureka and Resolute Bay July temperature ($r = 0.82$).

The average Eureka/Resolute Bay SATs are highly correlated with the regional glacier mass balance (PC1) ($r=0.79$). July SATs also show a significant regime shift from cooler to warmer temperatures between 1986 and 1987 (Figure 2.4). The SAT series contains a weakly significant linear trend towards warmer temperatures ($r^2 = 0.13$). This shift in regional temperature corresponds with the 1987 acceleration in the rate of annual glacier mass loss identified in glacier mass balance section. A similar shift is found in the regionally averaged NCEP/NCAR 850-mbar air temperatures.

It should be noted that in the 15 years prior to 1963 (the first year of record used in this study) mean July SATs taken from the Environment Canada meteorological stations of Resolute Bay and Eureka were 1 °C warmer than those in the period 1963-1986. The difference between the two is statistically significant and has previously been documented by Bradley and England (Bradley and England 1978).

500-mbar Arctic Circumpolar Vortex

For all years examined, the center locations of the July circumpolar vortices were grouped into three sectors (Figure 2.5a): Sector I: 75-90N and 0-180E, Sector II: 75-90N and 0-180W, and Sector III: 60-75N and 90-60W. To show the relationship between the position and strength of the circumpolar vortex and the mass balance of Canadian high Arctic glaciers, the relative vortex strength (standardized and inverted minimum Northern Hemisphere July 500-mbar geopotential height) and the Canadian high Arctic regional glacier mass balance signal (PC1) have been grouped by the sector in which the vortex center is located and sorted from the strongest to the weakest strength vortex within that group (Figure 2.5b).

For Sector I vortices there is a well-defined linear relationship between vortex strength and regional glacier mass balance, wherein strong vortices result in moderately positive mass balance anomalies and weak vortices result in extremely negative mass balance anomalies. A similar relationship exists for Sector II vortices except that strong vortices produce extremely positive mass balance anomalies and weak vortices produce neutral to moderately negative mass balance anomalies. As for Sector III vortices, there is little variation in vortex strength or regional glacier mass balance, with both indices close to neutral. If the extreme year of 1993 (see discussion section) is excluded from the analysis, there are statistically significant relationships between vortex strength and regional glacier mass balance for both Eastern (Sector I) and Western (Sector II and III) Hemisphere centered vortices.

Looking solely at the relationship between vortex location and regional glacier mass balance, 67% of all negative mass balance anomalies exceeding one standard deviation from the mean occurred during years when the vortex was located in the Eastern Hemisphere. 67% of all positive mass balance anomalies exceeding one standard deviation from the mean occurred during years when the vortex was located in the Western Hemisphere. In 18 of the 24 years prior to the 1987 decrease in regional glacier mass balance, the July vortex center was located in the Western Hemisphere. By contrast, the July vortex was centered in the Western Hemisphere in only 6 of the 17 years between 1987 and 2003. Analysis of the NCEP/NCAR climate reanalysis data available for the 15 years prior to 1963 shows an equal distribution of Eastern and Western centered vortices.

1987-2003 Atmospheric Anomalies

To examine atmospheric differences between the time periods before and after the 1987 shift in regional glacier mass balance, the differences between the 1963-1986 and 1987-2003 mean July NCEP/NCAR 850-mbar atmospheric temperature and 500-mbar geopotential height anomalies were determined. Relative to 1963-86, the mean 1987-2003 July 850-mbar temperature increased by 1-2 °C over the Canadian high Arctic, Siberia and the Barents Sea and decreased by 1-2 °C over the Kara and Labrador Seas (Figure 2.6a). The mean July 500-mbar geopotential height shows a similar pattern, with increases in geopotential height over regions where there was atmospheric warming and decreases in geopotential height over regions with atmospheric cooling (Figure 2.6b). The 1987-2003 decrease in mean July 500-mbar geopotential height in the region bounded by 75-90°N and 0-180°E and the increase in 500-mbar geopotential height in the region bounded by 75-90°N and 0-180°W reflects the increasing tendency for the July circumpolar vortex to be centered in the Eastern Hemisphere during the period of 1987-2003.

A time series (1963-2003) of mean area weighted July 500-mbar geopotential height over the region 70-85 ºN, 75-115 ºW was created to determine whether there were any significant regime shifts in mean 500-mbar geopotential height over the Canadian Arctic and whether they corresponded with the abrupt change in regional glacier mass balance. No significant shift or trend was identified. Regional 500-mbar geopotential heights are however highly correlated with the time series of regional glacier mass balance (r = 0.66).

Discussion

On a hemispheric scale, both Angell (1998; 2006) and Frauenfeld and Davis (2003) have shown that variability in the extent of the summer mid-tropospheric Arctic circumpolar vortex, as defined by the 700 to 300-mbar geopotential height contour that consistently falls within the primary baroclinic zone, is significantly correlated with variability in Northern Hemisphere mid to lower-tropospheric temperatures. Alt (1987) showed that inter-annual changes in the shape, strength, and position of the July 500-mbar Arctic circumpolar vortex have a strong influence on Canadian high Arctic regional glacier surface mass balance.

To illustrate the influence of both vortex strength and position on the regional glacier mass balance, July vortices were categorized into four Types: I-A, I-B, II-A, II-B, and III. The first type, Type I-A, includes years when the July 500-mbar circumpolar vortex was strong and its center was located in the Eastern Hemisphere. This type included all years with July vortices that had centers located in Sector I with positive strength anomalies. For Type I-A years it was most common for the area of low geopotential height surrounding the vortex center to extend into Baffin Bay (1973, 1982, 1992, 1994, 1996, and 2003). July 1992 exemplifies the regional influence of vortices with these characteristics (Figure 2.7a). Under these conditions, the regional influence of continental high-pressure systems over the Canadian high Arctic during July is greater than in years when a strong July vortex is located in the Western Hemisphere (Type II-A). In Type I-A years, average July temperatures result in neutral regional glacier mass balance anomalies.

In years when the July vortex is weak (negative strength anomaly) and centered in the Eastern Hemisphere (Type I-B conditions: 1963, 1971, 1972, 1976, 1987, 1988, 1991, 1998, 1999, and 2000) or is strong but the region of lowest geopotential height is not elongated over the Canadian high Arctic (1993) (Figure 2.7b), the Canadian high Arctic becomes almost thermally homogeneous with continental North America. This results in anomalously warm July SATs and extremely negative regional glacier mass balance. The 11 years with these characteristics contain 4 of the 5 warmest years in the 41-year record and 6 of the 8 most negative regional glacier mass balance years. Type I-B conditions compare well with Alt's (1987) synoptic analog for an extreme melt year (1962), when there was an anomalously high percentage of open water in the Queen Elizabeth Islands channels and a cloud cover minimum. Type I-B vortices were identified as having centers located in Sector I with negative strength anomalies or as having centers located in Sector I with the area of low geopotential heights constrained strictly to the Eastern Hemisphere with positive strength anomalies.

For years when the July 500-mbar vortex is strong and centered in the Western Hemisphere (Type II-A conditions) cyclonic conditions prevail over the Canadian high Arctic. July 1964 (Figure 2.7c) was selected as a representative year with these vortex characteristics. During this year, strong cyclonic conditions prevented North American high-pressure ridges from extending northward over the Canadian high Arctic, keeping July surface air temperatures (SATs) exceptionally low. Cold SATs in turn resulted in below average glacier ablation rates and highly positive annual glacier mass balance anomalies. 1964 was also a year of above average summer precipitation, which resulted from a succession of barotropic cyclones that transported Arctic Ocean moisture southward and deposited snow over the Canadian high Arctic (Alt 1987). Of the 41 years investigated, 1964 had the coldest mean July SAT, and the most positive annual regional glacier mass balance. Similar July vortex characteristics prevailed during 9 out of the 41 years investigated (1964, 1967, 1969, 1975, 1984, 1986, 1989, 1990 and 2002). Out of these 9 years, 8 were among the 10 most positive mass balance years on record. All years with vortex centers located in Sector II with positive strength anomalies were grouped in this category.

In years when the July circumpolar vortex is located in the Western Hemisphere but the vortex strength is decreased (higher minimum geopotential height) (Type II-B conditions: 1965, 1966, 1970, 1974, 1977, 1979, 1980, 1981, 1985, 1997 and 2001), the circumpolar vortex does not so effectively block warm North American continental air from moving into the Canadian high Arctic. These conditions result in average regional SATs and neutral regional glacier mass balance anomalies. All vortices with centers located in Sector II and having negative strength anomalies were placed in this category.

The last grouping of July vortices consists of years when there are two 500-mbar geopotential minima, the strongest of which (lowest geopotential height) is located in Sector III. The two minima are located to the south of, and to the north of, the Canadian high Arctic (Type III: 1968, 1978, 1983, and 1995). 500-mbar geopotential height contours for 1978, a representative year, are shown in Figure 2.7d. These vortex characteristics are associated with above average July SATs and below average Canadian high Arctic regional glacier mass balance.

Analysis of the NCEP/NCAR climate reanalysis data for the15-year period prior to 1963 shows a much higher occurrence (40%) of Type I-B vortices, which are associated with extreme melt conditions, and a reduced occurrence (20%) of Type II-B vortices, which are associated with average glacier mass balance conditions, relative to the period 1963-1986. This suggests that the period 1948-1962 closely resembles the 1987-2003 period, when there was a more negative glacier mass balance regime. This is also consistent with the above average July SATs observed during this period.

Analysis of July mean precipitation records from the Environment Canada meteorological stations at Eureka and Resolute Bay shows that in years when the vortex is strong and located in the Western Hemisphere (Type II-A) there is a nearly threefold increase (~20 mm) in total July precipitation compared to years when the vortex is weak and located in the Eastern Hemisphere (Type I-B), or when the vortex is located to the south of the Canadian high Arctic (Type III). During Type I-B and Type III years average regional July SATs measured at

Eureka and Resolute Bay, both of which are located at elevations near sea level, are 5.6 °C compared to 3.8 °C for Type II-A years. Assuming a cooling factor of 3 °C for SATs over glaciers, as was done by Atkinson and Gajewski (Atkinson and Gajewski 2002) when estimating high-resolution summer SATs for the Canadian Arctic Archipelago, this lowers the mean July sea level SATs over glaciers to 2.6 °C and 0.8 °C for Type I-B, Type III and Type I-A years, over Eureka and Resolute Bay respectively. Since Type II-A years have mean July temperatures near 0°C, it is likely that more of the precipitation will fall as snow during Type II-A years than in Type II-B and Type III years. Thus, the influence of vortex characteristics on summer precipitation in the Canadian high Arctic likely amplifies the thermally driven response of regional glacier mass balance to changes in the strength and location of the July 500-mbar circumpolar vortex.

Comparing the mean July 500-mbar geopotential heights in the 24 year period prior to the 1987 shift in regional glacier mass balance with those in the following 17 years (Figure 2.6b), there is a large decrease (40m) in mean geopotential height on the eastern side of the Arctic Ocean and a large increase (30m) on the western side. This is consistent with Angell's (1998; 2006) conclusion that the summer circumpolar vortex adopted a more easterly position in the latter part of the period 1963-2001.

In more general terms, when the mean July 500-mbar vortex is located in the Western Hemisphere the mass of cold polar air is more frequently situated over the Canadian high Arctic and warm high pressure ridges that build over continental Canada are more effectively blocked from moving northward over this region. When the mean July vortex is centered in the Eastern Hemisphere, warm continental high-pressure ridges are not so effectively blocked from pushing northward and the Canadian high Arctic becomes more thermally homogeneous with Continental North America. In terms of the influence of vortex characteristics on Canadian high Arctic glacier mass balance, only 17% of years between 1963 and 1986 had easterly positioned Type I-B July vortices, that result in extreme glacier melt conditions. In the 17 years that followed, 41% of years had Type I-B July vortices and the overall occurrence of westerly positioned July vortices (Types II-A, II-B, III) decreased by 40%.

In the results section it was shown that regional July 500-mbar geopotential heights are significantly correlated with the regional glacier mass balance, but the regional 500-mbar geopotential height time series does not show the 1986-1987 regime shift identified in both the air temperature and regional glacier mass balance time series. This suggests that it is not solely the absolute change in July 500-mbar height over the region that resulted in the inferred 1986-87 shift in regional glacier mass balance, but rather the combination of changes in the strength and position of the July circumpolar vortex. This can be illustrated by comparing regional July 500-mbar geopotential heights during Type I-A and Type II-B vortex years. During Type I-A vortex years (strong vortex centered in the Eastern Hemisphere), regional July 500-mbar geopotential heights over the Canadian high Arctic are on average 0.32 standard deviations below the 41-year mean. During Type II-B vortex years (weak vortex centered in Western Hemisphere) regional 500-mbar geopotential heights over the Canadian high Arctic are on average 0.40 standard deviations greater than for Type I-A vortex years. Despite the higher regional 500-mbar geopotential heights for years with Type II-B vortices, there is little difference in the regional glacier balance or station derived July SATs between years with Type II-B vortices and years with Type I-A vortices. This suggests that the combination of vortex position and strength must be accounted for when describing the relationship between the circumpolar vortex and the regional glacier mass balance.

The absence of significant correlations between the regional glacier mass balance record and the July temperature record from Alert (Figure 2.1), and between the Alert and Resolute/Eureka July temperature records suggests that mass balance variations of glaciers located in northern Ellesmere Island might differ from the pattern depicted by the regional glacier mass balance signal (PC1) of the four existing mass balance records for the Canadian high Arctic and therefore their relationships with the July 500-mbar vortex may differ from those presented here.

Other climate regime shifts that have previously been identified and shown to influence climate in Arctic regions are briefly examined. One of the most well known climate regime shifts is the 1976 shift in North Pacific sea surface temperatures, which is commonly referred to as the 1976 shift in the Pacific Decadal Oscillation (PDO; Mantua et al. 1997). By inspection of Figure 2.3, it can clearly be seen that the shift in PDO had little if any impact on the regional glacier mass balance of the Canadian high Arctic. Additional statistical analysis of the relationship between monthly and annual PDO indices (taken as the first empirical orthogonal function (EOF) of Pacific sea surface temperatures poleward of 20 °N; available at http://jisao.washington.edu/pdo/) shows no significant correlation between the PDO and the regional glacier mass balance. Another well-studied climate regime shift is the 1989 upward shift in the wintertime North Atlantic Oscillation (NAO; Hurrell 1995) / Arctic Oscillation (AO; Thompson and Wallace 1998) index, taken here as the first EOF of sea level pressure poleward of 20 °N. The majority of the variability in the Canadian high Arctic regional glacier mass balance is governed by melt processes that occur during summer months, so it is not surprising that no significant correlation exists between the National Weather Service Climate Prediction Center's winter AO index (available at www.cpc.noaa.gov) and the regional glacier mass balance. The only significant correlation that exists between monthly AO indices and the regional glacier mass balance signal is for the month of July ($r = 0.42$). The July AO is also significantly correlated ($r = 0.50$) with the average area weighted regional 500-mbar geopotential height and, like the regional 500-mbar geopotential height, the July AO does not contain a 1986-1987 regime shift. Less well-known regime shifts that did occur in 1987 affected central Arctic annual sea level pressures (Walsh et al. 1996) and Northern Hemisphere snow extent (Robinson and Frei 2000), suggesting that the inferred 1987 climate regime shift may have affected areas beyond the Canadian high Arctic.

Conclusions

A significant decrease in the Canadian high Arctic mean regional glacier mass balance anomaly, as represented by our 41-year time series of the first principal component of four glacier mass balance records, was detected between 1986 and 1987. For the four glaciers examined, variability in summer mass balance determines variability in the annual glacier mass balance. Regional glacier mass balance is strongly correlated with July mean air temperature at Eureka and Resolute Bay and with the regionally averaged 850-mbar July temperature from the NCEP/NCAR climate reanalysis. Significant shifts to higher July mean temperatures after 1987 were found in both station derived SATs and NCEP/NCAR 850-mbar temperatures.

Consistent with the findings of Alt (1987), inter-annual changes in the strength and position of the July 500-mbar circumpolar vortex exert a strong influence on Canadian high Arctic regional SATs and glacier mass balance. In general, when the July circumpolar vortex is strong and its center is located in the Western Hemisphere, positive mass balance anomalies prevail. In contrast, when the July circumpolar vortex is either weak, or strong without elongation over the Canadian high Arctic, and the vortex center is located in the Eastern Hemisphere, highly negative mass balance anomalies prevail. Since the late 1980s, there has been a significantly higher occurrence of July vortex types that produce anomalously high SATs over the Canadian high Arctic. This, in-turn, has resulted in a sharp decrease in the regional glacier mass balance. The tendency for more easterly centered July circumpolar vortices is reflected in 1987-2003 anomalies in NCEP/NCAR 500-mbar geopotential heights (Figure 2.6), which show a decrease of up to 40m in mean geopotential height over the eastern side of the Arctic Ocean and an increase of up to 30m in geopotential height over the Canadian Arctic relative to the 1963-1987 period.

These findings highlight the importance of understanding the dynamics behind the climatic forcings that have resulted in accelerated glacier melt in the Canadian high Arctic and show that the observed changes in July mean SATs and glacier mass balance in the region are not appropriately characterized by simple linear trends. To identify the mechanisms behind the regional patterns of warming and mass balance change in the Canadian high Arctic, it is necessary to analyze the dominant synoptic scale pressure systems and regional circulation patterns over the Arctic. The results presented here clearly show that changes in the strength and center position of the July 500-mbar circumpolar vortex have resulted in the acceleration of glacier ablation in the Canadian high Arctic since 1986-87. Further research is needed to determine what has caused these changes in the July 500-mbar circumpolar vortex.

References

Alt, B. T., 1978: Synoptic climate controls of mass-balance variations on Devon Island Ice-Cap. *Arctic and Alpine Research*, **10,** 61-80.

______, 1979: Investigation of summer synoptic climate controls on the mass balance of Meighen Ice Cap. *Atmosphere-Ocean*, **17,** 181-199.

______, 1987: Developing synoptic analogs for extreme mass balance conditions on Queen Elizabeth Island ice caps. *Journal of Climate and Applied Meteorology*, **26,** 1605-1623.

Angell, J. K., 1998: Contraction of the 300 mbar north circumpolar vortex during 1963-1997 and its movement into the Eastern Hemisphere. *Journal of Geophysical Research-Atmospheres*, **103,** 25887-25893.

______, 2006: Changes in the 300-mb North Circumpolar Vortex, 1963-2001. *Journal of Climate*, **19,** 2984-2994.

Atkinson, D. E. and K. Gajewski, 2002: High-resolution estimation of summer surface air temperature in the Canadian Arctic Archipelago. *Journal of Climate*, **15,** 3601-3614.

Bradley, R. S. and J. England, 1978: Recent climatic fluctuations of the Canadian High Arctic and their significance for glaciology. *Arctic and Alpine Research*, **10,** 715-731.

Braithwaite, R. J. and S. C. B. Raper, 2002: Glaciers and their contribution to sea level change. *Physics and Chemistry of the Earth*, **27,** 1445-1454.

Braun, C., D. R. Hardy, and R. S. Bradley, 2004: Mass balance and area changes of four High Arctic plateau ice caps, 1959-2002. *Geografiska Annaler: Series A - Physical Geography*, **86,** 43-52.

Burgess, D. O., M. J. Sharp, D. W. F. Mair, J. A. Dowdeswell, and T. J. Benham, 2005: Flow dynamics and iceberg calving rates of Devon Ice Cap, Nunavut, Canada. *Journal of Glaciology*, **51,** 219-230.

Cogley, J. G. and W. P. Adams, 1998: Mass balance of glaciers other than the ice sheets. *Journal of Glaciology*, **44,** 315-325.

Cogley, J. G., W. P. Adams, M. A. Ecclestone, F. Jung-Rothenhäusler, and C. S. L. Ommanney, 1996: Mass balance of White Glacier, Axel Heiberg Island, NWT, Canada, 1960-91. *Journal of Glaciology*, **42,** 548-563.

Dowdeswell, J. A., 1995: Glaciers in the High Arctic and recent environmental-change. *Philosophical Transactions of the Royal Society of London Series A-Mathematical Physical and Engineering Sciences*, **352,** 321-334.

Dowdeswell, J. A., J. O. Hagen, H. Bjornsson, A. F. Glazovsky, W. D. Harrison, P. Holmlund, J. Jania, R. M. Koerner, et al., 1997: The mass balance of circum-Arctic glaciers and recent climate change. *Quaternary Research*, **48,** 1-14.

Dyurgerov, M. and G. J. McCabe, 2006: Associations between accelerated glacier mass wastage and increased summer temperature in coastal regions. *Arctic Antarctic and Alpine Research*, **38,** 190-197.

Dyurgerov, M. and M. F. Meier, 1997: Year-to-year fluctuations of global mass balance of small glaciers and their contribution to sea-level changes. *Arctic and Alpine Research*, **29,** 392-402.

______, 1999: Analysis of winter and summer glacier mass balances. *Geografiska Annaler: Series A - Physical Geography*, **81A,** 541-554.

______, 2000: Twentieth century climate change: Evidence from small glaciers. *Proceedings of the National Academy of Sciences of the United States of America*, **97,** 1406-1411.

______, 2005: Glaciers and the changing earth system: A 2004 snapshot. Institute of Arctic and Alpine Research, University of Colorado, 268.

Dyurgerov, M., M. F. Meier, and R. L. Armstrong, 2005: Mass balance of mountain and sub-Polar glaciers outside the Greenland and Antarctic ice sheets: Supplement to the Dyurgerov Occasional Paper #55, 2002. Institute of Arctic and Alpine Research, University of Colorado.

Dyurgerov, M. B., 2002: Glacier mass balance and regime: Data of measurements and analysis. INSTAAR, University of Colorado Occasional Paper 55, 268 pp.

Frauenfeld, O. W. and R. E. Davis, 2003: Northern Hemisphere circumpolar vortex trends and climate change implications. *Journal of Geophysical Research-Atmospheres*, **108,** doi:10.1029/2002JD002958.

Hagen, J. O., K. Melvold, F. Pinglot, and J. A. Dowdeswell, 2003: On the net mass balance of the glaciers and ice caps in Svalbard, Norwegian Arctic. *Arctic Antarctic and Alpine Research*, **35,** 264-270.

Houghton, J. T., Y. Ding, D. J. Griggs, M. Noguer, P. J. Van Der Linden, D. Xiaosu, K. Maskell, and C. A. Johnson, Eds., 2001: *Climate Change 2001: The Scientific Basis*. Cambridge University Press, 881 pp.

Huber, P. J., 1964: Robust estimation of location parameter. *Annals of Mathematical Statistics*, **35,** 73-101

Hurrell, J. W., 1995: Decadal trends in the North Atlantic Oscillation: Regional temperatures and precipitation. *Science*, **269,** 676-679.

IAHS/UNESCO, 2005: Glacier mass balance bulletin No. 8, 108 pp.

Jóhannessen, O. M., L. Bengtsson, M. W. Miles, S. I. Kuzmina, V. A. Semenov, G. V. Alekseev, A. P. Nagurnyi, V. F. Zakharov, et al., 2004: Arctic climate change: Observed and modeled temperature and sea-ice variability. *Tellus Series A-Dynamic Meteorology and Oceanography*, **56A,** 559-560.

Kaiser, H. F., 1960: The application of electronic-computers to Factor-Analysis. *Educational and Psychological Measurement*, **20,** 141-151.

Kalnay, E., M. Kanamitsu, R. Kistler, W. Collins, D. Deaven, L. Gandin, M. Iredell, S. Saha, et al., 1996: The NCEP/NCAR 40-year reanalysis project. *Bulletin of the American Meteorological Society*, **77,** 437-471.

Kanamitsu, M., W. Ebisuzaki, J. Woollen, S. K. Yang, J. J. Hnilo, M. Fiorino, and G. L. Potter, 2002: NCEP-DOE AMIP-II Reanalysis (R-2). *Bulletin of the American Meteorological Society*, **83,** 1631-1643.

Kistler, R., E. Kalnay, W. Collins, S. Saha, G. White, J. Woollen, M. Chelliah, W. Ebisuzaki, et al., 2001: The NCEP-NCAR 50-year reanalysis: Monthly means CD-ROM and documentation. *Bulletin of the American Meteorological Society*, **82,** 247-267.

Koerner, R. M., 1996: Canadian Arctic. *Report on Mass Balance of Arctic Glaciers: IASC Report No. 5*, J. Jania and J. O. Hagen, Eds., Working Group on Arctic Glaciology, 5-8.

______, 2002: Glaciers of the Arctic Islands. Glaciers of the High Arctic Islands USGS Professional Paper 1386-J-1, J111-J146 pp.

Mantua, N. J., S. R. Hare, Y. Zhang, J. M. Wallace, and R. C. Francis, 1997: A Pacific interdecadal climate oscillation with impacts on salmon production. *Bulletin of the American Meteorological Society*, **78,** 1069-1079.

Maxwell, J. B., 1980: *The Climate of the Canadian Arctic Islands and Adjacent Waters* Vol. 1, *Climatological Studies*, Environment Canada, Department of supply services, 532 pp.

McCabe, G. J., M. Dyurgerov, and A. G. Fountain, 2000: Variability in winter mass balance of Northern Hemisphere glaciers and relations with atmospheric circulation. *Arctic Antarctic and Alpine Research*, **32,** 64-72.

Meier, M. F., 1984: Contribution of small glaciers to global sea-level. *Science*, **226,** 1418-1421.

Raper, S. C. B. and R. J. Braithwaite, 2006: Low sea level rise projections from mountain glaciers and icecaps under global warming. *Nature*, **439,** 311-313.

Robinson, D. A. and A. Frei, 2000: Seasonal variability of Northern Hemisphere snow extent using visible satellite data. *Professional Geographer*, **52,** 307-315.

Rodionov, S. N., 2004: A sequential algorithm for testing climate regime shifts. *Geophysical Research Letters*, **31,** doi:10.1029/2004GL019448.

______, 2006: Use of prewhitening in climate regime shift detection. *Geophysical Research Letters*, **33,** doi:10.1029/2006GL025904.

Serreze, M. C. and R. G. Barry, 2005: *The Arctic Climate System*. 1st ed. *Cambridge Atmospheric and Space Science Series*, Cambridge University Press, 385 pp.

Thompson, D. W. J. and J. M. Wallace, 1998: The Arctic Oscillation signature in the wintertime geopotential height and temperature fields. *Geophysical Research Letters*, **25,** 1297-1300.

Venegas, S. A., 2001: *Statistical Methods for Signal Detection in Climate*. DCESS Report No. 2, 96 pp.

Walsh, J. E., W. L. Chapman, and T. L. Shy, 1996: Recent decrease of sea level pressure in the central Arctic. *Journal of Climate*, **9,** 480-486.

Wang, L., M. J. Sharp, B. Rivard, S. Marshall, and D. Burgess, 2005: Melt season duration on Canadian Arctic ice caps, 2000-2004. *Geophysical Research Letters*, **32,** doi:10.1029/2005GL023962.

Figures

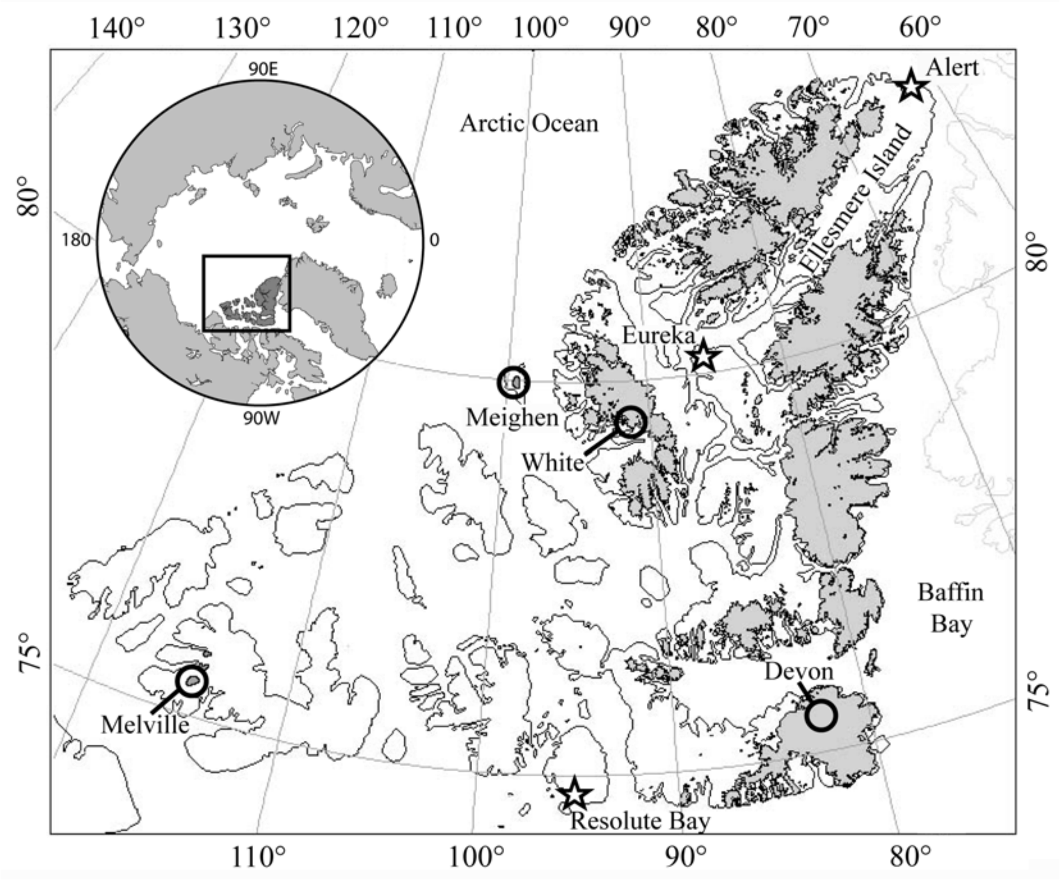

Figure 2.1: Canadian high Arctic: Locations at which long term glacier mass balance records have been collected (circles) and locations of long term Environment Canada meteorological stations (stars).

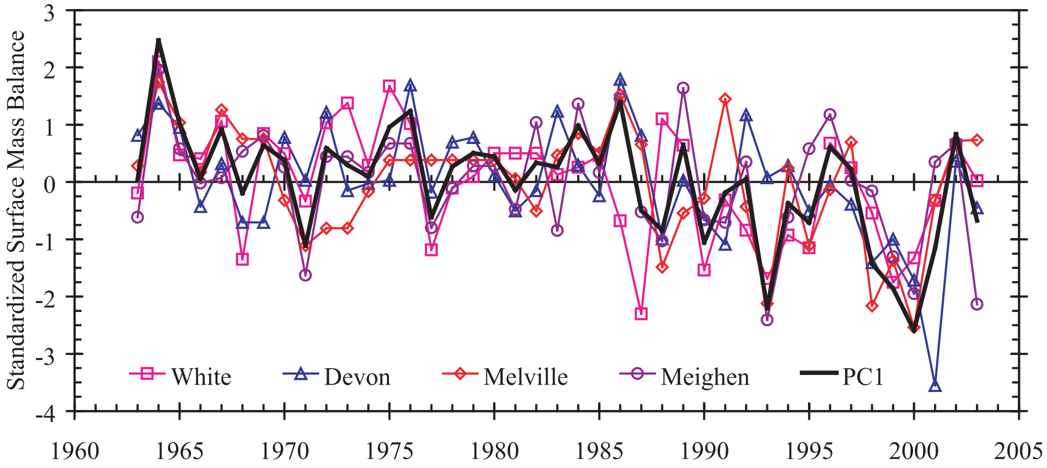

Figure 2.2: Annual mass balance records from individual glaciers expressed as standardized anomalies with the scores of the first principal component (PC1) plotted in bold.

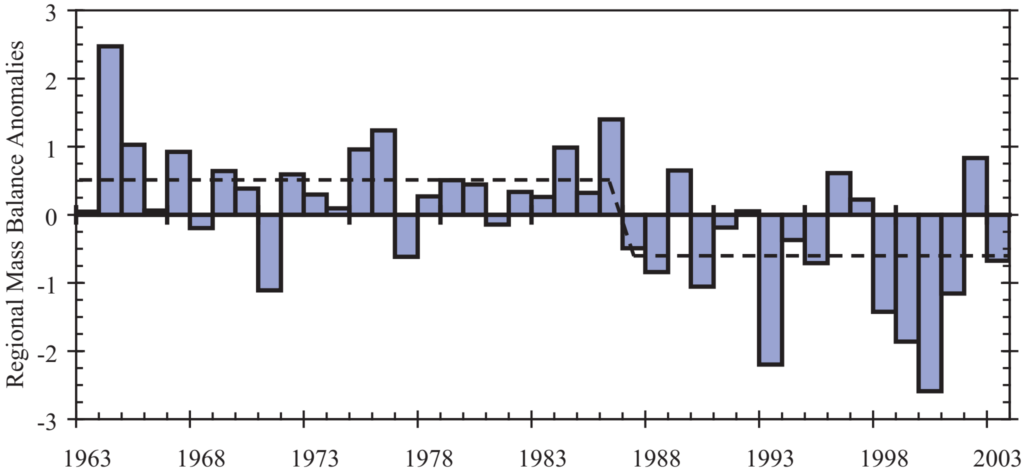

Figure 2.3: Standardized anomalies of the first principal component (PC1) of the four glacier mass balance records. Inferred mass balance regimes are represented by a dashed line.

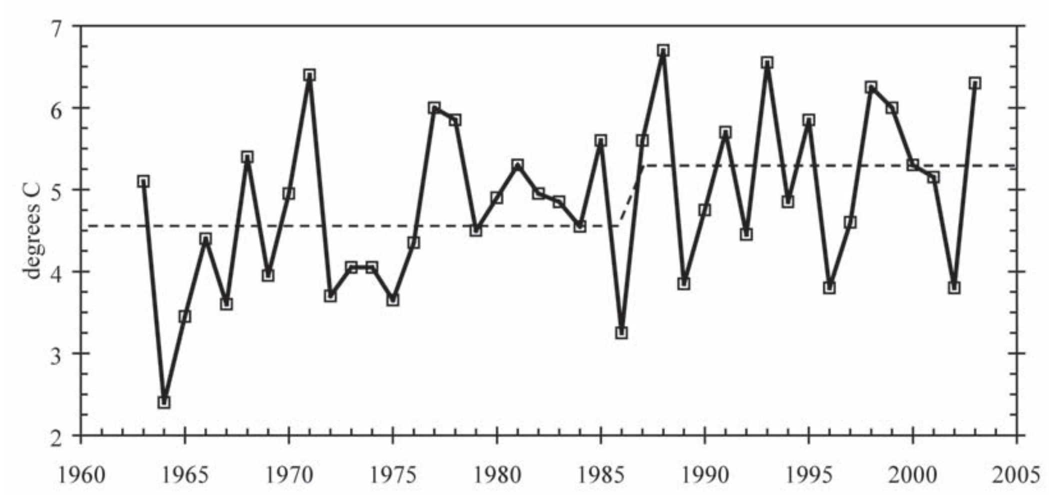

Figure 2.4: Regional mean July station derived surface air temperature (SAT), taken as the average temperature observed at the Environment Canada meteorological stations of Eureka and Resolute Bay. The dashed line displays the two significant temperature regimes.

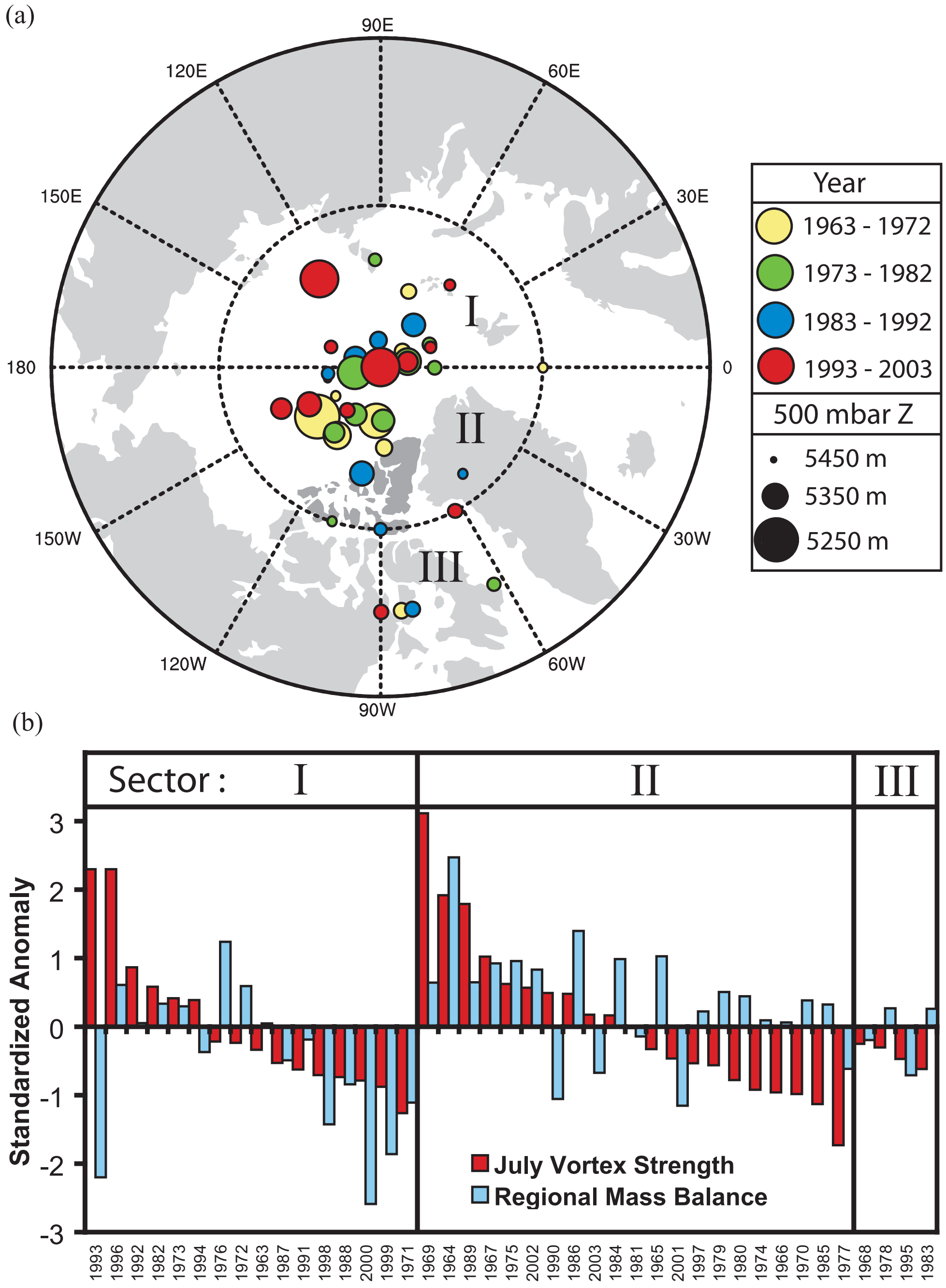

Figure 2.5: (a) Sector boundaries and July 500-mbar Arctic circumpolar vortex center location and strength, defined as the location and magnitude of the minimum Northern Hemisphere 500-mbar geopotential height (Z). Years of anomalously low (high) minimum geopotential heights are classified as years with a "strong" ("weak") circumpolar vortex. (b) Inverse of the standardized minimum Northern Hemisphere 500-mbar Z (vortex strength) and Canadian high Arctic regional glacier mass balance (PC1) grouped by year into the sectors in which the vortex center is located and sorted by vortex strength.

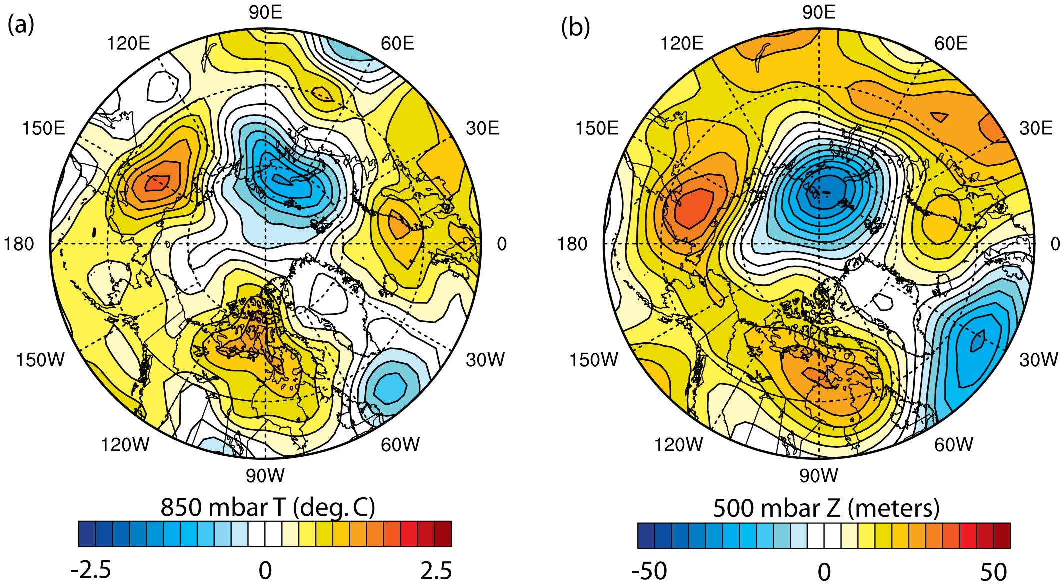

Figure 2.6: Mean July 1987-2003 (a) 850-mbar air temperature (T) and (b) NCEP/NCAR 500-mbar geopotential height (Z) anomalies based on a 1963-1986 base period.

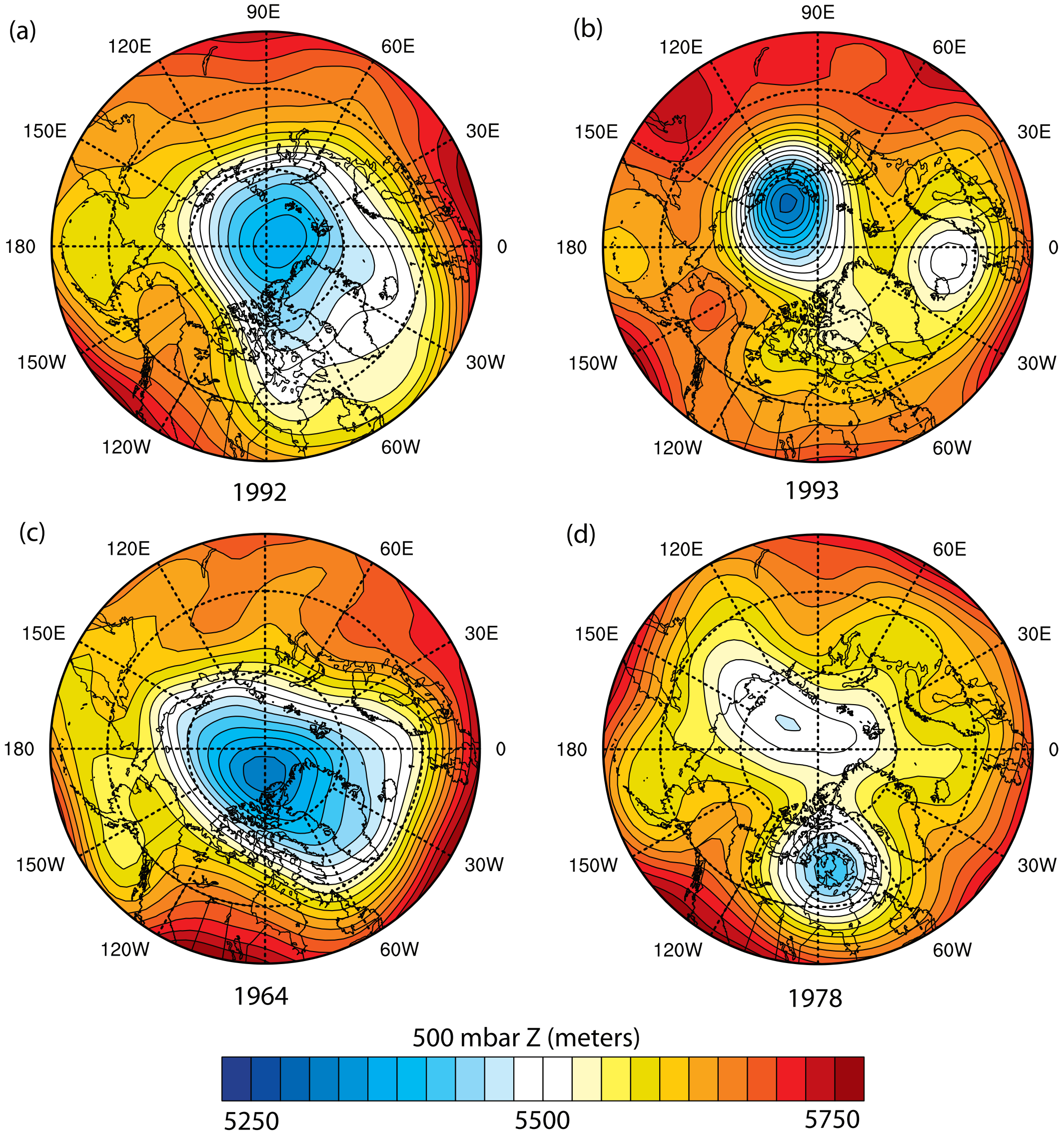

Figure 2.7: Mean July NCEP/NCAR 500-mbar geopotential heights (Z) for 1992, 1993, 1964 and 1978 (a through d), representative examples of Type I-A, Type I-B, Type II-A, and Type III July vortex types.

Tables

Table 2.1: Principal Component Analysis of four Canadian high Arctic glacier mass balance records (1963-2003).

Component	Eigenvalue	% of Variance	Component Loading			
			White	Devon	Melville	Meighen
1	2.13	53.30	0.71	0.75	0.81	0.64
2	0.85	21.22	-0.53	0.30	-0.30	0.62
3	0.58	14.53	0.29	-0.12	-0.12	0.45

CHAPTER 3 : NEAR-SURFACE TEMPERATURE LAPSE RATES OVER ARCTIC GLACIERS AND THEIR IMPLICATIONS FOR TEMPERATURE DOWNSCALING*

Introduction

Mass loss from glaciers and ice caps is likely the second largest contribution to global sea level rise after ocean thermal expansion (Meier et al., 2007). Quantifying past contributions from this source is challenging because of the limited availability of measurements of glacier surface mass balance and rates of iceberg calving. Glacier surface mass balance models are widely used to compensate for this lack of measurements and can be used to predict how climate change will influence future glacier contributions to global eustatic sea level (Gregory and Oerlemans, 1998; Braithwaite and Raper, 2002; Marshall et al., 2004; Bougamont and Bamber, 2005; Hanna et al., 2005).

Mass balance models calculate snow and ice melt using two main approaches: the energy balance approach and the temperature-index or “degree-day” approach. The latter approach assumes an empirical relationship between melting and near-surface air temperature, while the former involves the assessment of all the major energy fluxes to and from the glacier surface in order to determine the energy available for melt. In either case, spatially distributed modeling is required to capture spatial and temporal patterns of surface melt (Glover, 1999; Arnold et al., 2006). Such modeling requires accurate downscaling of coarse-resolution temperature fields derived from climate models or reanalysis to produce near-surface air temperature fields with an appropriate spatial resolution. Downscaling can be performed either by running a regional climate model (forced at its boundaries with coarse-resolution climate model

---

* Previously published material: Gardner, A. S., M. J. Sharp, R. M. Koerner, C. Labine, S. Boon, S. J. Marshall, D. O. Burgess, and D. Lewis, 2009: Near-surface temperature lapse rates over Arctic glaciers and their implications for temperature downscaling. *Journal of Climate*, **22,** 4281-4298.

output or data from climate reanalysis) at the desired resolution, or by computing near-surface temperatures from climate model fields using a digital elevation model of the glacier surface and an assumed temperature lapse rate.

"Lapse rate" is defined as "the decrease of an atmospheric variable with height, the variable being temperature, unless otherwise specified" (Glickman 2000), and it often refers to the environmental lapse rate in a vertical profile of the atmosphere. Here we use lapse rate to refer to the decrease in near-surface temperature with elevation following the glacier surface. We define lapse rates to be positive when temperature decreases as elevation increases in order to be consistent with usage in the atmospheric science community. However, we note that most previously published glacier near-surface lapse rates have been given the reverse sign convention (positive lapse rate = increase in temperature with increasing elevation: Braun and Hock 2004, Hanna et al. 2005, Otto-Bliesner et al. 2006b, Marshall et al. 2007, Gardner and Sharp 2009). This difference in sign convention should be noted when comparing our results with those presented in these other studies.

Regional climate modeling at high spatial resolution requires extensive computational resources, so this approach is best suited for downscaling temperature fields spanning short time periods to either relatively small ice masses or larger ice masses with low spatial gradients in melt rates. For large and complex regions like the Canadian High Arctic, running a regional climate model for multiple years at a resolution desirable for modeling glacier melt (~1 km) is computationally challenging, so statistical temperature downscaling remains an attractive proposition. The lapse rate used to downscale near-surface temperatures is often taken to be the moist adiabatic lapse rate (MALR = 6 to 7°C km^{-1}; Glover, 1999; Flowers and Clarke, 2002; Thomas et al., 2003; Arnold et al., 2006; Bassford et al., 2006; Bassford et al., 2006; de Woul et al., 2006; Otto-Bliesner et al., 2006; Raper and Braithwaite, 2006). However, temperature lapse rates measured close to glacier surfaces can differ substantially from the MALR (Greuell and Böhm, 1998; Braun and Hock, 2004; Hanna et al., 2005; Marshall et al., 2007). Neglecting to account for these differences may result in large errors in downscaled temperature fields and in the magnitude and spatial distribution of modeled glacier melt (Greuell and Böhm, 1998; Otto-Bliesner et al., 2006; Gardner and Sharp, 2009).

Near-surface temperature lapse rates vary on diurnal and seasonal time scales due to changes in the sensible heat flux between the free atmosphere and the underlying surface. This flux is influenced by temporal and spatial changes in free-atmosphere and surface temperatures, surface roughness, and wind speed. Because near-surface air temperatures are intermediate between those of the free atmosphere and the surface and surface temperatures over a melting glacier are fixed at the melting point temperature, near-surface lapse rates over melting glaciers are often lower than lapse rates in the free atmosphere (Greuell and Böhm, 1998). Marshall et al. (2007) found that measured near-surface lapse rates over a Canadian Arctic icefield were systematically lower than free-air lapse rates, and that daily changes in lapse rates were associated with changes in synoptic weather patterns. In the summer, lapse rates were closer to the free-air MALR when there was enhanced cyclonic activity, but were considerably lower than the MALR (< 2°C km^{-1}) when anticyclonic circulation prevailed.

Here we discuss measurements of surface air temperatures and lapse rates made on four large ice masses in the Canadian High Arctic at various intervals during the period 1988-2007. The Canadian High Arctic contains the largest volume of land ice in the world outside Greenland and Antarctica and is a potentially significant contributor to global sea level change. Mass balance measurements have been made at five sites in the region for over forty years (Cogley et al., 1996; Koerner, 2005) but little is known about the magnitude, trends, and inter-annual variability of glacier mass balance across much of the region. Distributed, regional-scale mass balance modeling is required to better estimate both past and future contributions of glacier melt in this region to global sea level change. The goals of this study are therefore (i) to determine whether the relationships identified by Marshall et al. (2007) apply throughout the region, (ii) to develop and validate an empirical method to model temporally variable lapse rates that can be used to downscale temperature fields derived from climate models or reanalysis to the complex surface topography of these ice masses, and (iii) to compare the results from this method with those generated by downscaling using the MALR.

Our analysis is based on six datasets from the Prince of Wales Icefield, Agassiz Ice Cap, and John Evans Glacier on Ellesmere Island, and from the Devon Island Ice Cap (Figure 3.1). These datasets contain over 58,000 measurements of daily mean temperature from 69 sensors covering the period June 1988 to May 2007. Near-surface lapse rates were calculated from these datasets and compared with estimates of daily mean lower-troposphere temperatures derived from the National Centers for Environmental Prediction's North American Regional Reanalysis (NARR: Mesinger et al., 2006). We present an empirical approach to downscaling the NARR temperatures that involves the prediction of near-surface lapse rates over glaciers from NARR 750-mbar mean daily air temperature standardized anomalies, where anomalies are taken relative to the 1979-2006 summer mean temperature and have been standardized by dividing the anomalies by their respective standard deviation. NARR bias-corrected summit elevation air temperatures were then downscaled using the modeled near-surface lapse rate for each day.

Site details

Agassiz Ice Cap

The 21,000 km^2 Agassiz Ice Cap, located on the eastern side of Ellesmere Island (Figure 3.1), is the second largest ice cap in the Canadian High Arctic (Sharp et al., 2003). In the spring of 1988, an automatic weather station (A_1) was erected at the site where two surface-to-bedrock boreholes were drilled by the Geological Survey of Canada in 1984 and 1987 (Koerner and Fisher, 1990; Fisher et al., 1995). Two more stations were installed at lower elevations along a northeast-oriented transect in June 1991 (A_2) and April 1994 (A_3). All three stations are equipped with Campbell Scientific (CS) 107F temperature sensors. These stations are still in operation, are maintained annually by CS Canada Ltd.

and the Geological Survey of Canada, and comprise the Agassiz transect, which extends 30 km horizontally and ranges in elevation from 880 to 1740 m a.s.l..

Devon Island Ice Cap

The dome-shaped Devon Island Ice Cap (area ~14,000 km^2) on the eastern side of Devon Island (Figure 3.1) is the southernmost glacier included in this study. Two of the six temperature-elevation transects are located on this ice cap. The longest running transect, Devon_N, is located on the north slope of the ice cap and spans a horizontal distance of >40 km and an elevation range from 330 to 1880 m a.s.l. It consists of six automatic weather stations installed between 1992 and 2005, four of which are currently in operation and are maintained by the Geological Survey of Canada (Koerner, 2005). All temperatures are measured with CS 107F sensors.

The second transect, Devon_S, is located on the south-facing slope of the ice cap and consists of three CS 107F sensors and 17 HOBO H8-PRO sensors manufactured by Onset Scientific Ltd. Sensors were installed between 2004 and 2006 and were distributed at ~2 km intervals along a 50 km transect from the ice cap summit to its southern margin. Most sensors on this transect, which spans an elevation range from 480 to 1800 m a.s.l., are currently operational and are maintained by the Arctic and Alpine Research Group at the University of Alberta.

John Evans Glacier

John Evans Glacier, the only valley glacier included in this study, is located on the east coast of Ellesmere Island to the south of the Agassiz Ice cap (Figure 3.1). In June 1996, three HMP35CF relative humidity/temperature sensors were installed on automatic weather stations located at elevations of 260, 820 and 1180 m a.s.l. (Arendt and Sharp, 1999; Boon et al., 2003). In May 2001, 16 HOBO H8-PRO temperature sensors were installed at ~100 m vertical intervals along a 15 km transect (JEG transect) following the centerline of the glacier from its terminus (140 m) to its summit (1470 m). The weather stations and the 16 HOBO sensors were removed in June 2003.

Prince of Wales Icefield

The Prince of Wales Icefield is located in eastern Ellesmere Island, to the south of John Evans Glacier (Figure 3.1). Two temperature-elevation sensor transects were operated on the icefield between 2001 and 2003 (Marshall et al., 2007). The 170 km POW_N transect, which crosses the northern part of the icefield, was installed in spring 2001. It consisted of one CS 107, one Veriteq Instruments Inc. SP-2000, and 12 HOBO H8-PRO temperature sensors located at elevations ranging from 130 to 1730 m a.s.l. The 130 km southern transect, POW_S, which spanned an elevation range from 550 to 1350 m a.s.l, was installed in spring 2002 and consisted of two SP-2000 and four HOBO H8-PRO temperature sensors. All sensors were removed in spring 2003. Marshall et al. (2007) provide a more detailed description of the icefield and the datasets derived from these transects.

Data and methods

Near-surface temperatures

All temperature sensors were installed in solar radiation shields mounted on metal or plastic poles drilled into the glacier surface. Sensors were mounted between 1 and 1.5 m above the surface and in open locations representative of the surrounding area. Temperatures were originally recorded as 15 min, 30 min, 1 hr, 2 hr or daily averages, and were post-processed to produce daily averages. A list of all temperature sensors used in the study, locations and periods of operation can be found in the appendix (Table A.1) along with sensor specifications (Table A.2).

Sensor measurement accuracies range between ±1.0°C at low (<-30°C) temperatures and ±0.2°C at 0°C (Table A.2). Marshall et al. (2007) conducted an extensive study to determine additional errors due to instrument calibration (0.1 to 0.7°C) and varying sensor height relative to the glacier surface (±0.1°C for daily averages). They estimated the overall uncertainty in the daily average temperature measurements to be ±1.3°C. This value is also adopted for the measurement error in this study.

Gaps in sensor records exist (mostly during winter months) where stations were removed for servicing, because the battery or sensor failed, when sensors were found less than 0.5 m (high accumulation) or more than 2.5 m (high ablation) above the surface, and where sensor poles collapsed due to ablation or interference from polar bears. Figure 3.2a shows the annual number of daily averaged temperature measurements made along each transect. All quality-controlled daily average temperature measurements for each transect have been included as supplementary material for this manuscript and can be found on the University of Alberta Arctic and Alpine Research Group's website: arctic.eas.ualberta.ca.

Lapse rates

Using daily mean temperatures and assuming constant sensor elevations, daily lapse rates were calculated for each transect using simple linear regression. For the Devon_S, JEG, POW_N and POW_S transects, measured temperatures below -30°C were excluded from lapse rate calculations due to increased instrument errors at these temperatures. For the Agassiz and Devon_N transects, where CS 107F temperature sensors were used, all temperatures below -50°C were excluded. Lapse rates were only calculated when three or more separate temperature measurements were available along a transect, and when the elevation difference between the lowest and highest available stations exceeded 500 m. These criteria reduce the impact of temperature measurement errors on calculated lapse rates, but also reduce the number of days for which lapse rates can be calculated. For the six transects, between 44% and 91% of days with temperature measurements yielded lapse rates (Figure 3.2b). There are less than twenty days of data for POW_S in January, February, and March, so no values are reported for these months and the POW_S transect is omitted from the discussion of winter lapse rates.

Regional Climate Reanalysis

The NARR dataset (32-km and 45-layer) is available for the period from 1979 to 2006 for the entire North American region. Data were provided by the

NOAA/OAR/ESRL Physical Sciences Division, Boulder, Colorado, USA, from their website at www.cdc.noaa.gov (accessed October, 2007).

The variables 500-mbar geopotential height (500Z) and 750-mbar air temperature (750T) were selected to characterize atmospheric conditions over the four Canadian High Arctic glaciers. 500Z was chosen to describe synoptic scale variability in the mid-troposphere, which has a strong influence on lower-troposphere temperatures, regional glacier melt, and near-surface lapse rates in the Canadian High Arctic (Alt, 1987; Wang et al., 2005; Gardner and Sharp, 2007; Marshall et al., 2007). 750T was selected to describe free-air temperatures at an elevation of ~2200 m a.s.l., which is at least 500 m above the NARR model topography in the regions of the four glaciers examined in this study. The influence of changes in free-atmospheric temperatures was investigated because these temperatures can affect near-surface lapse rates directly by modifying the sensible heat flux to and from the surface and indirectly by altering other surface energy balance components (i.e. the amount of absorbed solar radiation through melt-induced modification of the surface albedo). The influence of atmospheric winds was also investigated because winds can modify both free-air and near-surface lapse rates through the horizontal advection of air masses of different temperatures and moisture contents, by forcing the ascent/descent of advected air masses over terrain, and by altering the turbulent heat fluxes between the free atmosphere and the surface. However, no consistent relationships were found between wind components and lapse rates.

Daily average time series for the selected NARR variables were created for each glacier by averaging over a six grid-cell domain (96 km by 64 km) centered over each glacier. All time series were generated for the period January 1988 to December 2006, which extends from the first year of on-glacier temperature data to the last year of NARR data available from the NOAA/OAR/ESRL Physical Sciences Division's website.

To ensure that the NARR data accurately model climatic variability over the region of interest, 750T (averaged over the regions occupied by each glacier) was correlated with individual temperature series from on-glacier sensors located above 1000 m a.s.l. on each glacier. All near-surface measurements are highly positively correlated with the corresponding NARR 750T (annual: $r = 0.84 – 0.98$, summer: $r = 0.71 – 0.92$). As with other correlations presented in this paper, monthly means were subtracted from the time series prior to correlation.

Statistical analysis

Pearson product-moment correlation analysis (Shumway and Stoffer, 2006) was used to identify relationships between NARR meteorological variables, lapse rates, and glacier surface temperatures. Before correlation coefficients (r) were calculated, a centered three-day moving average low-pass filter was applied to all time series. This removed local noise that was present at daily frequencies and improved comparisons between time series from field sites that are separated by up to 700 km and may be affected by the same synoptic events but at different times. As with most sub-annual meteorological time series, there are strong red-noise (seasonal cycle) components in the datasets that must be removed before representative correlation coefficients can be determined. This was accomplished by subtracting monthly means from all time series before correlation coefficients were calculated. The significance of the correlation coefficients was determined using a two-tailed Student's t-test with the null hypothesis that the time series were uncorrelated ($r = 0$). The low-pass filter introduces lag-1 and -2 serial correlations into the time series that might affect the assessment of the statistical significance of correlation coefficients, although "inferences about the correlation coefficient seem to be relatively weakly affected by serial correlation" (von Storch and Zwiers, 1999, p. 149). To err on the side of caution, we adopted a 99% confidence level ($p < 0.01$) as the threshold for statistical significance.

Results

Near-surface temperatures

Mean annual temperatures averaged over all sensors ranged from -18.9 to -15.5°C for the Agassiz and JEG transects respectively. Average monthly transect temperatures are lowest in February (-35 to -29°C) and highest in July (-1 to +2°C). There are pronounced seasonal cycles in the monthly mean standard deviations of daily temperatures, with higher standard deviations (3.5 to 7.1°C) during the winter (DJF) and lower values (2.0 to 3.7°C) during the summer (JJA). The lower standard deviations in summer are in part due to fixed temperatures (0°C) at the melting surface.

The relationship between elevation and seasonal mean temperature is much stronger during the summer (average $r = -0.94$; Figure 3.3b) than in the winter (average $r = -0.68$; Figure 3.3a). This suggests that a constant regional near-surface lapse rate is a better description of the near-surface temperature field during the summer than in the winter. There is also a significant correlation ($r = 0.73$) between elevation and the standard deviation of the daily near-surface temperatures in summer (Figure 3.3d) but not in winter (Figure 3.3c). The atmospheric controls governing this observed relationship will be discussed in a later section.

Lapse rates

Daily near-surface lapse rates ranged between -11.9°C km^{-1} (recorded during a strong temperature inversion over the JEG transect in March 2003) and 14.8°C km^{-1} (recorded over the Devon_S transect in November 2002). Centered 3-day moving average lapse rates for each of the 6 transects are presented in Figure 3.4. Lapse rates are generally lower during colder months and higher during warmer months. Monthly mean values (Figure 3.5) are on average 1.8°C km^{-1} higher in summer than in winter. Monthly mean daily temperature-elevation correlation coefficients are also larger in summer ($r = 0.82 – 0.97$) than in winter ($r = 0.63 – 0.85$), suggesting that the assumption of a linear near-surface lapse rate is most appropriate during the summer months. Lower lapse rates are expected during winter months due to a persistent lower-troposphere temperature inversion that is observed throughout the Arctic (Serreze and Barry 2005, p.139-143). During polar night, when there is little or no solar radiation, an atmospheric temperature inversion results from long-wave radiative equilibrium between the highly emissive colder snow surface and the less emissive and warmer lower troposphere. It is maintained by the northward advection of warmer sub-arctic air (Overland and Guest 1991). The strength of the lower-troposphere temperature inversion is strongly influenced by the presence of diamond dust (Overland and Guest 1991) and occurrence of cloud cover (Serreze et al. 1992). Near-surface lapse rates over JEG are on average 2.2°C km^{-1} lower than lapse rates over the other five transects in summer and 4.4°C km^{-1} lower in winter (Figure 3.5). The Agassiz transect has the highest average summer (6.4°C km^{-1}) and winter (4.6°C km^{-1}) lapse rates. This is likely due to the Agassiz transect's generally colder climate, which results in less frequent summer melt and a less extensive melting zone than is observed at the other three sites (Wang et al., 2005). Less melt area leads to less area at lower elevations with surface temperatures fixed at 0˚C, resulting in slightly higher near-surface lapse rate. Lower temperatures also result in higher MALRs because the MALR tends towards the dry air lapse rate as temperatures cool. All other mean summer and winter lapse rates lay within the ranges 4.9 ±0.4°C km^{-1} and 3.2 ±0.5°C km^{-1} respectively. These values are systematically lower than standard MALRs, which is consistent with most previously published values for Arctic glaciers and the Greenland ice sheet (Table 3.1).

Cross-correlations between daily lapse rates along the different glacier transects are stronger during summer months than in winter (Table 3.2). This suggests that regional-scale processes account for a larger fraction of the variance in lapse rates during summer than winter. To illustrate the strength of this regional influence, all available lapse rates for summer 2002 are plotted in Figure 3.6.

Relationship between near-surface lapse rates and atmospheric conditions

Summer daily mean lapse rates measured over all six temperature-elevation transects are significantly lower than the free-air MALR when summit elevation temperatures are anomalously high (Fig. 3.7). The relationship between measured lapse rates and temperatures is strongest when lapse rates are compared with temperature measurements taken at higher elevations. In addition, when near-surface lapse rates are correlated with NARR 500Z and 750T (averaged over each of the four glaciers) the strongest relationships are between summer lapse rates and 750T (Fig. 3.8).

Variations in summer 750T over the Canadian High Arctic are associated with synoptic scale southerly advection of warm North American continental air and northerly advection of cold polar air masses that affect temperatures on a regional scale (Alt, 1987; Gardner and Sharp, 2007). Mean summer correlation coefficients with summer 750T are negative and significant for all lapse rate series and range between $r = -0.55$ and -0.81. These findings show that lower lapse rates are associated with warmer air masses and higher rates with colder air masses.

Influence of free-atmospheric temperatures on near-surface temperatures and lapse rates

To explain what drives the relationship between free-air temperatures and near-surface lapse rates we focus on a vertical cross section of the atmospheric boundary layer between the glacier surface and the free atmosphere, and discuss the "climate sensitivity" of the near-surface air temperature. This is defined here as the change in near-surface temperature relative to a change in the free-atmospheric temperature. During the summer, the glacier surface gains energy through a positive net radiation flux and, to a lesser extent, through turbulent heat transfer and rainfall. The snow and glacier-ice warm until the surface reaches the melting point, after which further net inputs of energy produce melt while the surface temperature remains fixed at 0° C. Because surface temperatures are fixed over a melting glacier surface and free-atmosphere temperatures decrease with increasing elevation, the free atmosphere becomes warmer relative to the surface as the surface elevation decreases. This gradient drives a flux of sensible heat from the atmosphere to the glacier surface that modifies the temperature of the air within the boundary layer. A larger sensible heat flux will result in greater cooling of the boundary layer relative to the temperature of the free atmosphere, so the climate sensitivity of the near-surface air temperature over a melting surface will be less than unity.

The upper portions of Arctic glaciers will often remain frozen while melt occurs at lower elevations. Where the surface is frozen, the temperature of the snow/ice surface can vary with changes in the free-air temperature. Because of this, vertical temperature gradients in the boundary layer over frozen surfaces are generally not as large as those found over melting surfaces. Thus, near-surface air temperatures over frozen surfaces have larger climate sensitivities than temperatures over melting surfaces. Consistent with this argument, Denby et al. (2002) showed that the climate sensitivity of near-surface air temperatures over the Greenland ice sheet was close to unity in the dry snow zone (no melt) and that it decreased with elevation to a value of only 0.3 in the lower ablation zone. This explains the observed increase in the standard deviation of glacier near-surface temperatures at higher surface elevations (Figure 3.3d).

The sensible heat flux, and therefore the degree to which the temperature of the atmospheric boundary layer air is modified, is also influenced by the wind speed. Observations (van den Broeke, 1997) and modeling studies (Denby et al., 2002) in Greenland show that down-slope glacier winds increase systematically with increases in free-atmospheric temperatures during the ablation season. This has the effect of increasing the sensible heat flux at lower elevations when warm air is advected into the region. However, the climate sensitivity of the glacier wind is relatively low (0 – 0.2 m $s^{-1}°C^{-1}$), so changes in the near-surface temperature will be primarily governed by changes in the sensible heat flux that result from changes in free-air temperatures (Denby et al., 2002). Glacier winds over the ice masses examined in this study are not as well developed as those observed over the Greenland Ice Sheet, and will have less impact on the sensible heat flux variability than was observed by Denby et al. (2002). Summer mean daily wind speed and direction measurements from three weather stations located on JEG and three stations located on the Devon Island Ice Cap show an increase in the frequency of down slope (katabatic) winds at lower elevations, but neither transect shows an increase in mean wind speed at lower elevations or any consistent relationship between wind speed and 750T.

The relationship between the climate sensitivity of near-surface temperature and elevation means that when warm air is advected into the region, near-surface temperatures over glaciers will not rise uniformly. Because of larger near-surface air temperature sensitivities at higher elevations, near-surface air temperature will increase more at higher elevations than at lower elevations in response to an increase in free-atmospheric temperature. This has the effect of reducing the lapse rate, consistent with the strong negative correlation between 750T and lapse rates (Figure 3.8). Ablation season dependence of surface roughness on elevation (preference for snow at higher elevations and ice at lower elevations) may also play a role in modifying the glacier near-surface lapse rate, but is not investigated in this study.

Implications for the modeling of near-surface temperatures

During the melt season, the variability in measured lapse rates is strongly related to the variability in 750T (Figure 3.8). This relationship was used to develop simple empirical models to predict daily near-surface lapse rates from standardized daily anomalies in 750T (summer means removed and divided through by respective standard deviation). Using least-squares regression analysis, model coefficients were calculated for each of the four glaciers (Table 3.3). Because the regression models are based on standardized anomalies (mean = 0), all model y-intercepts (β) are equal to respective glacier mean summer lapse rates. Where more than one daily lapse rate measurement was available for the same glacier (i.e. Devon and POW), the lapse rate was taken to be the mean of the two estimated values.

Non-ablation season lapse rates are important for the determination of end-of-winter snowpack temperatures. However, the relationship between free-air temperatures and lapse rates breaks down outside the ablation season and there is no strong relationship between non-ablation season lapse rates and either winds or geopotential height that can be used to model them. Thus we chose not to attempt to downscale winter temperatures. If winter temperatures are needed for a mass balance modelling study, we suggest setting the lapse rate for days outside the ablation season to the mean non-ablation season lapse rate (Table 3.3). A lapse rate minimum threshold of 0°C km^{-1} should also be applied to summer values to prevent unrealistically low lapse rates during extreme warm periods. This threshold does not impact the results presented here, but might be relevant if the lapse rate models developed here were applied to years that are anomalously warm compared to the years examined in this study.

Validation of temperature extrapolation methods

Prior to comparing long term differences in surface air temperature estimates made using modeled daily lapse rates with those made using a constant MALR (6.5°C km^{-1}), the modeled daily lapse rate downscaling method was validated over the Devon Island Ice Cap for the summer of 2006. Coefficients for the Devon lapse rate model were first calibrated by excluding 2006 data. Daily lapse rates were then calculated for the 2006 melt season using daily NARR 750T standardized anomalies. Daily observed, modeled, and constant measured mean summer (5.1°C km^{-1}) lapse rates are plotted together with the MALR (6.5°C km^{-1}) in Figure 3.9. There is reasonably good consistency between the patterns of variability in the observed and modeled lapse rates ($r = 0.68$) and their means, which are not statistically different when compared using a two-tailed Student's t-test with the null hypothesis that the means are equal. Both lapse rates are significantly lower than the MALR.

For the validation process, least-squares linear regression was used to reconstruct daily summit elevation temperatures (1880 m) by extrapolating 2006 daily temperature measurements made along the Devon_S transect. This effectively minimizes the local error associated with single station measurements and provides a temporally continuous summit elevation temperature that can be extrapolated to lower elevations using a specified lapse rate.

To assess the errors associated with lapse rate choice when downscaling near-surface temperatures, measured and modeled daily lapse rates, a constant lapse rate equal to the 2006 summer mean (5.1°C km^{-1}), and the MALR were used to extrapolate reconstructed summit temperatures to the elevation of each Devon_S transect temperature sensor with a complete 2006 summer record. Taking the daily mean temperature measured at each station as the true temperature, mean and standard errors in daily mean temperatures were determined for each of the four extrapolation methods (Figure 3.10). Averaged over all stations, temperatures extrapolated using mean daily and summer measured lapse rates have a mean error of zero as they have been derived directly from the 2006 summer station data (Figure 3.10a). Temperatures extrapolated using modeled lapse rates have a small mean cold bias (-0.3°C) while those extrapolated using the MALR have a strong warm bias (0.8°C) that decreases with increasing elevation. Compared with air temperatures extrapolated using a constant lapse rate, modeled daily lapse rates offer a slight improvement in the standard error of the estimated temperatures (Figure 3.10b).

A similar error analysis for estimates of positive degree days (PDD), a quantity that is strongly related to glacier melt (Braithwaite, 1981; Hock, 2003), reveals that only those extrapolation methods that employ variable lapse rates can reproduce the observed annual PDD values (mean error ≈ 0 ±10°C d yr^{-1}; Figure 3.10c, d). Because near-surface lapse rates vary systematically with temperature, employing the constant mean summer lapse rate results in temperature underestimation during relatively cold periods and overestimation during relatively warm periods. Across all stations, this results in an average PDD overestimation of 25°C d yr^{-1}, with a mean error as high as 75°C d yr^{-1} at the lowest station. Using the MALR greatly overestimates total PDDs with mean errors as high as 160°C d yr^{-1}.

Comparison between PDDs downscaled using daily modeled lapse rates and a constant MALR

To illustrate differences in surface air temperature estimates when differing lapse rates are employed, we compared daily mean temperatures downscaled to glacier surfaces (Canada3D DEM: available from Natural

Resources Canada) from NARR 750T using both daily modeled lapse rates and the MALR for the period 1994 – 2006. Results are displayed as total PDDs. As part of the downscaling process, 750T was first adjusted to the temperature at the highest available station on each glacier by subtracting the monthly mean difference between 750T and the station temperatures. The derived station temperature was then downscaled over the entire glacier surface at the 3D DEM resolution (30 seconds ~ 900 × 200 m) using the two different lapse rates.

Using the model coefficients provided in Table 3.3 and daily 750T standardized anomalies, mean annual total PDDs for the period 1994-2006 were estimated for each of the four glaciers (Figure 3.11). Average annual PDD totals for the Agassiz Ice Cap, Devon Island Ice Cap, John Evans Glacier, and Prince of Wales Icefield were 80, 130, 180 and 80°C d yr^{-1} respectively. Averaged over each glacier, the annual total PDDs derived from near-surface temperatures downscaled using daily modeled lapse rates are 20, 160, 130 and 140°C d yr^{-1} less than PDD totals generated using the constant MALR for the Agassiz and Devon Island Ice Caps, John Evans Glacier, and Prince of Wales Icefield respectively. Except for the Agassiz Ice Cap (which has the lowest mean summer temperatures, one of the lowest estimated average annual PDD totals, and the highest near-surface temperature lapse rates), downscaling with the MALR results in a substantial overestimation of near-surface air temperatures and annual PDDs. In the case of the Prince of Wales Icefield, using the MALR produces annual PDD estimates nearly three times those derived using modeled lapse rates. This large difference is due not only to the nearly 2°C km^{-1} difference between the mean of the modeled lapse rate and the MALR but also to: (i) the large vertical distance over which temperatures are downscaled (~1800 m), (ii) the high sensitivity of lapse rates to changes in 750T standardized anomalies (-1.39°C km^{-1}), (iii) low annual PDD totals, and (iv) the large number of days (averaged over all stations: 43 d yr^{-1}) with near-surface temperatures within ±2°C of the freezing point.

To illustrate the spatial differences in PDD estimates, mean annual PDDs estimated from surface air temperatures downscaled using modeled daily lapse rates (a) and the MALR (b) are shown for the Devon Island Ice Cap in Figure

3.12. Because both downscaling methods extrapolate from the same summit point location temperature series, our model comparisons show good agreement between downscaling methods near summit elevations, and larger disagreement at lower elevations. If adjusted sea-level temperatures had been extrapolated instead, the MALR would result in an underestimate of near-surface temperatures and total PDDs relative to those determined using modeled daily lapse rates, as opposed to the overestimates reported here.

Discussion

Consistent with previous studies (Greuell and Böhm, 1998; Steffen and Box, 2001; Lowe and Porter, 2004; Hanna et al., 2005; Mair et al., 2005; Wright et al., 2005; Marshall et al., 2007; Shepherd et al., 2007) we found that ablation season near-surface lapse rates observed over Arctic glacier surfaces are consistently lower than the MALR. Higher near-surface lapse rates of 7 to 9°C km^{-1} have been reported for some valley glaciers (Schuler et al., 2005; Brock et al., 2006). In these cases, however, lapse rates were derived using air temperatures measured at two weather stations, one of which was located at a higher elevation on glacier ice and the other at a lower elevation on exposed ice-free ground. This has the effect of producing artificially high near-surface glacier lapse rates because the temperatures recorded at the lower weather stations are not as strongly affected by the cooling effects of the glacier surface as those at the upper stations. Using these lapse rates to extrapolate near-surface temperatures over large altitudinal distances over ice could result in significant errors.

Near-surface lapse rates over glaciers vary on seasonal and daily time scales, a phenomenon that, although well documented (Braun and Hock, 2004; Steffen et al., 2004; Hanna et al., 2005; Marshall et al., 2007), is rarely accounted for in the downscaling or extrapolation of near-surface air temperatures (Greuell and Böhm, 1998; Gardner and Sharp, 2009). Unlike previous studies, our work has shown that the variability in glacier near-surface lapse rates during summer months is significantly correlated on a regional-scale and that this co-variability appears to be controlled by regional-scale changes in lower-troposphere (750-mbar) temperatures that are associated with the passage of synoptic weather systems (Alt, 1987, Gardner and Sharp, 2007; Marshall et al., 2007). During the ablation season, the sensitivity of glacier near-surface air temperature to changes in free-atmosphere temperature increases with elevation (Denby et al., 2002). This is because surface temperatures are fixed at 0°C over melting glacier surfaces while free-atmosphere temperatures decrease with increasing elevation. As the surface elevation decreases, the free atmosphere becomes warmer relative to the surface, which drives a sensible heat flux that cools the atmospheric boundary layer at a rate that is proportional to the vertical temperature gradient. The less frequent occurrence of melt at higher elevations reinforces this relationship as near-surface temperatures have a higher climate sensitivity over frozen surfaces than over melting surfaces (Denby et al., 2002). To a lesser extent, glacier winds (which are known to increase in strength with the magnitude of the atmospheric boundary layer temperature inversion (van den Broeke, 1997)), also support an increase in sensible heat flux with decreasing elevation (Denby et al., 2002). Therefore, near-surface air temperatures will increase more at higher elevations than at lower elevations in response to an increase in free-atmospheric temperature. This effectively reduces the near-surface lapse rate and results in the negative relationship between 750T and near-surface lapse rates.

This relationship was used successfully to develop glacier specific models for the downscaling of coarse-resolution temperature fields. Through the model validation process it was shown that summer near-surface air temperatures downscaled using modeled daily lapse rates substantially improve estimates of total PDDs over glaciers relative to use of a constant lapse rate equal to either the mean ablation season lapse rate or the moist adiabatic lapse rate (MALR). When lower-troposphere temperatures were downscaled over each of the four glaciers examined in this study for the period from 1994 to 2006, the use of a constant MALR overestimated annual total PDDs by an average of 110 ±64°C d yr^{-1} relative to values estimated using modeled lapse rates. In the case of the Prince of Wales Icefield, annual mean PDDs estimated using a constant MALR were nearly three times greater than those estimated using modeled lapse rates. The chronic overestimation of PDDs when the MALR is employed can result in significant errors in glacier mass balance estimates when the near surface temperature is used to model glacier melt. Following a similar methodology to the one outlined here, Gardner and Sharp (2009) showed that, for the Devon Island Ice Cap over the period 1980-2006, estimates of glacier mass balance made using a degree-day model can be as much as 4 times more negative when summit elevation temperatures are downscaled with the MALR than estimates made using a variable lapse rate modeled from lower-troposphere temperatures and 2.5 times more negative when downscaling is performed using a mean measured summer lapse rate.

Despite good regional correlations and success at downscaling temperatures over individual glaciers, lapse rate model coefficients differ between glaciers (Table 3.3). There is generally good agreement in the model slopes (*m*) (-0.83° to -1.39°C km^{-1}), but mean summer lapse rates (β: *y*-intercept) vary greatly (6.4 to 3.1°C km^{-1}) between glaciers. This suggests that lapse rate models should be calibrated for individual glaciers. If it is necessary to downscale temperatures over Arctic glaciers for which there are insufficient measurements to calibrate a model, we suggest using $m = -1.1°$ and $\beta = 4.9°\text{C km}^{-1}$. These model parameters correspond to the average model slope for the four glacier specific models (Table 3.3) and the mean ablation season lapse rate for the six transects and all previously published Arctic ablation season lapse rates included in Table 3.1. For the four glaciers examined in this study, applying this model to downscale 750T to near-surface temperatures for the period of 1994 to 2006 produces total PDD estimates that are on average 17 ±35°C d yr^{-1} larger than total PDD estimates derived using the site specific lapse rate models. Similar estimates made using a constant lapse rate equal to the mean ablation season lapse rate (4.9°C km^{-1}) produce total PDD estimates that are on average 33 ±46°C d yr^{-1} too large.

In this study, near-surface lapse rates were parameterized using standardized 750-mbar temperature anomalies because temperatures at this pressure level are representative of free-air temperatures for all 4 glaciers examined and provide the highest correlations (not shown) with near-surface lapse rates when compared to surface and other lower- and mid-troposphere temperatures. This being said, model coefficients are relatively insensitive to the temperature used for the parameterization of the lapse rate model. Parameterizations based on NARR surface, 900-mbar, 850-mbar or 500-mbar standardized temperature anomalies, derived in the same way as done for 750T, result in model slopes that are within ~±20% of those reported for the glacier specific lapse rate models based on 750T (Table 3.3) and within ~±15% of the regional model. All alternative models have the same mean lapse rate (intercept) but have slightly lower regression coefficients when averaged across all four glaciers. Standardized surface air temperature anomalies provide the poorest model fit as they are the least representative of free-air temperatures.

Near-surface air temperatures were downscaled from glacier summit temperatures to lower elevations. This approach was used because NARR temperatures (surface or lower-troposphere) show increased correlation with on-glacier temperature measurements as the elevation of the on-glacier measurement increases. This suggests that NARR, and likely other regional/global climate models, does a better job at simulating higher elevation temperatures (which are closer to free-air values) than temperatures at lower elevations (which are more strongly influenced by complex local effects e.g. topography, katabatic winds, higher frequency of surface melt (stronger sensible heat flux), and increased influence from low lying cloud). Our approach to downscaling involves two steps – interpolating the NARR lower-troposphere temperatures to an elevation on the ice cap, and then downscaling from that elevation using a computed lapse rate. Errors arising from the first step are minimized by interpolating measured temperatures to the ice cap summit elevation, while those arising from the lapse rate based downscaling are independent of the choice of height from which to interpolate. Thus total error in surface air temperature estimates should be minimized by the approach that we have adopted.

Conclusion

The negative relationship between near-surface lapse rates and lower-troposphere temperatures suggests that lower lapse rates can be expected under a warming climate. This trend is driven by the increase in free-air temperatures, the migration of the glacier melt zone to higher elevations earlier in the season (larger glacier area with a fixed surface temperature) and, to a lesser extent, by enhanced glacier winds. This means that as ablation season temperatures warm over the Arctic, temperatures near the glacier surface may become less sensitive to temperature changes in the free atmosphere. If this behavior were incorporated into glacier mass balance models, it could reduce projections of Arctic glacier melt and its contributions to sea level in a warmer climate. The opposite would be true if variable lapse rates were used to extrapolate terminus (lower elevation) near-surface temperatures to higher elevations.

References

Alt, B. T. (1987) Developing synoptic analogs for extreme mass balance conditions on Queen Elizabeth Island ice caps. Journal of Climate and Applied Meteorology, 26, 1605-1623.

Arendt, A. and M. Sharp (1999) Energy balance measurements on a Canadian High Arctic glacier and their implications for mass balance modelling. Proceedings of the IUGG Symposium, Birmingham 1999: Interactions Between the Cryosphere, Climate and Greenhouse Gases, M. Tranter, R. Armstrong, E. Brun, G. Jones, M. Sharp, and M. Williams, Eds., 165–172.

Arnold, N. S., W. G. Rees, A. J. Hodson, and J. Kohler (2006) Topographic controls on the surface energy balance of a High Arctic valley glacier. Journal of Geophysical Research-Earth Surface, 111, doi:10.1029/2005JF000426.

Bassford, R. P., M. J. Siegert, and J. A. Dowdeswell (2006) Quantifying the mass balance of ice caps on Severnaya Zemlya, Russian High Arctic. II: Modeling the flow of the Vavilov Ice Cap under the present climate. Arctic Antarctic and Alpine Research, 38, 13-20.

Bassford, R. P., M. J. Siegert, J. A. Dowdeswell, J. Oerlemans, A. F. Glazovsky, et al. (2006) Quantifying the mass balance of ice caps on Severnaya Zemlya, Russian High Arctic. I: Climate and mass balance of tle Vavilov Ice Cap. Arctic Antarctic and Alpine Research, 38, 1-12.

Boon, S., M. Sharp, and P. Nienow (2003) Impact of an extreme melt event on the runoff and hydrology of a High Arctic glacier. Hydrological Processes, 17, 1051-1072.

Bougamont, M. and J. L. Bamber (2005) A surface mass balance model for the Greenland Ice Sheet. Journal of Geophysical Research-Earth Surface, 110, doi:10.1029/2005JF000348.

Box, J. E. and A. Rinke (2003) Evaluation of Greenland Ice Sheet surface climate in the HIRHAM regional climate model using automatic weather station data. Journal of Climate, 16, 1302-1319.

Braithwaite, R. J. (1981) On glacier energy balance, ablation, and air temperature. Journal of Glaciology, 27, 381-391.

Braithwaite, R. J. and S. C. B. Raper (2002) Glaciers and their contribution to sea level change. Physics and Chemistry of the Earth, 27, 1445-1454.

Braun, M. and R. Hock (2004) Spatially distributed surface energy balance and ablation modelling on the ice cap of King George Island (Antarctica). Global and Planetary Change, 42, 45-58.

Brock, B. W., I. C. Willis, and M. J. Sharp (2006) Measurement and parameterization of aerodynamic roughness length variations at Haut Glacier d'Arolla, Switzerland. Journal of Glaciology, 52, 281-297.

Cogley, J. G., W. P. Adams, M. A. Ecclestone, F. Jung-Rothenhäusler, and C. S. L. Ommanney (1996) Mass balance of White Glacier, Axel Heiberg Island, NWT, Canada, 1960-91. Journal of Glaciology, 42, 548-563.

de Woul, M., R. Hock, M. Braun, T. Thorsteinsson, T. Johannesson, et al. (2006) Firn layer impact on glacial runoff: A case study at Hofsjoekull, Iceland. Hydrological Processes, 20, 2171-2185.

Denby, B., W. Greuell, and J. Oerlemans (2002) Simulating the Greenland atmospheric boundary layer - Part II: Energy balance and climate sensitivity. Tellus Series A-Dynamic Meteorology and Oceanography, 54, 529-541.

Fisher, D. A., R. M. Koerner, and N. Reeh (1995) Holocene climatic records from Agassiz Ice Cap, Ellesmere Island, NWT, Canada. Holocene, 5, 19-24.

Flowers, G. E. and G. K. C. Clarke (2002) A multicomponent coupled model of glacier hydrology - 2. Application to Trapridge Glacier, Yukon, Canada. Journal of Geophysical Research-Solid Earth, 107, doi:10.1029/2001JB001124.

Gardner, A. S. and M. Sharp (2007) Influence of the Arctic Circumpolar Vortex on the mass balance of Canadian High Arctic glaciers. Journal of Climate, 20, 4586–4598

Gardner, A. S. and M. J. Sharp (2009) Sensitivity of net mass balance estimates to near-surface temperature lapse rates when employing the degree-day method to estimate glacier melt. Annals of Glaciology, 50, 80-86.

Glover, R. W. (1999) Influence of spatial resolution and treatment of orography on GCM estimates of the surface mass balance of the Greenland Ice Sheet. Journal of Climate, 12, 551-563.

Gregory, J. M. and J. Oerlemans (1998) Simulated future sea-level rise due to glacier melt based on regionally and seasonally resolved temperature changes. Nature, 391, 474-476.

Greuell, W. and R. Böhm (1998) 2 m temperatures along melting mid-latitude glaciers, and implications for the sensitivity of the mass balance to variations in temperature. Journal of Glaciology, 44, 9-20.

Hanna, E., P. Huybrechts, I. Janssens, J. Cappelen, K. Steffen, et al. (2005) Runoff and mass balance of the Greenland Ice Sheet: 1958-2003. Journal of Geophysical Research-Atmospheres, 110, doi:10.1029/2004JD005641.

Hock, R. (2003) Temperature index melt modelling in mountain areas. Journal of Hydrology, 282, 104-115.

Koerner, R. M. (2005) Mass balance of glaciers in the Queen Elizabeth Islands, Nunavut, Canada. Annals of Glaciology, 42, 417-423.

Koerner, R. M. and D. A. Fisher (1990) A record of Holocene summer climate from a Canadian High-Arctic ice core. Nature, 343, 630-631.

Lowe, A. T. and P. R. Porter (2004) Variability of air temperatures lapse rates: Preliminary results from the Karakoram Himalaya, Pakistan. Geophysical Research Abstracts, 6, 04441.

Mair, D., D. Burgess, and M. Sharp (2005) Thirty-seven year mass balance of Devon Ice Cap, Nunavut, Canada, determined by shallow ice coring and melt modeling. Journal of Geophysical Research-Earth Surface, 110, doi:10.1029/2003JF000099.

Marshall, S. J., H. Bjornsson, G. E. Flowers, and G. K. C. Clarke (2004) Simulation of Vatnajokull ice cap dynamics. Journal of Geophysical Research-Earth Surface, 110, doi:10.1029/2004JF000262.

Marshall, S. J., M. J. Sharp, D. O. Burgess, and F. S. Anslow (2007) Surface temperature lapse rate variability on the Prince of Wales Icefield, Ellesmere Island, Canada: Implications for regional-scale downscaling of temperature. International Journal of Climatology, 27, 385-398.

Meier, M. F., M. B. Dyurgerov, U. K. Rick, S. O'Neel, W. T. Pfeffer, et al. (2007) Glaciers dominate eustatic sea-level rise in the 21st century. Science, 317, 1064-1067.

Mesinger, F., G. DiMego, E. Kalnay, K. Mitchell, P. C. Shafran, et al. (2006) North American Regional Reanalysis. Bulletin of the American Meteorological Society, 87, 343-360.

Otto-Bliesner, B. L., S. J. Marsha, J. T. Overpeck, G. H. Miller, and A. X. Hu (2006) Simulating arctic climate warmth and icefield retreat in the Last Interglaciation. Science, 311, 1751-1753.

Otto-Bliesner, B. L., S. J. Marsha, J. T. Overpeck, G. H. Miller, and A. X. Hu (2006) Support material: Simulating arctic climate warmth and icefield retreat in the Last Interglaciation. Science, 311, 1751-1753.

Raper, S. C. B. and R. J. Braithwaite (2006) Low sea level rise projections from mountain glaciers and icecaps under global warming. Nature, 439, 311-313.

Schuler, T. V., R. Hock, M. Jackson, H. Elvehoy, M. Braun, et al. (2005) Distributed mass-balance and climate sensitivity modelling of Engabreen, Norway. Annals of Glaciology, 42, 395-401.

Sharp, M., L. Copland, K. Filbert, D. Burgess, and S. Williamson (2003) Recent changes in the extent and volume of Canadian Arctic glaciers. Glaciological data report GD-32, papers and recommendations: Snow watch 2002 workshop and workshop on assessing global glacier recession, NSIDC, Boulder, USA, 73-75.

Shepherd, A., Z. Du, T. J. Benham, J. A. Dowdeswell, and E. M. Morris (2007) Mass balance of Devon Ice Cap, Canadian Arctic. Annals of Glaciology, 46, 249-254.

Shumway, R. H. and D. S. Stoffer (2006) Time Series Analysis and its Applications: With R Examples. 2nd ed. Springer-Verlag, 575 pp.

Steffen, K. and J. Box (2001) Surface climatology of the Greenland Ice Sheet: Greenland climate network 1995-1999. Journal of Geophysical Research-Atmospheres, 106, 33951-33964.

Steffen, K., S. V. Nghiem, R. Huff, and G. Neumann (2004) The melt anomaly of 2002 on the Greenland Ice Sheet from active and passive microwave satellite observations. Geophysical Research Letters, 31, doi:10.1029/2004GL020444.

Thomas, R. H., W. Abdalati, E. Frederick, W. B. Krabill, S. Manizade, et al. (2003) Investigation of surface melting and dynamic thinning on Jakobshavn Isbrae, Greenland. Journal of Glaciology, 49, 231-239.

van den Broeke, M. R. (1997) Structure and diurnal, variation of the atmospheric boundary layer over a mid-latitude glacier in summer. Boundary-Layer Meteorology, 83, 183-205.

von Storch, H. and F. W. Zwiers (1999) Statistical Analysis in Climate Research. Cambridge Univ. Press, New York, 484.

Wang, L., M. J. Sharp, B. Rivard, S. Marshall, and D. Burgess (2005) Melt season duration on Canadian Arctic ice caps, 2000-2004. Geophysical Research Letters, 32, doi:10.1029/2005GL023962.

Wright, A., J. Wadham, M. Siegert, A. Luckman, and J. Kohler (2005) Modelling the impact of superimposed ice on the mass balance of an Arctic glacier under scenarios of future climate change. Annals of Glaciology, 42, 277-283.

Figures

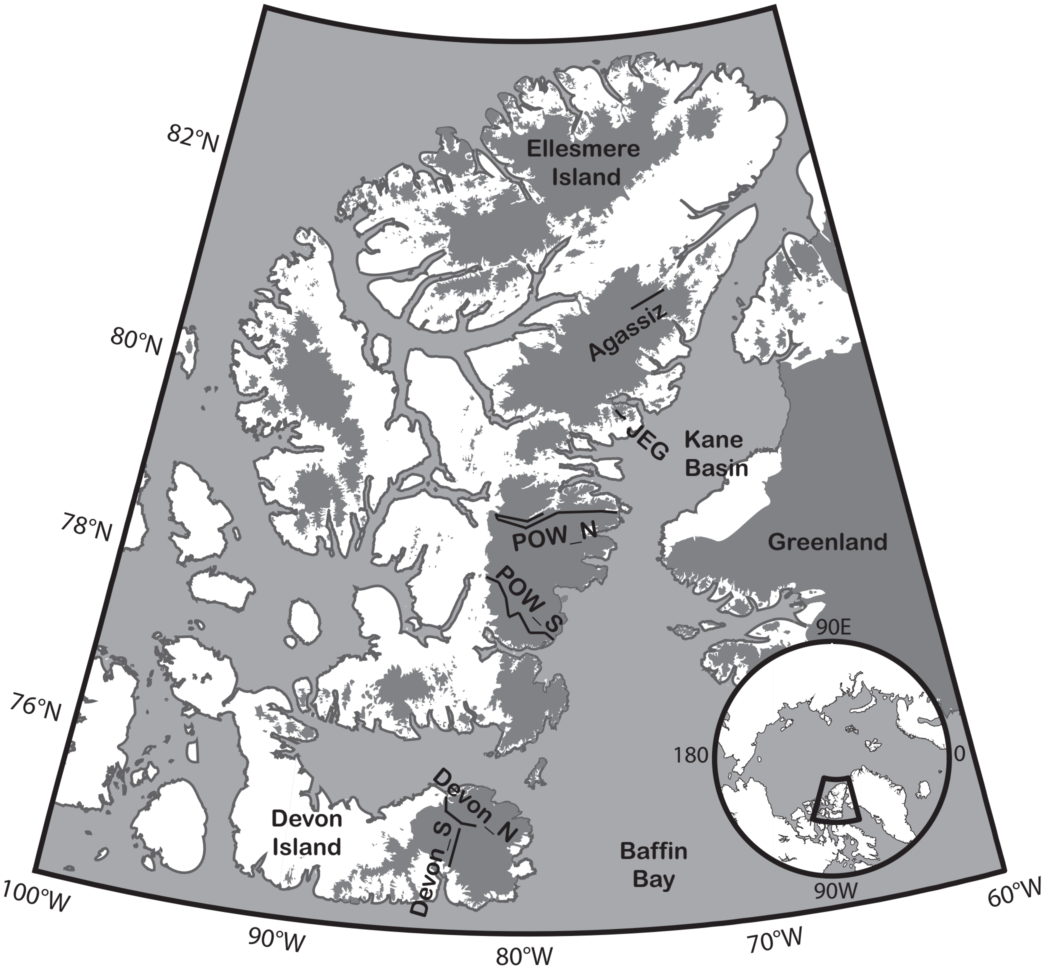

Figure 3.1: Map of Canadian High Arctic with the six temperature-elevation sensor transects shown with heavy black lines.

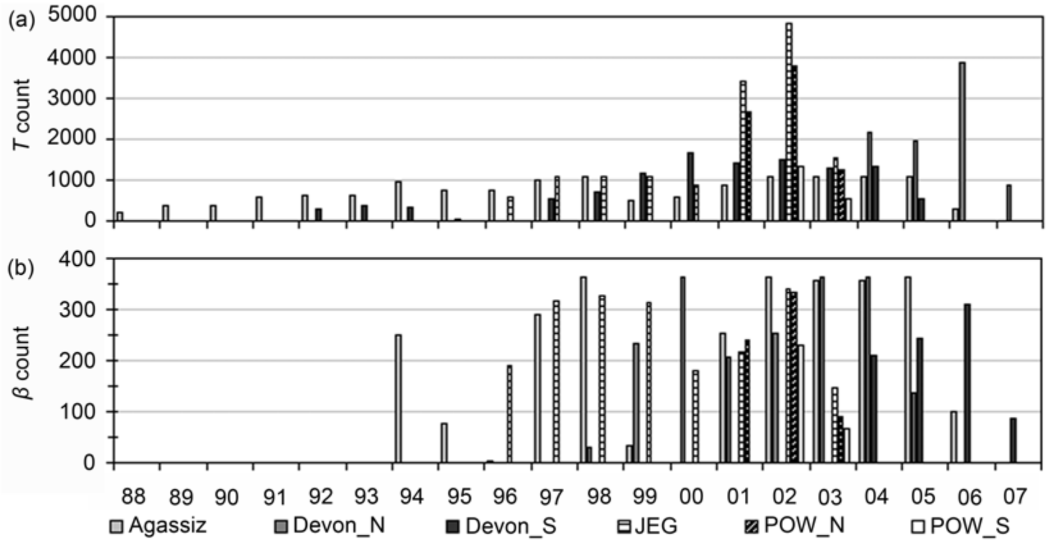

Figure 3.2: Annual number of daily averaged (a) temperature measurements and (b) calculated lapse rates (β) for each of the six near-surface glacier temperature-elevation transects.

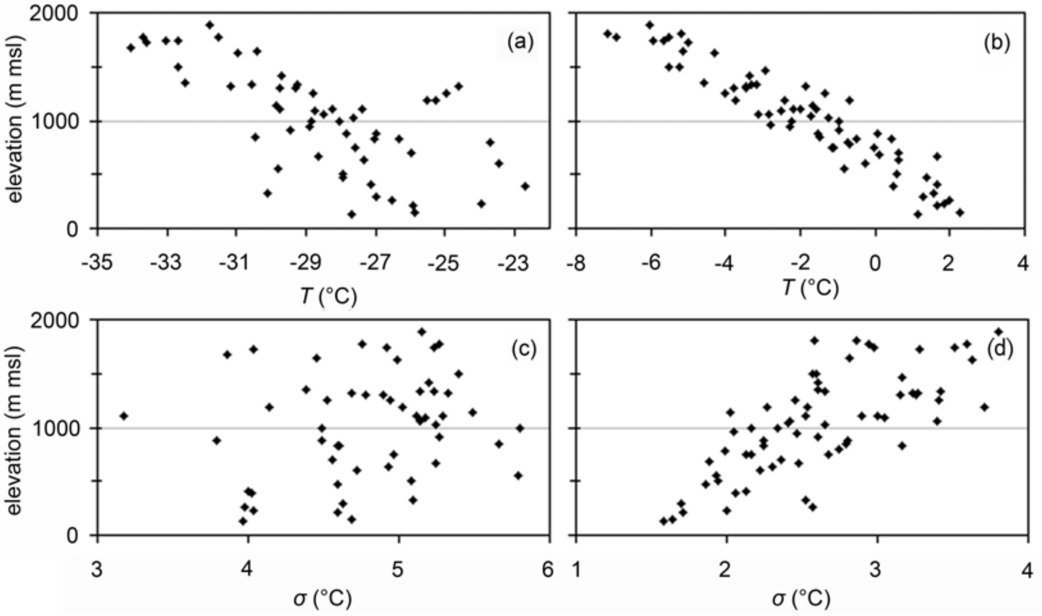

Figure 3.3: Average winter (DJF) (a) and summer (JJA) (b) near-surface temperatures and their standard deviations [DJF: (c), JJA: (d)] plotted with respect to sensor elevation. The relationship between temperature and elevation is much weaker in winter ($r = -0.68$) than in summer ($r = -0.94$) and standard deviations are significantly correlated with elevation in summer ($r = 0.73$) only.

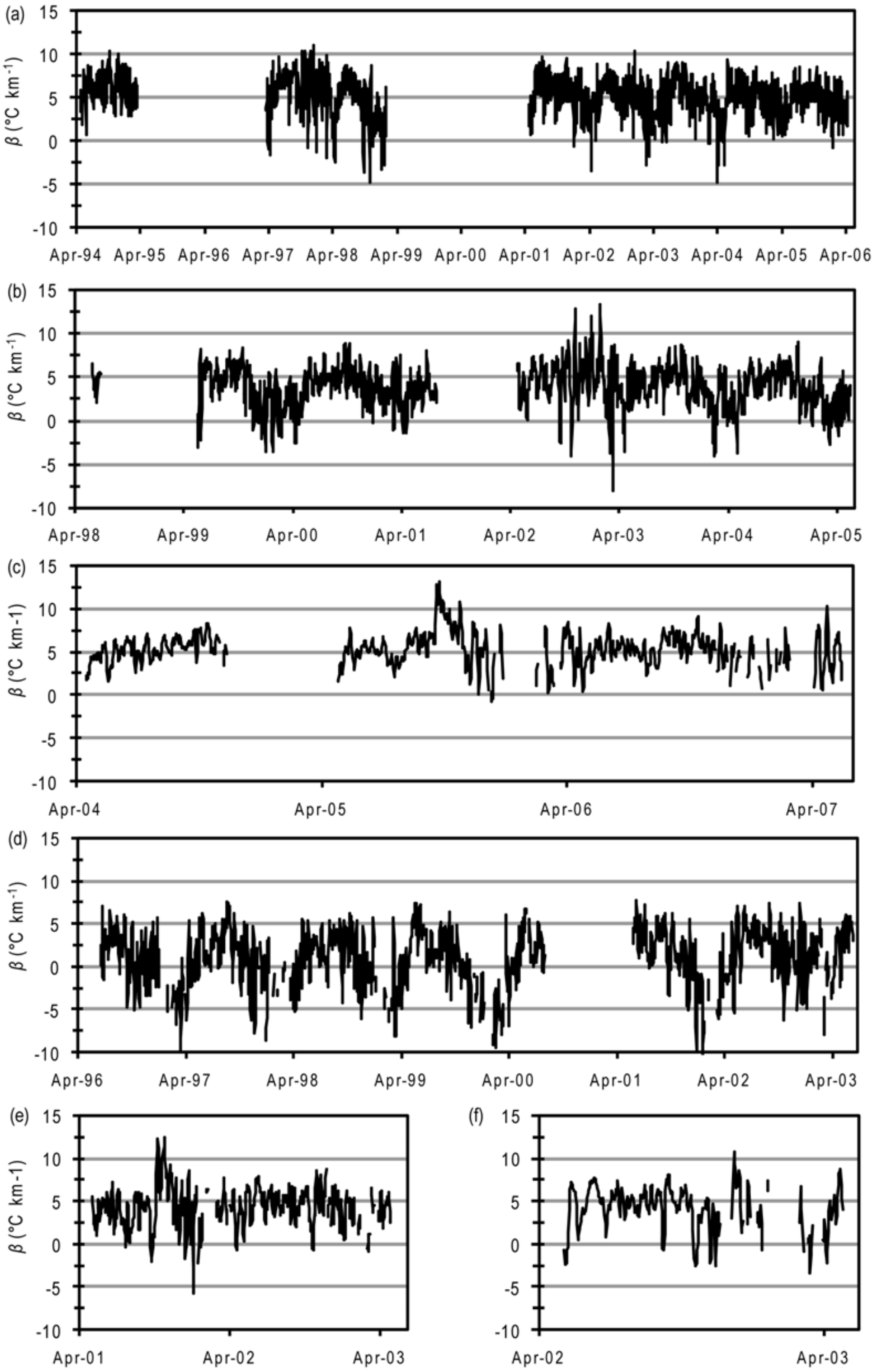

Figure 3.4: 3-day moving average lapse rates (β) for the Agassiz (a), Devon_N (b), Devon_S (c), JEG (d), POW_N (e), and POW_S (f) transects.

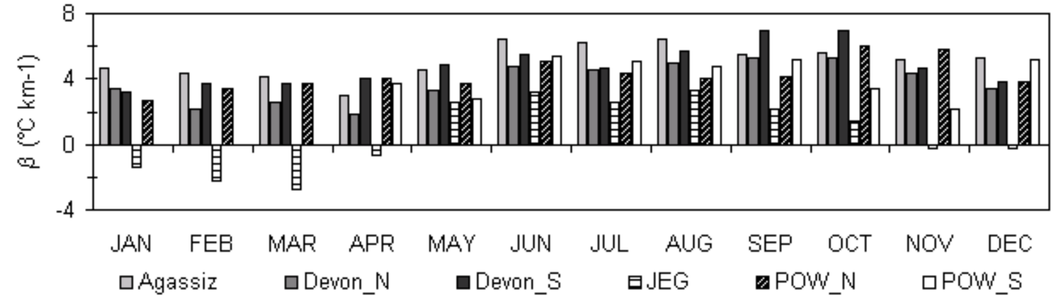

Figure 3.5: Monthly mean lapse rates (β) for all six transects.

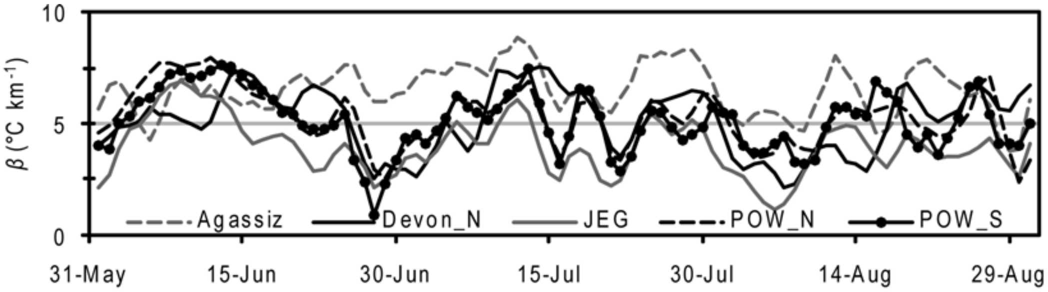

Figure 3.6: All available 2002 summer lapse rates (β).

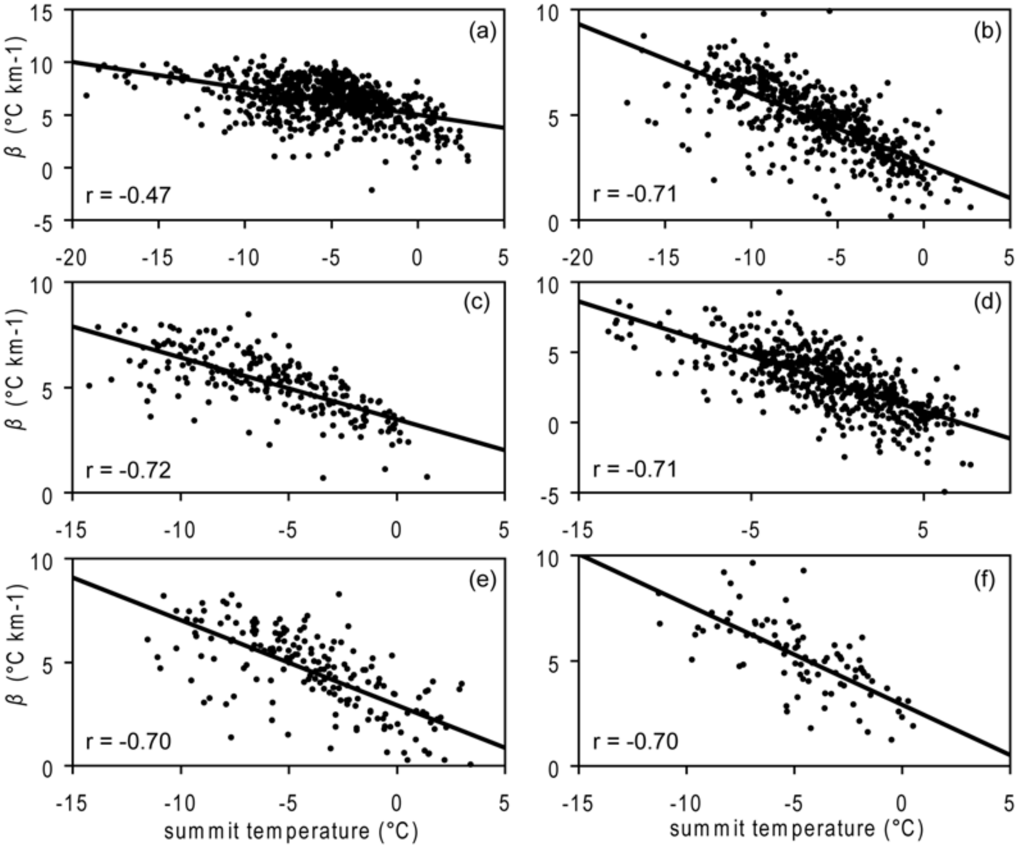

Figure 3.7: Summer daily mean lapse rates (β) plotted against measured summit elevation temperatures for the Agassiz (a), Devon_N (b), Devon_S (c), JEG (d), POW_N (e) and POW_S (f) temperature-elevation transects with heavy black lines showing the linear regression relationship between the two variables.

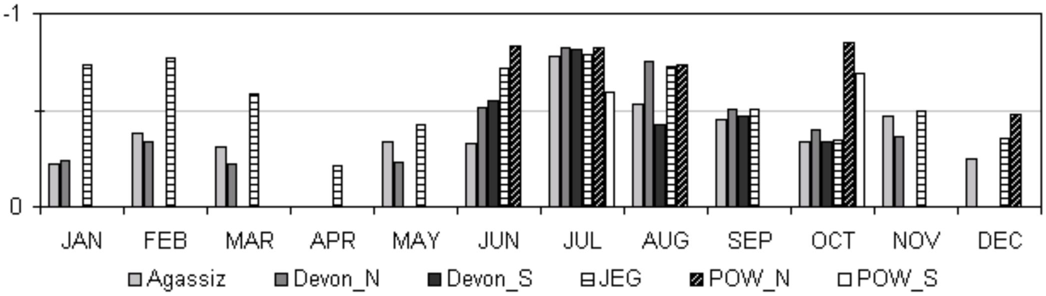

Figure 3.8: Mean monthly correlation coefficients between lapse rates and 750T. Only those values significant at the 0.01 level are shown.

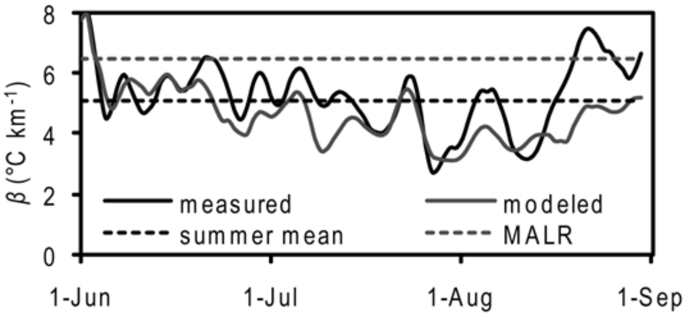

Figure 3.9: 3-day average measured and modeled near-surface lapse rates (β) for Devon Island Ice Cap. The mean measured summer lapse rate (5.1°C km^{-1}) and the MALR (6.5°C km^{-1}) are plotted for comparison. Modeled lapse rates were calculated using 750T and linear regression coefficients calibrated with temperature-elevation data from previous years. Measured and modeled lapse rates are fully independent and are significantly correlated ($r = 0.68$).

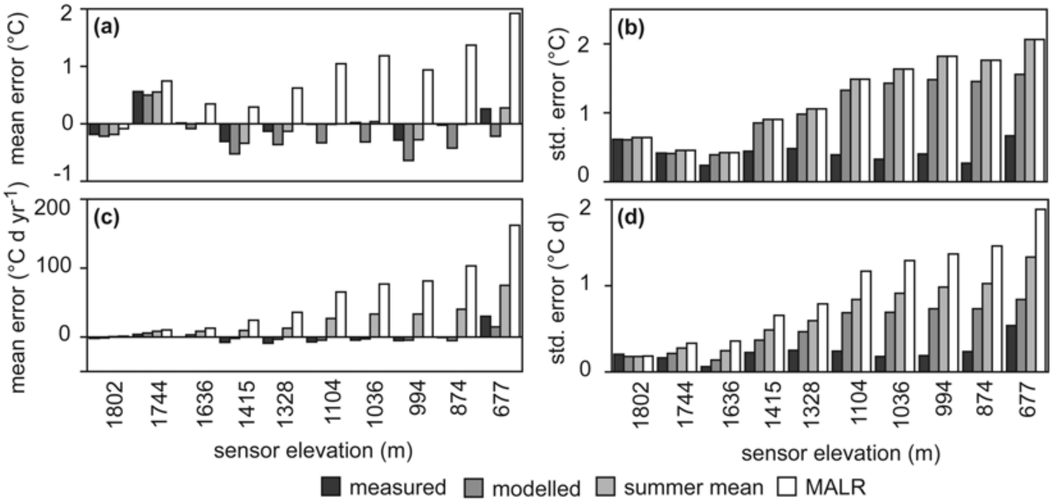

Figure 3.10: Mean and standard error in near-surface temperatures (a and b respectively) and positive degree days (c and d respectively) extrapolated from reconstructed summit elevation temperatures using variable daily mean measured and modeled lapse rates as well as constant lapse rates equal to the 2006 mean summer lapse rate (5.1°C km^{-1}) and MALR (6.5°C km^{-1}).

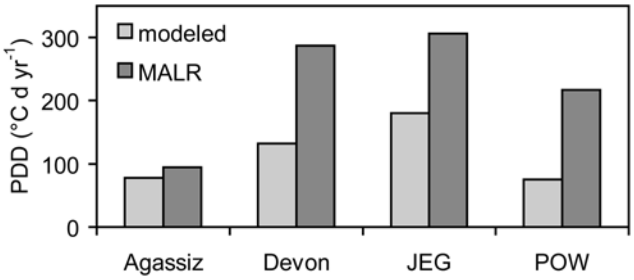

Figure 3.11: 1994-2006 area averaged mean annual positive degree days (PDDs) for the Agassiz Ice Cap, Devon Island Ice Caps, John Evans Glacier (JEG) and the Prince of Wales Icefield (POW) derived from near-surface temperature fields downscaled from NARR 750T using daily modeled and a constant lapse rate set equal to the MALR (6.5°C km^{-1}).

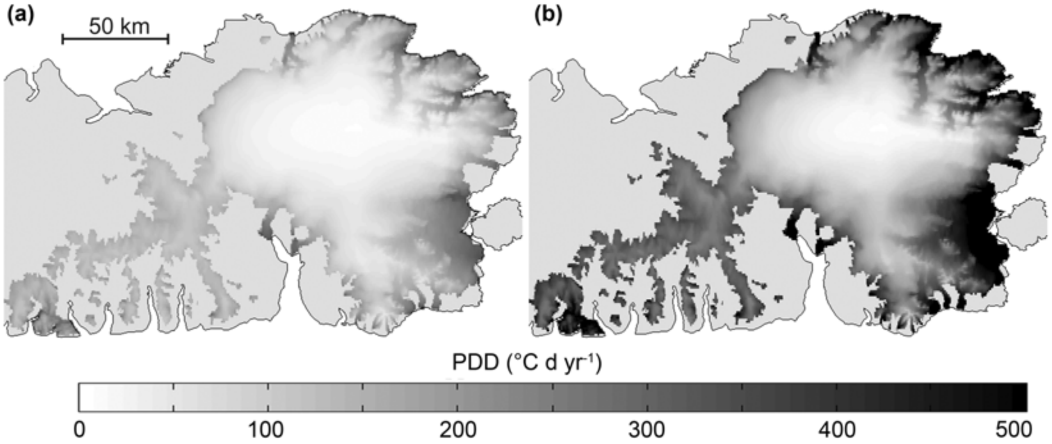

Figure 3.12: 1994-2006 mean annual positive degree days (PDD) for the Devon Island Ice Caps derived from near-surface temperature fields downscaled from NARR 750T using daily modeled lapse rates (a) and a constant lapse rate equal to the MALR (b).

Tables

Table 3.1: Previously reported Arctic glacier and ice-sheet near-surface temperature lapse rates (β)

Location	Study	Months	β (°C km^{-1})
Devon Island Ice Cap, Nunavut, Canada	Shepherd et al. (2007)	not given	4.6
Devon Island Ice Cap, Nunavut, Canada	Mair et al. (2005)	J,J,A	4.8
Greenland Ice Sheet	Steffen and Box (2001)	Annual	7.1
Greenland Ice Sheet	Steffen and Box (2001)	June	4.0
Greenland Ice Sheet	Box and Rinke (2003)	June, July	5.0
Greenland Ice Sheet (>1000 m a.s.l.)	Hanna et al. (2005)	J,J,A	7.9
Greenland Ice Sheet (≤1000 m a.s.l.)	Hanna et al. (2005)	J,J,A	4.3
Nigardsbreen, Norway	Jóhannesson et al. (1995)*	Summer	5.8
Ny-Alesund, Spitsbergen	Wright et al. (2005)	not given	4.0
Prince of Wales Icefield, Nunavut, Canada	Marshall et al. (2007)	J,J,A	4.7
Qamanarssup, West Greenland	Jóhannesson et al. (1995)*	Summer	6.6
Storstrommen, Northeast Greenland	Bøggild et al. (1994)	J,A	4.0
Satujokull, Iceland	Jóhannesson et al.(1995)*	Summer	5.3

* determined through model calibration (not measured)

Table 3.2: Summer (JJA) and winter (DJF) cross-correlations between each of the lapse rate time series of the 6 sensor transects. Significant ($p \leq 0.01$) correlations are shown in bold.

	WINTER				
	Agassiz	Devon_N	Devon_S	JEG	POW_N
Devon_N	0.34				
Devon_S	0.25	-			
JEG	0.35	0.40	-		
POW_N	0.37	0.31	-	0.50	
POW_S	-	-	-	-	-
	SUMMER				
	Agassiz	Devon_N	Devon_S	JEG	POW_N
Devon_N	0.29				
Devon_S	0.37	0.81			
JEG	0.45	0.25	-		
POW_N	0.25	0.47	-	0.83	
POW_S	0.09	0.52	-	0.76	0.89

Table 3.3: Best fit linear regression slope (*m*), mean summer (β: y-intercept) and non-ablation season (β_w) lapse rates and *r* values for modeling summer near-surface lapse rates with 750T standardized anomalies.

	Agassiz	Devon	JEG	POW
m (°C km^{-1})	-0.83	-0.84	-1.31	-1.39
β (°C km^{-1})	6.4	4.9	3.1	4.6
β_w (°C km^{-1})	4.8	4.0	0.4	4.2
r	0.55	0.61	0.75	0.80

CHAPTER 4 : SENSITIVITY OF NET MASS BALANCE ESTIMATES TO NEAR-SURFACE TEMPERATURE LAPSE RATES WHEN EMPLOYING THE DEGREE DAY METHOD TO ESTIMATE GLACIER MELT*

Introduction

The magnitude of glacier ablation depends on the energy balance at the glacier surface. For remote glacier locations, the large amounts of data required to determine this balance are often unavailable. For this reason, degree day models (DDMs) based on the strong observed relationship between glacier melt and near surface air temperatures are often used to estimate surface melt. Most studies that employ DDMs must downscale or interpolate climate model output and/or station observations to the area of interest. For spatially distributed models, temperature fields must be generated to reflect local conditions, which often include complex topography. This is most commonly done through the use of digital elevation models and a constant free air lapse rate‡ (change in temperature with elevation) that is often assumed to be the moist adiabatic lapse rate (-6- -7°C km^{-1}). The problem with this approach is that temperature lapse rates measured over melting glacier surfaces have been found to be systematically less steep than the free air values (Greuell and Böhm 1998; Braun and Hock 2004; Hanna et al. 2005; Marshall et al. 2007). These deviations are mainly the result of temperatures over melting surfaces being fixed at 0°C while free atmospheric temperatures generally increase with decreasing elevation. This can generate strong temperature gradients between the surface and overlying atmosphere that

---

* Previously published material: Gardner, A. S. and M. J. Sharp, 2009: Sensitivity of net mass balance estimates to near-surface temperature lapse rates when employing the degree-day method to estimate glacier melt. *Annals of Glaciology*, **50,** 80-86.

‡ Please note that in this chapter lapse rate is defined as negative when temperatures decrease with elevation. This is opposite to the convention used in Chapter 3. For further detatils see the Introduction of Chapter 3.

increase with decreasing elevation when air temperature is above 0°C. The strong temperature gradients drive a sensible heat flux that cools the near-surface atmosphere at lower elevations and effectively reduces the magnitude of the near-surface temperature lapse rates (Greuell and Böhm 1998).

Recent investigations into near-surface temperature lapse rates in the Canadian High Arctic have found that lapse rates vary on both seasonal and daily time scales (Marshall et al. 2007). Gardner et al. (2009) found that during the summer months (JJA) lapse rates vary systematically with daily mean air temperatures in the lower (i.e. 750 mbar) troposphere. They concluded that much of the observed covariability was due to an increase in the climate sensitivity of screen-level temperatures with increasing elevation (e.g. Denby et al. 2002), where "climate sensitivity" is defined as the change in near-surface temperature relative to a change in the free atmospheric temperature.

In this study we examine the implications of including variable near-surface lapse rates (VLR) in DDM simulations of the surface mass balance of the Devon Island Ice Cap, Nunavut, Canada. Surface mass balance estimates are determined for the years 1980-2006 and are evaluated against 23 years (1980-2003) of surface mass balance measurements from the north-west sector of the ice cap (Koerner 1970). These results are also compared with estimates derived using the assumption that model temperatures can be downscaled using a constant near surface lapse rate equal to either the measured summer (JJA) mean lapse rate (MMLR) or the moist adiabatic lapse rate (MALR).

Site and Data Description

The Devon Island Ice Cap is a large (14,000 km^2: Dowdeswell et al. 2004) dome-shaped ice mass covering much of the eastern part of Devon Island, Nunavut, Canada (Figure 4.1). From 1961 to present, the Geological Survey of Canada (GSC) has made physical measurements of the net surface mass balance b_n along a 40 km long stake network following a path from the glacier summit (1880 m a.s.l.) to the terminus of the Sverdrup outlet glacier in the northwest sector of the ice cap (Figure 4.1: Koerner 2005). Previous estimates of surface mass balance (mm w.e. yr^{-1}) for the main ice cap (excluding the south-west arm) vary greatly between study periods: -76 ± 50 (1961-66: Koerner 1970), -130 ± 60 (1963-2000: Mair et al. 2005) and +28 ± 70 (1996: Shepherd et al. 2007).

Continuous meteorological measurements have been made on the ice cap since 1997, with as many as 7 automatic weather stations and 13 temperature sensors operating along two transects in 2004 (Figure 4.1). Near-surface temperature lapse rates derived from these transects show strong linear relationships ($r = 0.72$) with summit elevation temperatures (Figure 4.2).

Mass Balance Model

Glacier melt

The Degree-Day glacier Mass Balance model (DDM) determines the daily quantity of melt m_t (mm w.e.) as a function of the mean daily air temperature T_t (°C) using a factor of proportionality referred to as the Degree-Day factor DDF (mm d^{-1} °C):

$$\begin{aligned} m_t &= DDF \cdot T_t && T_t \geq 0°C \\ m_t &= 0 && T_t < 0°C \end{aligned}$$

Owing to differences in the surface energy balance characteristics of snow and ice (including albedo, shortwave penetration, thermal conductivity, and surface roughness), separate values are used for snow (DDF_s) and ice (DDF_i). Reported factors vary greatly from study to study depending on local variations in the surface energy balance (albedo, incoming solar radiation, surface roughness, wind speed and air temperature), how melt was determined (measured or modeled), the time period over which the study was conducted, and how air temperatures were determined (daily or hourly mean). Hock (2003) provides a comprehensive review of the temperature-index melt modeling method. For this study we adopt the values DDF_s = 3.3 mm d^{-1} °C and DDF_i = 8.2 mm d^{-1} °C, which are the mean values determined by Braithwaite (1995) at two locations (880 and 790 m a.s.l.)

on the Greenland Ice Sheet. Braithwaite (1995) obtained these values through the use of an energy balance model over a six year period and these agree well with factors determined from stake measurements made at the same locations. These are the same factors used by Shepherd et al. (2007) to model melt over the Devon Island Ice Cap for 1996 and compare with $DDF_s = 4$ and $DDF_i = 6 - 14$ mm d^{-1} °C used by Mair and others (2005) to model melt over the ice cap for the years 1963-2000.

Surface air temperature & downscaling

Daily mean surface air temperatures were downscaled to the entire Ice Cap from summit elevation temperatures using both modeled mean daily and assumed constant lapse rates and a 30 by 30 second digital elevation model (DEM; Canada3D: available from Natural Resources Canada). Daily mean 2 m air temperatures from the North American Regional Reanalysis (NARR: Mesinger et al. 2006) were extracted for the model grid cell centered on the summit of the ice cap and were corrected for a mean summer (JJA) temperature offset of +4°C relative to 8 years (1997-2004) of air temperature measurements from an on-glacier weather station located near the summit of the ice cap. The 4°C offset in the NARR air temperature is partly due to the coarse resolution of the NARR model topography which models the maximum elevation of the Devon Island Ice Cap at an elevation that is 400 m lower than the true summit elevation. After adjusting for the mean difference, measured and modeled summer daily mean summit air temperatures show good agreement (r = 0.86) except for systematic underestimations of maximum and overestimation of minimum summer summit temperatures. To correct for this bias, we add or subtract corrections drawn randomly from a normal distribution with a range of 0 to 2 ºC to all NARR summer temperatures above -4.5 ºC and below -7.5 ºC respectively (Figure 4.3). Surface air temperatures were generated for both ablation season and non-ablation season days in order to determine mean annual and winter temperatures, which are needed for the calculation of maximum meltwater refreeze amounts and which are discussed in Section 3d.

To investigate the impact on mass balance of using different near-surface temperature lapse rates β to downscale air temperatures, three separate surface air temperature fields were generated. The first was generated using a near surface lapse rate equal to the moist adiabatic lapse rate ($\overline{\beta}_{MALR}$ = -6.5°C km^{-1}), the second using mean measured lapse rates ($\overline{\beta}_{MMLR} = -4.9$ °C km^{-1}) for all days during the ablation season (May 15 to Sept 15) and all winter days (Sept 16 to May 14: $\overline{\beta}_{MMLR\_w} = -3.3$ °C km^{-1}), and the third using a modeled variable daily lapse rate β_{VLR} (°C km^{-1}) during the ablation season and $\overline{\beta}_{MMLR\_w}$ in winter. β_{VLR} was estimated using the lapse rate equation developed from over 10 years of screen-level air temperature measurements made over the Devon Island Ice Cap (Gardner et al. 2009):

$$\beta_{VLR} = 0.2T_{750} - 4.9$$

where T_{750} is the three day running mean of the daily anomaly (summer mean removed: not the same as the standardized anomaly used in Chapter 3) in NARR 750-mbar temperature. T_{750} was derived from a six grid cell domain (64 by 86 km) centered over the ice cap. To illustrate the range in variability of β_{VLR}, mean daily summit temperatures are plotted with β_{VLR} for the highest (1986: Figure 4.4a) and lowest (2001: Figure 4.4b) measured mass balance years in the study period. On July 26, 2001, when temperatures peaked at 5°C, $\beta_{VLR} = -3$ °C km^{-1}. On this day, downscaling summit temperatures with β_{VLR} results in sea level temperatures that are 4 and 7°C cooler than temperatures downscaled using $\overline{\beta}_{MMLR}$ and $\overline{\beta}_{MALR}$ respectively. This represents roughly 30-55 mm w.e. less ice melt for this day.

The three model runs forced with mean daily air temperature fields downscaled using β_{VLR}, $\overline{\beta}_{MMLR}$ and $\overline{\beta}_{MALR}$ are referred to throughout the manuscript as the VLR, MMLR and MALR runs respectively.

Precipitation

Daily precipitation was derived from the NARR and corrected for a mean over-precipitation bias of 100 mm w.e. yr^{-1}, which was determined from the comparison of NARR mean annual precipitation at the summit with the net mass balance measured at the same location for the years 1979-2003 (Koerner, personal communication). Taking point values at the center of the NARR grid cells, the bias adjusted coarse resolution (32 by 32 km) NARR daily precipitation fields were linearly interpolated based on horizontal distance to match the resolution of the DEM (~200 by 1000 m). The phase of the daily precipitation P_t (mm w.e.) was determined at each grid cell based on the estimated mean daily grid cell air temperature T_t :

$$\begin{aligned} P_t &= snow & T_t &\leq 0°C \\ P_t &= rain & T_t &> 0°C \end{aligned}$$

Here we have chosen the critical surface temperature for phase change to be 0°C as done by Bassford et al. (2006). Other studies use values as high as 2°C (Oerlemans 1991). Using a critical value of 2°C would increase net mass balance estimates of the Devon Island Ice Cap on average by 40 ± 14 mm w.e. relative to the value used here. At the summit of the ice cap, the standard error of the interpolated precipitation was determined to be 40 mm w.e. yr^{-1}.

Refreezing of meltwater

All liquid water (melt or rain) generated within any grid cell in a given year is assumed to refreeze in that grid cell until the volume of refrozen water $F = F_{\max}$, where $F_{\max}$ is the maximum amount of refreeze that can occur in that cell. Once the liquid water exceeds $F_{\max}$ all additional rain or melt generated in that year is assumed to leave the glacier as runoff. We use the term “refreeze” to refer to the total amount of melt water and rain that refreezes on the glacier during a given mass balance year and can re-melt later in that year and run off; the term “internal accumulation” we refer to as the amount of water that refreezes, does not run off, and remains on the glacier into the following mass balance year. There is no communication between grid cells, so meltwater only affects refreeze and internal accumulation quantities of the cell in which that meltwater is generated.

$F_{\max}$ was determined at each grid cell using the method proposed by Wright et al. (2007). This method determines $F_{\max}$ based on a simplified estimate of the total amount of energy required to change the temperature profile of the upper 10-15 m of the glacier from an end of winter temperature profile to a post-refreezing profile:

$$F_{\max} = \frac{c_i d_i}{2L_f}\left(\left(1-\frac{\pi}{2}\right)\overline{T}_a - \overline{T}_w\right),$$

where c_i is the specific heat capacity of ice at 0°C (2097 J kg^{-1} $°C^{-1}$), d_i is the maximum depth to which the annual temperature cycle penetrates, L_f is the latent heat of fusion for water (333.5 kJ kg^{-1}), $\overline{T}_a$ is the mean annual air temperature and $\overline{T}_w$ is the mean winter temperature (here taken as the mean temperature outside of the ablation season). On the Devon Island Ice Cap the annual temperature cycle penetrates to a depth of about 10-15 m. Using this value for d_i results in $F_{\max}$ values which are much too large (> 1000 mm w.e.). We instead set d_i = 1 m, which gives mean $F_{\max}$ values at the summit of the ice cap that are ~60% (130 mm) of the annual snow fall, the value often used for the upper threshold for meltwater refreezing on the Greenland Ice Sheet (Reeh 1991) and is supported by field measurements made near the equilibrium line altitude of the Greenland Ice Sheet (Braithwaite et al. 1994.

Results

Mass balance components

Average (1980-2006) annual snowfall, rainfall, refreeze and melt generated from the VLR model run are shown in Figure 4.5. Similar spatial patterns in the four mass balance components are seen in all three model runs, but magnitudes vary as all components are dependent on the surface air temperature. Averaged over the entire ice cap (including the south-west arm) for the period of study, mean annual snowfall (156 ± 11 mm w.e. yr^{-1}), rainfall (43 ± 10 mm w.e. yr^{-1}), and melt water refreeze (90 ± 7 mm w.e. yr^{-1}) vary little between model runs with slightly lower (20 mm w.e. yr^{-1}) snowfall and slightly higher (20 mm w.e. yr^{-1}) rainfall amounts for the MALR run due to a higher frequency of above zero temperatures in that run. There are, however, large differences in melt quantities, with mean annual estimates of 730 ± 250, 960 ± 350 and 1840 ± 440 mm w.e. yr^{-1} for the VLR, MMLR, and MALR model runs respectively. Because the model runs differ greatly in both the melt amounts and the altitudes at which melt occurs, the three model runs produce very different internal accumulation distributions (Figure 4.6) and thicknesses (8, 12 and 3 mm w.e. yr^{-1} for the VLR, MMLR, MALR model runs respectively).

Comparison with measurements (north-west sector)

Modeled point-location net mass balance (b_n) estimates were extracted from the model output along the GSC's north-west transect and compared with their respective stake measurements at 100 m elevation intervals from 150 to 1750 m a.s.l. for the period of available data (1980-2003: Koerner, personal communication) (Figure 4.7). All model estimates are similar and agree well with the stake measurements at elevations above 1450 m, but they diverge with decreasing elevation as estimated melt quantities increase. At 150 m, all model runs significantly overestimate melt quantities relative to measurements by as much as 2800 mm for the MALR run. Overall, the VLR and MMLR model runs significantly outperform the MALR model run, with 23 year mean ± standard errors averaged across all elevations of +25 ± 260 and -140 ± 340 mm w.e. yr^{-1} respectively compared with -880 ± 920 mm w.e. yr^{-1} for the MALR. Using the sector boundaries outlined by Koerner (1970), cumulative annual net mass balances B_n for the three model runs were estimated for the north-west sector of the ice cap and are shown together with an estimate derived from stake measurements in Figure 4.8. B_n estimates vary greatly between model runs with mean ± standard errors of 9 ± 120, -113 ± 150, -577 ± 223 mm w.e. yr^{-1} for the VLR, MMLR and MALR runs relative to measured values. The VLR model run produces B_n that are close to measured values with a 1980-2003 cumulative difference of only 0.2 m w.e..

Net mass balance of the Devon Island Ice Cap

Annual B_n values were calculated for the main portion of the ice cap (south-west arm excluded: 12100 km^2: Dowdeswell et al. 2004) and are shown in Figure 4.9. The MALR model run produces mass balance values that are, on average, four times more negative than values determined from the VLR model run and ~2.5 times more negative than values determined from the MMLR run. During more positive mass balance years (e.g. 1986 and 2004) there is good agreement between the VLR and MMLR model runs, but the differences are larger during more negative years (e.g. 2001 and 2006). This is because the total annual Positive Degree Days (PDDs) for the two runs are most similar when lower tropospheric temperatures are seasonally low and most different when temperatures are seasonally warm (i.e. during high melt years). For the whole ice cap (south-west arm included), B_n values are 24–41% more negative than for the main ice cap because the entire south-west arm lies below 900 m elevation and often lies completely within the ablation zone (Figure 4.10).

Using perturbed historical accumulation measurements and a constant lapse rate of -4.6°C km^{-1} (mean 2001 lapse rate measure over the Devon Island Ice Cap) to extrapolate sea level temperature data from the International Arctic Buoy Program over different sectors of the ice cap, Shepherd et al. (2007) estimated the 1996 net mass balance for the main ice cap to be 28 mm w.e.. This value is 42, 140 and 730 mm w.e. larger than 1996 estimates computed using the VLR, MMLR, and MALR respectively. We attribute most of the difference between the VLR model run and this estimate to the slightly higher (12 mm w.e.) snow fall estimate used by Shepherd et al., which results in both greater net accumulation at higher elevations and less melt at lower elevations since snow has a lower *DDF* than ice does. The differences between Shepherd et al. (2007)'s estimate and the estimates generated using MMLR and MALR are attributed to an overestimation of surface air temperatures in the MMLR and MALR simulations (much higher melt and slightly lower snowfall) due to the use of overly steep lapse rates.

Based on our comparisons with independent model estimates of the 1996 net glacier mass balance for the main Ice Cap and 24 years of measurements made along the north-west stake transect, we take the VLR model results as the best estimate of surface mass balance. We estimate that the main ice cap lost an average of 333 ± 120 mm w.e. yr^{-1} over the period 1980-2006, where the error associated with this estimate is taken to be the standard error of the modeled, relative to measured, net mass balance for the north-west sector.

Discussion and Conclusion

The use of different air temperature lapse rates in the downscaling of surface air temperatures over the Devon Island Ice Cap has a large impact on estimates of glacier mass balance produced with the Degree-Day method. Using the moist adiabatic lapse rate (-6.5°C km^{-1}) to downscale summit elevation temperatures over the ice cap generates net mass balance estimates that are four times more negative than estimates made using a modeled variable lapse rate and ~2.5 times more negative than estimates made using a mean measured summer lapse rate. Over the main ice cap, mass balance estimates made from temperature fields downscaled with the mean measured summer lapse rate overestimate melt by ~180 ± 100 mm w.e yr^{-1} on average relative to estimates made from temperature fields downscaled using a modeled variable lapse rate. During more positive mass balance years, model results generated using the two methods agree closely, but they diverge by as much as 550 mm w.e. yr^{-1} during the most negative mass balance years.

When the DDM is forced with surface air temperature fields downscaled using modeled variable daily lapse rates it produces estimates of net surface mass balance that agree well (9 ± 120 mm) with the 23 years of measurements made along the north-west transect. This same method produces a 1996 estimate of net mass balance for the main ice cap that agrees closely (42 mm w.e. higher) with the previous 1996 estimate made by Shepherd et al. (2007). This being said, forcing the model with these surface air temperatures only results in a 25% (80 mm w.e. yr^{-1}) improvement in the standard error of point location net mass balance estimates relative to estimates made from temperature fields downscaled using a mean summer lapse rate. Like all DDMs, model results are highly sensitive to the choice of degree day factors. While we have chosen not to tune the model using the degree day factors, similar model root-mean-square errors as those achieved when the DDM is forced with a variable lapse rate could be achieved by adjusting the degree-day factor for ice to ~4.5-6.5 and ~2-3.5 mm w.e. d^{-1} when employing the mean measured summer lapse rate and the moist adiabatic lapse rate respectively. Comparing against previously published values (Hock 2003), a degree-day factor < 5.0 mm w.e. d^{-1} for ice is unrealistic. Therefore, the model can only be tuned with a realistic degree-day factor for ice to produce comparable results to those achieved using the untuned variable lapse rate when the mean measured summer lapse rate is employed. The root-mean-square error across all three models is relatively insensitive to the choice in degree day-factor for snow (2-6 mm w.e. d^{-1}).

Our best estimate of the net surface mass balance of the main ice cap over the years 1980-2006 is -330 ± 120 mm w.e. yr^{-1}, which is much lower than previous estimates of -76 ± 50 (1961-66; Koerner 1970), -130 ± 60 (1963-2000; Mair et al. 2005) and 28 ± 70 mm w.e. yr^{-1} (1996; Shepherd et al. 2007). The more negative model estimate can be attributed to differences in mean summer conditions between the different time periods for which estimates have been derived and to large uncertainties in estimated accumulation rates due to large spatial variations in snowfall (Koerner 1966) which are poorly reproduced by the 32 by 32 km resolution NARR output. In particular, total accumulation amounts measured by Koerner (1966) were found to be 2 to 6 times larger for the south-east (largest sector) than for the north-west sector of the ice cap and are nearly equivalent in the regridded NARR model output.

In conclusion, DDMs are highly sensitive to the choice of lapse rate when models are forced with downscaled temperature fields. For the DDM used in this study, use of a variable daily lapse rate estimated from lower tropospheric (750-mbar) temperatures to downscale surface air temperatures gives significantly better mass balance estimates than a constant lapse equal to either the summer mean or the moist adiabatic lapse rate.

References

Bassford, R. P., M. J. Siegert, J. A. Dowdeswell, J. Oerlemans, A. F. Glazovsky, and Y. Y. Macheret, 2006: Quantifying the mass balance of ice caps on Severnaya Zemlya, Russian High Arctic. I: Climate and mass balance of the Vavilov Ice Cap. *Arctic Antarctic and Alpine Research*, **38,** 1-12.

Braithwaite, R. J., 1995: Positive degree-day factors for ablation on the Greenland Ice-Sheet studied by energy-balance modeling. *Journal of Glaciology*, **41,** 153-160.

Braithwaite, R. J., M. Laternser, and W. T. Pfeffer, 1994: Variations of near-surface firn density in the lower accumulation area of the Greenland Ice Sheet, Pakitsoq, West Greenland. *Journal of Glaciology*, **40,** 477-485.

Braun, M. and R. Hock, 2004: Spatially distributed surface energy balance and ablation modelling on the ice cap of King George Island (Antarctica). *Global and Planetary Change*, **42,** 45-58.

Denby, B., W. Greuell, and J. Oerlemans, 2002: Simulating the Greenland atmospheric boundary layer - Part II: Energy balance and climate sensitivity. *Tellus Series a-Dynamic Meteorology and Oceanography*, **54,** 529-541.

Dowdeswell, J. A., T. J. Benham, M. R. Gorman, D. Burgess, and M. J. Sharp, 2004: Form and flow of the Devon Island Ice Cap, Canadian Arctic. *Journal of Geophysical Research-Earth Surface*, **109,** -.

Gardner, A. S., M. J. Sharp, R. M. Koerner, C. Labine, S. Boon, S. J. Marshall, D. O. Burgess, and D. Lewis, 2009: Near-surface temperature lapse rates over Arctic glaciers and their implications for temperature downscaling. *Journal of Climate*, **22,** 4281-4298.

Greuell, W. and R. Böhm, 1998: 2 m temperatures along melting mid-latitude glaciers, and implications for the sensitivity of the mass balance to variations in temperature. *Journal of Glaciology*, **44,** 9-20.

Hanna, E., P. Huybrechts, I. Janssens, J. Cappelen, K. Steffen, and A. Stephens, 2005: Runoff and mass balance of the Greenland Ice Sheet: 1958-2003.

Journal of Geophysical Research-Atmospheres, **110,** doi:10.1029/2004JD005641.

Hock, R., 2003: Temperature index melt modelling in mountain areas. *Journal of Hydrology*, **282,** 104-115.

Koerner, R. M., 1966: Accumulation on the Devon Island Ice Cap, Northwest Territories, Canada. *Journal of Glaciology*, **6,** 383-92.

______, 1970: The mass balance of the Devon Island ice cap, Northwest Territories, Canada, 1961-66. *Journal of Glaciology*, **9,** 325-336.

______, 2005: Mass balance of glaciers in the Queen Elizabeth Islands, Nunavut, Canada. *Annals of Glaciology*, **42,** 417-423.

Mair, D., D. Burgess, and M. Sharp, 2005: Thirty-seven year mass balance of Devon Ice Cap, Nunavut, Canada, determined by shallow ice coring and melt modeling. *Journal of Geophysical Research-Earth Surface*, **110,** doi:10.1029/2003JF000099.

Marshall, S. J., M. J. Sharp, D. O. Burgess, and F. S. Anslow, 2007: Surface temperature lapse rate variability on the Prince of Wales Icefield, Ellesmere Island, Canada: Implications for regional-scale downscaling of temperature. *International Journal of Climatology*, **27,** 385-398.

Mesinger, F., G. DiMego, E. Kalnay, K. Mitchell, P. C. Shafran, W. Ebisuzaki, D. Jovic, J. Woollen, et al., 2006: North American Regional Reanalysis. *Bulletin of the American Meteorological Society*, **87,** 343-360.

Oerlemans, J., 1991: A model for the surface balance of ice masses: Part I: Alpine glaciers. *Zeitschrift für Gletscherkunde und Glazialgeologie*, **27,** 63–83.

Reeh, N., 1991: Parameterization of melt rate and surface temperature on the Greenland Ice Sheet. *Polarforschung*, **59,** 113–128.

Shepherd, A., Z. Du, T. J. Benham, J. A. Dowdeswell, and E. M. Morris, 2007: Mass balance of Devon Ice Cap, Canadian Arctic. *Annals of Glaciology*, **46,** 249-254.

Wright, A. P., J. L. Wadham, M. J. Siegert, A. Luckman, J. Kohler, and A. M. Nuttall, 2007: Modeling the refreezing of meltwater as superimposed ice on a high Arctic glacier: A comparison of approaches. *Journal of Geophysical Research-Earth Surface*, **112,** doi:10.1029/2007JF000818.

Figures

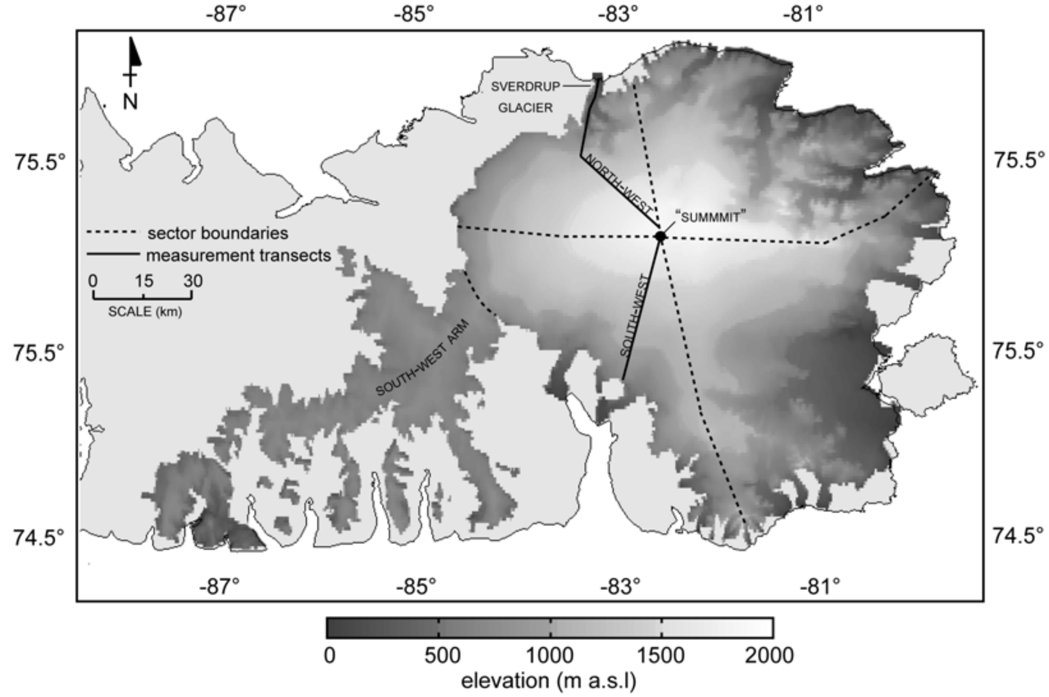

Figure 4.1: The Devon Island Ice Cap shown with region boundaries and transects along which field measurements have been taken.

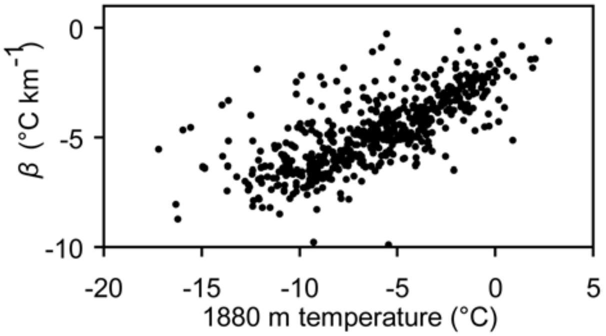

Figure 4.2: 1998-2004 average daily summer JJA lapse rates β for the north-west transects plotted against respective mean daily summit air temperatures.

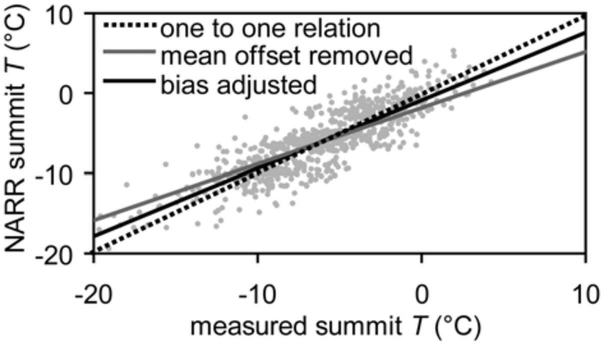

Figure 4.3: NARR bias adjusted summer (JJA) daily summit air temperatures (*T*) plotted against measured summit temperatures (1880 m). The two solid lines show the linear regression relationship between NARR and measured summit temperatures before (grey: $r = 0.86$) and after (black: $r = 0.85$) the temperatures have been adjusted for overly warm temperatures on relatively cool days and overly cool temperatures on relatively warm days.

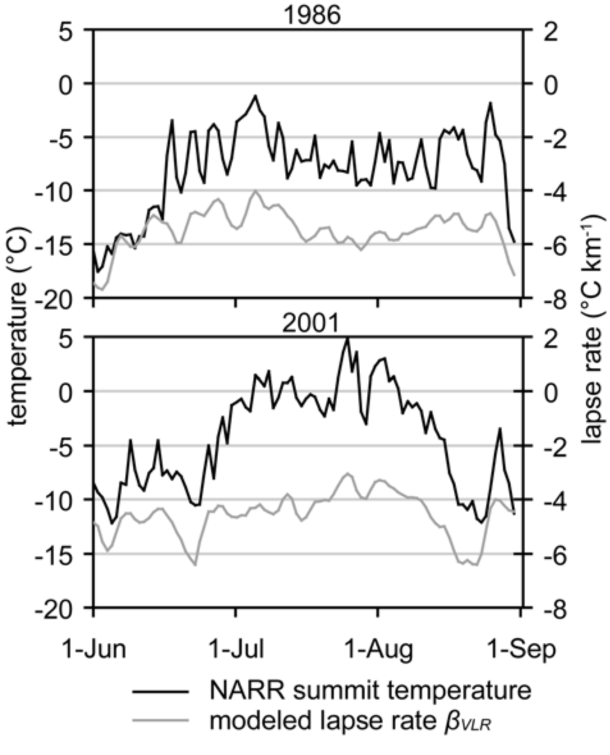

Figure 4.4: NARR summit elevation temperatures plotted with variable modeled daily lapse rates β_{VLR} for representatively cold (a) and warm (b) years. Modeled lapse rates are less steep when temperatures are anomalously warm and steeper when temperatures are anomalously cold.

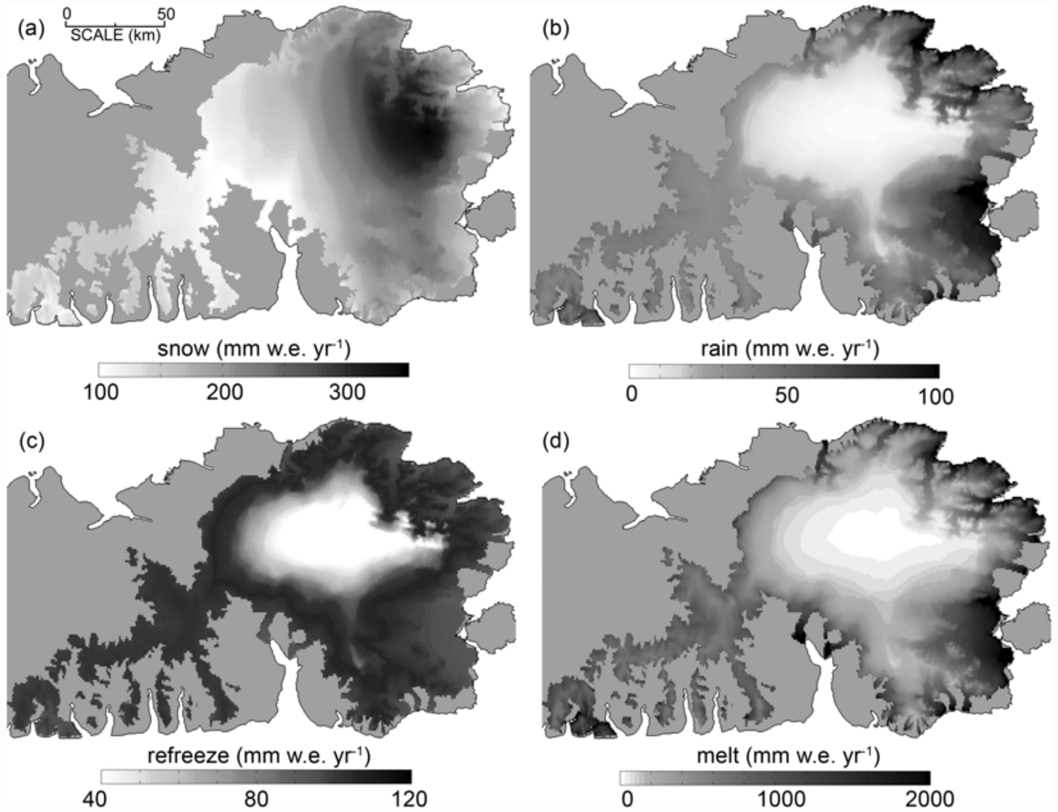

Figure 4.5 Mean annual snow (a), rain (b), melt water refreeze (c) and melt (d) for the Devon Ice Cap averaged over the years 1980-2006. Values determined from the VLR model run, see text for details.

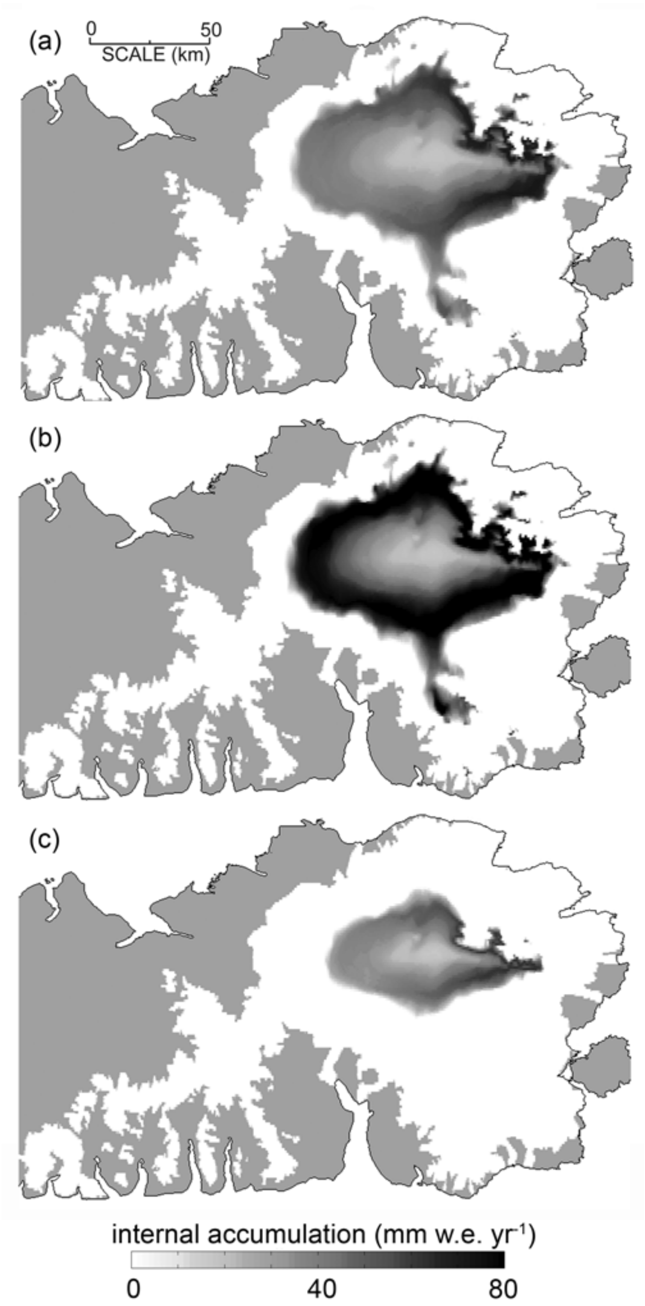

Figure 4.6: Annual mean internal accumulation formation estimated from the VLR (a), MMLR (b), and MALR (c) model runs.

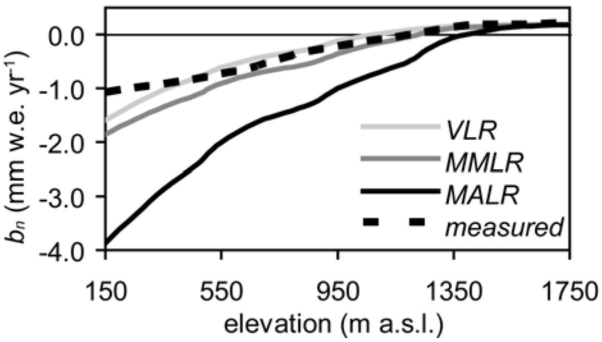

Figure 4.7: Average (1980-2001) annual point-location net mass balance (b_n) model estimates extracted at 100 m intervals along the north-west transect shown with respective mass balance stake network measurements.

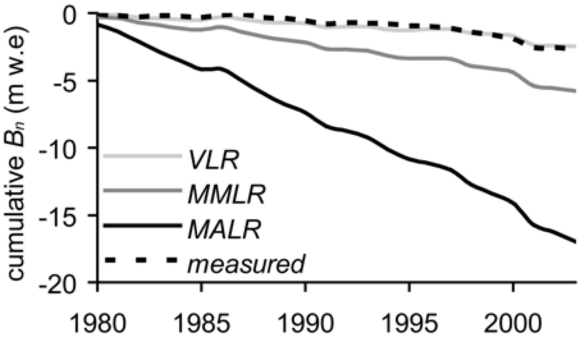

Figure 4.8: Modeled cumulative surface mass balance for the north-west sector of the Devon Island Ice Cap plotted with estimates derived from measurements.

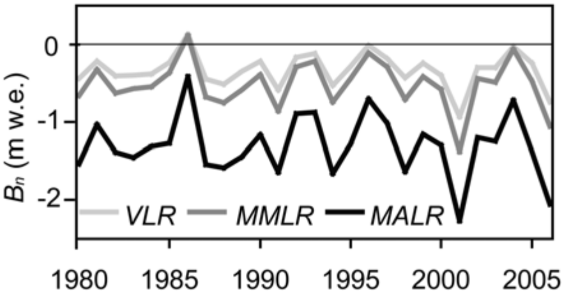

Figure 4.9: Net mass balance B_n for the main Devon Ice Cap (south-west arm excluded) for all three model runs.

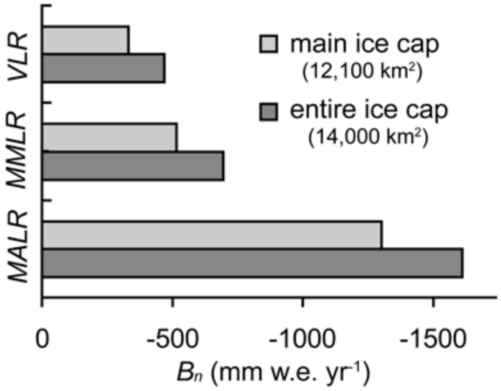

Figure 4.10: Model run estimates of mean annual net mass balance B_n for the main (excluding south-west arm) and whole Devon Island Ice Cap.

CHAPTER 5 : A REVIEW OF SNOW AND ICE ALBEDO AND THE DEVELOPMENT OF A NEW PHYSICALLY BASED BROADBAND ALBEDO PARAMETERIZATION*

Introduction

Under most atmospheric conditions, absorption of shortwave radiation is the largest energy source for melting snow and ice (Male and Granger 1981; Paterson 2000). The amount of shortwave radiation absorbed is dependent on both the incident radiation and the surface albedo, both of which are highly variable in space and time (Stroeve et al. 1997; Klok et al. 2003). It is therefore critical to incorporate the temporal variability of snow and ice albedo in numerical models of the surface energy balance. This can be done either by specifying the albedo on the basis of continuous observations, or by computing it with a physical model or empirically based parameterization. Direct surface measurements of snow and ice albedo are sparse, discontinuous, and often contain large errors if the instrumentation is not continuously monitored (van den Broeke et al. 2004). Satellite derived albedos offer more spatially continuous datasets but are limited to times of clear sky overpasses and may contain significant sources of error, especially over complex terrain (Stroeve et al. 1997; Klok et al. 2003). For these reasons, numerical models of snow and ice albedo are often incorporated into surface energy balance and climate models.

Sophisticated radiation transfer models do a very good job at producing snow and ice albedo estimates that closely match observations (Grenfell et al. 1994; Aoki et al. 2000; Painter et al. 2007), but they are computationally demanding and require many inputs that are not routinely available. Thus, surface energy balance and climate models typically employ computationally simple albedo parameterizations that require minimal inputs in one or more spectral

---

* Previously published material: Gardner, A. S. and M. J. Sharp, 2010: A review of snow and ice albedo and the development of a new physically based broadband albedo parameterization. *Journal of Geophysical Research*, **115,** F01009, doi:10.1029/2009JF001444.

bands. Despite the strong influence of snow and ice albedo on climate, surface energy balance, and melt rates (Cess et al. 1991; Klok and Oerlemans 2004), there is little consensus on which albedo parameterizations are most appropriate for large scale modeling.

The theoretical determinants of the spectral albedo (a_λ) of snow and ice are well established (Warren and Wiscombe 1980; Wiscombe and Warren 1980; Warren 1982; Mullen and Warren 1988; Askebjer et al. 1997; Warren et al. 2002; Ackermann et al. 2006; Warren and Brandt 2008), but there have been few attempts to derive theoretically based, computationally simple broadband (spectrally integrated) albedo parameterizations that are easily implemented in surface energy balance and climate models (Marshall 1989; Brun et al. 1992). Thus, most such models employ empirical parameterizations (e.g. Brock et al. 2000; Pedersen and Winther 2005) developed from observational datasets. These parameterizations are practical in that they provide a reasonable approximation of snow and ice albedo whilst requiring minimal knowledge of the physical characteristics of the snow, ice and atmosphere. They are, however, somewhat limited in their applicability as they are based on statistical fits to albedo measurements that are representative of the characteristics of the snow, ice, and atmosphere for specific time periods and locations.

This motivates the development of a computationally simple, theoretically-based parameterization for snow and ice albedo that can accurately reproduce theoretical broadband albedos under a wide range of snow, ice, and atmospheric conditions. The parameterization is derived by fitting equations to broadband albedo estimates generated with a 16-stream plane-parallel, discrete ordinates radiative transfer model of snow and ice that is coupled to a similar model of the atmosphere. This allows for simulation of multiple reflections between the surface and atmosphere that alter the spectral distribution of solar irradiance. This is important because the modification of the spectral distribution of solar irradiance by clouds can significantly modify the broadband albedo of snow and ice (Grenfell and Maykut 1977; Carroll and Fitch 1981; Grenfell and Perovich 1984; Jonsell et al. 2003; Grenfell and Perovich 2008).

As the goal of this study is to develop a theoretically-based parameterization, we start by reviewing what is known about radiative transfer in snow and ice and discussing the physical determinants governing its albedo. This review supplements earlier works (Grenfell and Maykut 1977; Warren and Wiscombe 1980; Wiscombe and Warren 1980; Grenfell et al. 1981; Warren 1982; Mullen and Warren 1988; Grenfell et al. 1994) with a more complete discussion of the solar irradiance and the inclusion of many new references.

Radiative transfer modeling of snow, ice and the atmosphere

Single scattering

To define the optical characteristics of snow and ice we must first determine the single scattering properties of its individual constituents (e.g. ice grains, air bubbles and impurities). As long as the individual particles are sufficiently separate that they act as independent scatterers, the scattering properties of a single element can be characterized by three dimensionless optical characteristics; the absorption efficiency Q_{abs}, scattering efficiency Q_{sca} and asymmetry factor g (mean cosine of the scattering angle). For ease of calculation, particles are often assumed to scatter as spheres. If one knows the radius r of the sphere and the complex refractive index of the medium ($m_\lambda = n_\lambda + ik_\lambda$), then the dimensionless optical characteristics can be determined using Mie theory (Bohren and Huffman 1998).

In models which resolve the absorption and scattering of shortwave radiation by snow and ice, the optical geometries of ice grains can be well described by a collection of spheres that have the same specific surface area ($\hat{S}$:surface area per unit mass) as the snow grains they describe (Hansen and Travis 1974; Warren 1982; Grenfell et al. 1994). The area-weighted mean radius of these optically equivalent grains is referred to as the effective radius, r_e, and is directly related to specific surface area as:

$$r_e = \frac{3}{\rho_i \hat{S}}$$

where ρ_i is the density of ice (910 kg m^{-3}). Optical properties relevant to energy balance studies modeled using this definition of effective radius agree well with observations and exact model results for a wide range of grain sizes, wavelengths, optical depths and several different crystal shapes (Grenfell and Warren 1999; Neshyba et al. 2003; Grenfell et al. 2005). This allows for significant model simplification as complex snow grain geometries and orientations can be modeled as optically equivalent spheres.

In a pure ice sample that contains only air bubbles, all photon absorption events will occur within the ice and all scattering will occur at the ice-bubble boundaries. Scattering efficiencies and asymmetry parameters are, therefore, purely a function of the effective bubble size and can be calculated using Mie theory in the same way as for snow grains but with the absorption set equal to zero ($m_\lambda = n_\lambda$, Mullen and Warren 1988). Absorption, on the other hand, is solely a function of the amount of ice per unit volume and the absorbance of ice.

In this analysis Q_{abs}, Q_{sca} and g for spherical ice grains, air bubbles and light-absorbing carbon were determined for 381 wavelengths from 0.2-4.0 μm using the algorithms developed by Mätzler (2002). The complex refractive index for ice was taken from Warren and Brandt (2008). The optical properties of light—absorbing carbon, commonly referred to as "black carbon" or "soot", were determined using the spectrally uniform complex index of refraction suggested by Bond and Bergstrom (2006: $m = 1.95 + 0.79i$). There are large uncertainties regarding the absorptive properties of light-absorbing carbon in snow and ice. This is because typical ratios of internally (particles residing within the ice grains) to externally (carbon particles located outside the ice grains) mixed carbon particles in terrestrial snow are not well known, and carbon particle densities, sizes, and refractive indices vary with production sources and residence times in the atmosphere (Bond and Bergstrom 2006). For this study, carbon particles are assumed to be externally mixed, have an effective radius of 0.1 μm (Horvath 1993; Hansen and Nazarenko 2004), and a mean density of 1.8 g cm^{-3} (Bond and Bergstrom 2006). The mass absorption coefficient (MAC) of the prescribed light absorbing carbon varies across the solar spectrum. The MAC decreases rapidly from its largest value of 6.8 m^{2} g^{-1} at 0.4 μm to 3.6 m^{2} g^{-1} at 1 μm and continues to decreases to 0.7 m^{2} g^{-1} at 4 μm.

For the sake of computational simplicity, we chose not to model dust within snow and ice. This choice is justifiable because: i) carbon is ~200 times more absorbent by mass than crustal dust at visible wavelengths, ii) dust has been shown to have significantly less impact on snow albedo than light-absorbing carbon in remote areas devoid of local dust sources, and iii) the effects on broadband albedo of dust loading in snow and ice should be similar to those of optically equivalent concentrations of light-absorbing carbon (Warren and Wiscombe 1980; Warren 1984; Warren and Clarke 1990). Effects of other snow impurities, such as organic debris and algae, that can reduce albedo (Grenfell 1991) are not examined in this study.

All Mie calculations (for ice, soot and air) were averaged over 1000 effective radii with a Gaussian distribution ($u = r_e, \sigma = 0.15r_e$). This minimized ripple effects in calculated Mie values which are not observed in natural media that contain a range of particle sizes (Bohren and Huffman 1998, p. 296-305).

Multiple scattering

The single scattering properties were used to determine snow and ice layer optical depths and single scattering albedos. Scattering phase functions were determined using the Henyey–Greenstein approximation, which has been shown to work well for the calculation of snow spectral albedo (Aoki et al. 2000). These derived variables were then used to define varying snow and ice conditions in a 16-stream plane-parallel discrete ordinates radiative transfer model (DISORT: Stamnes et al. 1988).

For accurate estimation of spectrally integrated broadband albedo, it was necessary to couple the snow and ice model with the Santa Barbara DISORT

Atmospheric Radiative Transfer model (SBDART 2.4: Ricchiazzi et al. 1998). This allowed for simulation of multiple reflections between the surface and the atmosphere that can have a significant influence on the amount, spectral distribution, and fractions of direct and diffuse solar radiation incident at the surface, all of which influence the broadband albedo of snow (Grenfell and Maykut 1977; Carroll and Fitch 1981; Grenfell and Perovich 1984; Grenfell and Perovich 2008). Within SBDART, we assigned a sub-Arctic summer standard atmospheric profile (McClatchey et al. 1972) and a surface elevation of sea level. A schematic diagram illustrating key components of the coupled snow and ice – atmosphere model is provided in Figure 5.1.

Where radiative transfer modeling was performed for cloudy conditions, clouds were assigned the characteristics of Arctic summertime lower-level stratus clouds. This is the predominant cloud type in the Arctic during summer months (when snow and ice melt occurs) and accounts for approximately 85-90% of all summer cloud cover observed over the Arctic Ocean (Serreze and Barry 2005, p. 48). All clouds were assumed to be evenly distributed between the elevations of 1000 to 2500 m a.s.l. and were assigned an effective droplet radius of 7.5 μm, a value typical of Arctic summertime low-level stratus (Curry et al. 1996). The uncertainty in the effective radius of cloud droplets introduces little error in estimates of cloud radiative properties (Fitzpatrick et al. 2004).

Determinants of the albedo of snow and ice

The amount of energy absorbed by a medium at a specific wavelength is dependent on its spectral albedo α_λ which is defined as the ratio of the reflected $F_\lambda^{\uparrow}$ to incident $F_\lambda^{\downarrow}$ flux as referenced to a specified surface. The spectral albedo of snow and ice is dependent on the optical properties of its individual constituents, the location and frequency of scattering and absorption events, and radiation's angle of incidence. When shortwave radiative fluxes are discussed in terms of one or more spectral bands, the amount of energy absorbed by the medium is determined using spectrally integrated albedos (α). Spectrally integrated albedos are dependent on both the spectral albedo of the medium and the spectral distribution of the incident irradiance within each spectral band. To understand the determinants of the spectrally integrated albedo of snow and ice, it is therefore necessary to examine the determinants of their spectral albedos and the characteristics of the solar spectral irradiance.

Location and frequency of scattering and absorption events

The spectral albedo α_λ of snow and ice varies greatly across the solar spectrum (Figure 5.2), with $\alpha_\lambda \approx 1$ in the near-ultraviolet and visible regions ($\lambda = 0.3 – 0.7$ μm), and $\alpha_\lambda < 0.4$ in the short-wave infrared region ($\lambda = 1.5$ — 5.0 μm). Outside the near-ultraviolet wavelengths, the albedo of pure snow is highly sensitive to effective grain size (Figure 5.2). This can best be understood by considering radiative transfer as a statistical process. Neglecting internal scattering (scattering not at snow grain boundaries) and absorption by interstitial air, a photon has a chance of being scattered at the air-ice interface and a chance of being absorbed while passing through the ice. An increase in the average radius of the ice grains effectively increases the length of the photon's travel path through the ice and decreases the number of opportunities for the photon to scatter out of the snowpack. This increases the probability of the photon being absorbed and, in more general terms, reduces the surface albedo.

Small amounts of strongly absorbent impurities, such as soot, dust and volcanic ash, lower snow albedo in the spectral region where absorption by ice is weakest ($\lambda < 0.9$ μm). Light-absorbing impurities within the snow cause the greatest reductions in albedo for coarse-grained snow (Warren and Wiscombe 1980). This is illustrated in Figure 5.3, which shows the reduction in the spectral albedo when light-absorbing carbon is added to three semi-infinite snow layers with different effective radii. At shorter wavelengths, photons generally experience more scattering events and travel a greater distance through the snow, increasing the probability that the photon will encounter an absorbing impurity and not re-emerge from the snowpack. As the effective grain radius of snow increases, the average travel path lengthens, further increasing the probability of encountering an absorbing impurity. For wavelengths $\lambda > 0.9$ μm, snow spectral albedo is negligibly influenced by the presence of impurities because the already strong absorption by ice at these wavelengths leads to short travel paths. Impurities located within ice grains (internal mixture) are 1.4 times as absorbent as impurities located in air (externally mixed) and can receive proportionally more incident radiation if located near the center of an ice sphere due to the refraction of light towards the sphere's center (Chýlek et al. 1983; Bohren 1986). Impurities concentrated near the surface have a greater impact on albedo (Aoki et al. 2000; Grenfell et al. 2002). Because impurities reduce the albedo at wavelengths where most of the downward solar flux occurs they can have a large impact on the overall energy budget of snow and ice.

Shortwave-infrared albedo is also influenced by the incident radiation's angle of incidence (Figure 5.4). At higher angles of incidence a photon will, on average, travel a path that is closer to the surface increasing its probability of experiencing a scattering event that will send it out of the snowpack (see Figure 11 of Warren 1982). In addition, the effective radius of snow grains is often smaller near the surface (where snow is younger), so photons entering at high angles of incidence will experience more scattering events near the surface. This is enhanced by significant asymmetric scattering in the near-infra red region of $\lambda > 1.4$ μm that strongly favors scattering in the forward direction (Aoki et al. 2000; Hudson et al. 2006). Near-ultraviolet and visible wavelengths experience such low absorption that nearly all radiation at these wavelengths eventually scatters back out of the snow regardless of angle of incidence.

Surface roughness can also affect surface albedo by decreasing the angle of incidence relative to a flat surface. This is because more incident radiation is absorbed by the slope facing the sun (lower angle of incidence) than by the slope facing away from it (higher angle of incidence). While surface roughness features can decrease the broadband albedo by as much as 4% at high solar zenith angles (Carroll and Fitch 1981), this has little impact on the overall surface energy balance because little solar energy is received at high solar zenith angles and the fraction of direct incident radiation decreases with increasing solar zenith angle (Warren et al. 1998).

Snow is relatively absorptive in the near-infrared, so, nearly all shortwave radiation with $\lambda > 1.5$ μm is absorbed within the top few millimeters of the snow. At near-ultraviolet and visible wavelengths scattering is high and absorption low, which allows radiation at these wavelengths to penetrate the snow to several meters depth. Where a homogeneous pure fine grained snow layer overlies pure white ice with a broadband albedo of 0.4, surface albedo in the near-ultraviolet and visible parts of the spectrum is minimally affected by the presence of the underlying white ice when snow depths are > 10 mm w.e., and completely unaffected in the short-wave infrared (Figure 5.5a). For very coarse snow, in which photons generally experience less scattering events per unit depth, the surface albedo is minimally affected when snow depths > 100 mm w.e. (Figure 5.5b). Of course, the albedo of snow overlying a surface that is strongly absorbent in the near-ultraviolet and visible parts of the spectrum (soil, dirt, or snow with a high impurity content) will be much more sensitive to snow depth than that of snow overlying white ice.

The optical properties of pure ice and water are very similar in the shortwave part of the spectrum, so the presence of liquid water in snow has little direct effect on snow albedo (Dozier 1989; Green et al. 2002). Liquid water does however indirectly alter snow albedo by enhancing grain growth and infilling voids between snow grains, increasing the effective grain size (Colbeck 1979). The infilling of voids is the reason that saturated snow tends to have a lower albedo than unsaturated wet snow. Liquid water ponding on the surface of glaciers (Zuo and Oerlemans 1996; Greuell 2000; Greuell et al. 2002) and sea ice (Grenfell and Maykut 1977; Perovich et al. 2002; Light et al. 2008) can greatly reduce shortwave albedo and increase transmittance by reducing the number of air-ice boundaries that exist near the ice surface. Both observational (Hanson 1965) and modeling studies (Lüthje et al. 2006) have shown that ice ablation rates below surface ponds can be 2-3 times greater than on nearby bare ice.

The albedo of glacier, lake and sea ice is influenced by the same factors as snow with the exception that, instead of being governed by grain size, the frequency and location of scattering events (air-ice interfaces) are determined by the size and distribution of air bubbles, brine inclusions and cracks within the ice (Mullen and Warren 1988; Askebjer et al. 1997; Warren et al. 2002; Light et al. 2003; Ackermann et al. 2006). In a pure ice sample that contains only air bubbles, all photon absorption events will occur within the ice and all scattering will occur at the ice-bubble boundaries (neglecting any surface reflection and internal scattering and absorption by interstitial air). Any size distribution of air bubbles within ice can be described by an effective bubble radius (r'_e) and an effective bubble concentration (n'_e) that has the same specific surface area ($\hat{S}$: $\mathrm{cm}^2\ \mathrm{g}^{-1}$) as the population of bubbles of the ice that it describes (Mullen and Warren 1988; Warren et al. 2002). An increase in either r'_e or n'_e causes an increase in the surface albedo at wavelengths $\lambda > 0.5$ µm. The influence of r'_e on the surface albedo of ice with a constant n'_e is shown in Figure 5.6.

Solar irradiance

As shortwave radiation passes through the earth's atmosphere it is modified by scattering, absorption and reflection. The shortwave irradiance incident upon the earth's surface is dependent on the solar zenith angle (Figure 5.7a), cloud optical thickness (Figure 5.7b), cloud amount, the transmission properties of the atmosphere, aerosol extinction, surface-atmosphere reflections (Figure 5.7c), surface slope and aspect, and shadowing and reflection by terrain.

As discussed in the previous section, the spectral albedo of snow and ice is dependent on the angle of incidence of the incoming radiation (Figure 5.4). The effective angle of incidence is dependent on both the fraction of diffuse radiation and the zenith angle of the direct solar beam (Figure 5.7d). Under clear sky conditions the total incident radiation decreases as the solar zenith angle increases, and the fraction of diffuse irradiance increases due to an increase in the atmospheric path length (Figure 5.8a). Since diffuse radiation has an effective solar zenith angle of ~50° over a horizontal snow surface (Warren 1982), the increase in spectral albedo of snow as the solar zenith angle increases is somewhat mitigated by an increase in the fraction of diffuse radiation.

The fraction of diffuse radiation also increases with the presence of clouds (Figure 5.8b). Thus, when the sun is low on the horizon, cloud cover decreases the effective solar zenith angle relative to clear sky conditions. Clouds, which have similar optical properties to snow, also alter the spectral distribution of incident shortwave radiation by preferentially absorbing near-IR wavelengths and returning near-UV and visible wavelengths that have been reflected from the surface (Figure 5.7b). This increases the fraction of total shortwave radiation incident at shorter wavelengths where the albedo of snow is highest (Figure 5.2). In general, the net effect of the spectral shift toward shorter wavelengths and the increase in the diffuse faction of incident radiation results in an increase in the spectrally integrated albedo of snow and ice (Grenfell and Maykut 1977; Carroll and Fitch 1981; Grenfell and Perovich 1984; Jonsell et al. 2003; Grenfell and Perovich 2008).

Broadband albedo of snow and ice and its parameterization

Theoretically determined broadband albedos

Broadband albedos determined with the snow and ice – atmosphere radiative transfer model show a nearly perfect logarithmic relationship with specific surface area ($\hat{S}$:Figure 5.9a) and an inverse logarithmic relationship with effective grain size (r_e: not shown). As shown by Bohren (1983), albedos are virtually identical for equivalent $\hat{S}$ regardless of whether the medium is modeled as an assemblage of independent spherical ice grains or as an assemblage of spherical air bubbles encased in ice. This is very important and highlights the significance of using $\hat{S}$ instead of r_e and r_e' for the modeling snow and ice albedo.

The modification of broadband albedo due to the presence of light-absorbing carbon is dependent on its concentration and the $\hat{S}$ of the snow/ice in which it resides (Figure 5.9a). Snow/ice with higher $\hat{S}$ is less impacted by carbon loading because solar radiation, on average, has a shorter travel path within the medium.

Under clear sky conditions, broadband albedos of both pure and contaminated snow/ice increase non-linearly with an increase in the solar zenith angle (θ_Z:Figure 5.9b). Snow/ice contaminated with light-absorbing carbon is most sensitive to changes in solar zenith angle. This is because the migration of scattering events towards the surface as the solar zenith angle increases results in less absorption in the ultraviolet and visible wavelengths by the carbon particles.

The broadband albedo of snow/ice also increases with cloud optical thickness (τ) due to a spectral shift in the incident solar irradiance towards shorter wavelengths (Figure 5.9c). For solar zenith angles < ~50°, this increase is enhanced by an increase in the diffuse fraction of incident solar irradiance. The varying sensitivities of broadband albedo to increasing cloud cover for different snow and ice types can be understood by examining the respective spectral albedos. Pure fresh snow with large $\hat{S}$ has a very high spectral albedo for wavelengths where the majority of incident solar radiation occurs (Figure 5.2). This means that a shift in the solar spectrum towards shorter wavelengths will have little impact on the broadband albedo. The opposite is true for pure snow/ice with low $\hat{S}$. In this case there is a much larger contrast between spectral albedos for wavelengths $> 0.8\mu$m and $< 0.8\mu$m (Figure 5.6), leading to larger sensitivities to cloud induced changes in the spectral distribution of the solar irradiance. Snow and ice containing significant amounts of light-absorbing carbon have much lower albedos at shorter wavelengths (Figure 5.3). This has two effects; it limits the number of surface-cloud reflections and, in turn, reduces the spectral shift in incident solar radiation, and it reduces the contrast in the spectral albedo across the wavelengths at which most of the solar radiation is incident (flattens the spectral albedo curve).

Previously proposed parameterizations

Where albedo values are unknown they are often modeled from one or more surrogate variables that include grain size, snow age, snow depth, snow density, melt rate, and air temperature (e.g. Brun et al. 1992; Brock et al. 2000; Greuell 2000; Klok et al. 2003). Some of the more sophisticated empirical models also account for albedo modification due to impurity loading, solar zenith angle, and cloud cover (e.g. Dickinson et al. 1986; Marshall 1989; Greuell and Konzelmann 1994). Here we introduce a selection of published albedo parameterizations that will be compared to the snow and ice – atmosphere radiative transfer model (hereafter: full model). As there are too many parameterizations to evaluate all of them, we focus the comparison on parameterizations that have been employed in the well established snow and ice metamorphism models CROCUS (Brun et al. 1989), SOMARS (Greuell and Konzelmann 1994), and SNTHERM (Jordan 1991).

Time-dependent albedo parameterizations such as those that are either linear (Winther 1993), exponential (Ranzi and Rossi 1991; Klok and Oerlemans 2004), and/or logarithmic (Brock et al. 2000) functions of the temperature sum since the previous snowfall event or exponential time decay models (Klok and Oerlemans 2004; Bougamont and Bamber 2005), use simple proxies to model the time evolution of snow albedo. This is largely the result of snow grain metamorphism, and likely includes effects of time dependent changes in grain size, impurity loading, snow depth and atmospheric conditions. The theoretical broadband albedos and solar incidence calculated using the snow and ice – atmosphere radiative transfer model are specific to the physical characteristics of the snow and ice, the evolution of which must be simulated with a snow grain metamorphism model (Marbouty 1980; Brun 1989; Legagneux et al. 2004; Flanner and Zender 2006; Taillandier et al. 2007). To avoid the need to perform such simulations, we restrict our analysis to the comparison of full model results with those albedo parameterizations that are independent of time.

The parameterizations we have selected for comparison are:

i. A density dependent albedo parameterization that was developed for use in the SOMARS snow and ice mass balance model (Greuell and Konzelmann 1994):

$$\alpha = \alpha_i + \left(\rho_{ss} - \rho_i\right)\left(\frac{\alpha_s - \alpha_i}{\rho_s - \rho_i}\right) \tag{1}$$

where α and ρ are albedo and density and subscripts i, s and ss are for ice, fresh snow and surface snow. ρ_s and ρ_i are generally taken to be ~300 and ~910 kg m^{-3}, the densities of fresh snow and ice respectively. α_s and α_i are constants that are often determined as part of the model tuning process. ρ_{ss} is calculated using a snow densification model. This parameterization is no longer used in SOMARS and has been replaced with a parameterization that is a function of the length of time that the surface has been wet. This parameterization is, however, still frequently used elsewhere in the snowmelt and glacier mass balance modeling community (Wright et al. 2005; Bassford et al. 2006; Wright et al. 2007) and adds diversity to our comparison.

ii. The albedo parameterization developed by Brun et al. (1992) approximates snow albedo in three spectral ranges as a function of effective grain diameter d_e (m) (updated parameterization provided by Jean-Marie Willamette, personal communication):

$$\alpha_{0.3-0.8\mu m} = \min\left[0.94, 0.96 - 1.58 d_e^{0.5}\right] \tag{2}$$

$$\alpha_{0.8-1.5\,\mu m} = 0.95 - 15.4 d_e^{0.5} \tag{3}$$

$$\alpha_{1.5-2.8\,\mu m} = 0.88 + 346.3 d_e^{'} - 32.31 d_e^{'0.5} \;\; where \; d_e^{'} = \min\left[d_e, 0.0023\right] \tag{4}$$

This albedo scheme is part of the CROCUS snow model (Brun et al. 1989) which has been used in numerous snow studies (e.g. Martin et al. 1996; Durand et al. 1999; Lefebre et al. 2003) and has been coupled with the French ARPEGE global climate model (Brun et al. 1997).

iii. An albedo parameterization that accounts for changes in albedo with solar zenith angle. The parameterization used most commonly to account for these changes was proposed by Dickinson et al. (1986) for use in the Biosphere-Atmosphere Transfer Scheme (BATS):

$$\alpha = \alpha_{\theta_Z < 60^\circ} + \max\left[0, 0.4\left(\frac{1-\alpha_{\theta_Z < 60^\circ}}{b}\right)\left(\frac{b+1}{1+2bu} - 1\right)\right] \tag{5}$$

where $u = \cos\theta_Z$, $\alpha_{\theta_Z < 60^\circ}$ is the constant snow albedo for solar zenith angles θ_Z less than 60°, b is a tunable parameter used to fit modeled to observed data and u' is the effective cosine of the solar zenith angle. If no observational data are available, b is often set equal to 2 (Segal et al. 1991; Lefebre et al. 2003). Albedos for zenith angles less than 60° are unchanged.

iv. An albedo parameterization that accounts for observed changes in albedo with increasing cloud cover (n_c) that was originally proposed by for use in SOMARS (Greuell and Konzelmann 1994):

$$\alpha_{cloud} = \alpha_{clear} + 0.05(n_c - 0.5) \tag{6}$$

v. The physically based parameterization developed by Marshall (1989) that was developed by fitting piecewise equations to theoretical model output (Warren and Wiscombe 1980; Wiscombe and Warren 1980). Marshall parameterized both visible and near-infrared albedos as a function of the square root of the effective grain radius and also accounted for the effects of solar zenith angle, soot contamination, and finite snow depth. This parameterization relies heavily on look-up tables and has been developed as a FORTRAN subroutine (SNOALB). This subroutine has been incorporated successfully into both regional and global climate models (Marshall and Oglesby 1994; Marshall et al. 1999; Marshall et al. 2003). A simplified adaptation of Marshall's parameterization is included in the SNTHERM snow model (Jordan 1991), which is maintained by the US Army Corps of Engineers, Cold Regions Research & Engineering Laboratory.

Comparison between theoretical results and selected parameterizations

Results from the five selected albedo parameterizations were compared with those from the full model:

i. Since the Greuell and Konzelmann (1994) albedo parameterization is based on density and not on effective grain size, the empirical relationship proposed by Dominé et al. [2007, equation (1)] was used to estimate snow density from the specific surface area of snow. In general, for $r_e < 2$mm, the Greuell and Konzelmann parameterization (Equation 1) underestimates the broadband albedo relative to full model results, with a maximum underestimation of 12% (Figure 5.10a).

ii. The Brun et al. (1992) grain size dependent albedo parameterization (Equations 2-4) does a good job of reproducing theoretical results for r_e < 0.5 mm but underestimates broadband albedos by as much as 15% relative to full model values for $r_e > 0.5$ mm (Figure 5.10a)..

iii. The Dickinson et al. (1986) parameterization (Equation 5) underestimates the theoretical increase in broadband albedo with increasing solar zenith angle by about 50% (Figure 5.10b). It does, however, do a good job of reproducing the increase in sensitivity of albedo to changes in the solar zenith angle as the effective radius of snow becomes larger.

iv. Overall, the Greuell and Konzelmann (1994) parameterization, which simulates the broadband albedo response to changes in cloud optical thickness (Equation 6), produces a similar shaped albedo response as seen in the full model results but slightly overestimates the magnitude of the response (Figure 5.10c). In order to compare the Greuell and Konzelmann parameterization with full model results it was necessary to estimate cloud amount from cloud optical thickness using the relationship proposed by Konzelmann et al. [1994, equation (3)]. This introduces additional uncertainty into the comparison, as is shown by the grey shading in Figure 5.10c.

v. Lastly, full model predictions of broadband albedo were compared with predictions from the Marshall (1989) parameterization for different grain sizes (Figure 5.10a), solar zenith angles (Figure 5.10b) and cloud optical thicknesses (Figure 5.10c). Clear-sky broadband albedos determined with the Marshall parameterization for snow with $r_e \leq 0.7$ mm and solar zenith angles < 80° were well matched with full model results. As r_e exceeded 0.8 mm and/or cloud cover increases the albedo is increasingly under predicted. Comparisons between the Marshall parameterization and the full model were also made for snow contaminated with varying amounts of light absorbing carbon. This comparison showed similar deviations as were evident in the comparisons for pure snow.

All five selected albedo parameterizations show varying degrees of disagreement with the full model results. Overall, the Marshall (1989) parameterization compares most favorably with the full model, but none of the parameterizations examined perform well for effective grain radii $r_e > 1$ mm or under cloudy sky conditions. The numerical details of the comparison between theoretical results and these selected parameterizations can be found in Appendix B.

A new broadband albedo parameterization

Here we develop a simple broadband albedo parameterization that closely matches full model results and is valid for a diverse array of snow, ice, and atmospheric conditions. The full model was run at a spectral resolution of 0.01 μm for the spectral range 0.2 – 4 μm, and for a wide range of semi-infinite homogeneous snow and ice media. Spectral snow surface albedos were determined for 352 snow types, defined by 22 effective ice grain radii between 0.025 – 5 mm and 16 light-absorbing carbon concentrations between 0 – 2 ppmw. This range of light-absorbing carbon concentrations covers the full range of published values (Hansen and Nazarenko 2004). Spectral ice surface albedos were determined for 192 ice types defined by 12 effective air bubble radii between 0.04 – 0.9 mm at an effective bubble concentration of 0.3 mm^{-3} and 16 light-absorbing carbon concentrations. In total, spectral albedos were calculated for 544 snow and ice types at 18 solar zenith angles between 0 – 85° and 11 cloud optical thicknesses ranging between 0 – 30. Integrating across the solar spectrum and dividing the total reflected irradiance by the total incident irradiance, 108 thousand broadband snow and ice albedos were determined. Atmospheric, snow and ice properties assigned to each model run are summarized in Table C.1 of Appendix C.

Pure snow and ice broadband albedos are asymptotically related to specific surface area ($\hat{S}$: cm^2 g^{-1}) and are nearly identical for equivalent specific surface areas of spherical ice grains and air bubbles (Figure 5.9a). For a solar zenith angle and cloud optical depth of zero, pure snow and ice broadband albedos ($\alpha_{\hat{S}}$) can be modeled accurately for specific surface areas in the range 0.07-1300 cm^2 g^{-1} ($R^2 = 0.997$, standard error $S_e = 0.008$, absolute maximum error $M_e = 0.02$) using the simple asymptotic function:

$$a_{\hat{S}} = 1.48 - \hat{S}^{-0.07} \tag{7}$$

The relationship between broadband snow and ice albedo and specific surface area changes as the concentration of light-absorbing carbon (c : ppmw) in the snow/ice increases (Figure 5.9a). The change in broadband snow and ice albedo due to loading by light-absorbing carbon from 0-2 ppmw ($d\alpha_c$) can be modeled using the equation (R^2 =0.999, $S_e = 0.007$, $M_e = 0.02$):

$$da_c = \max\left(0.04 - a_{\hat{S}}, \frac{-c^{0.55}}{0.16 + 0.6\hat{S}^{0.5} + 1.8c^{0.6}\hat{S}^{-0.25}}\right) \tag{8}$$

where the broadband albedo of the loaded snow/ice is $\alpha_c = \alpha_{\hat{s}} + d\alpha_c$, if there are no impurities $\alpha_c = \alpha_{\hat{s}}$.

The change in clear sky broadband snow and ice albedo with change in solar zenith angle ($d\alpha_{\theta_Z}$:Figure 5.9b) can be modeled using ($R^2 = 0.997$, $S_e =$ 0.007, $M_e = 0.03$):

$$d\alpha_{\theta_Z} = 0.53\alpha_{\hat{S}}\left(1-\alpha_c\right)\left(1-u\right)^{1.2} \tag{9}$$

where u is the cosine of the solar zenith angle.

Next, a set of equations was developed that can reproduce the increase in broadband albedo of snow and ice resulting from an increase in cloud cover for clouds with optical thicknesses ranging between 0-30 (Figure 5.9c). The increase in the diffuse fraction of the incident radiation as the cloud optical thickness increases from 0 to 3 can be approximated with a linear weighting function that adjusts the cosine of the effective solar zenith angle (u') towards that of diffuse radiation (~50°) as both the cloud optical thickness and solar zenith angle increase:

$$u' = 0.64x + \left(1-x\right)u \tag{10}$$

$$\text{where } x = \min\left[\left(\frac{\tau}{3u}\right)^{0.5}, 1\right]$$

Using u' in Equation 9, the additional change in broadband albedo due to the spectral shift in incident radiation caused by an increase in cloud optical thickness ($d\alpha_\tau$) can be modeled with (R^2 =0.998, $S_e = 0.01$, $M_e = 0.06$):

$$d\alpha_\tau = \frac{0.1\tau\alpha_c^{1.3}}{\left(1+1.5\tau\right)^{\alpha_{\hat{S}}}} \tag{11}$$

The resultant broadband albedo (α) is determined by summing all contributing components:

$$\alpha = \alpha_{\hat{S}} + d\alpha_c + d\alpha_{u'} + d\alpha_\tau \tag{12}$$

The newly proposed snow and ice albedo parameterization performs slightly better for snow with $r_e \leq 2$ mm and under clear sky conditions (S_e = 0.006, M_e = 0.03) than for snow, ice and atmospheric conditions outside of this range. That being said, deviations from full model results are minimal (S_e = 0.01, M_e = 0.06) under all 108 thousand modeled snow, ice and atmosphere conditions (Figure 5.11).

Equations 7-12 are for homogenous semi-infinite snow/ice. Because finite snow depth only impacts spectral albedos in the near-UV and visible (see Wiscombe and Warren 1980: Figure 8), its effects are similar to adding or reducing the amount of light-absorbing carbon in semi-infinite snow. Therefore, the surface albedo for a finite snow layer of depth z (m w.e.) overlying semi-infinite ice layer can be accounted for by replacing $d\alpha_c$ in equations 8-12 with a value which has been corrected for finite snow depth $d\alpha'_c$:

$$d\alpha'_c = \left(\alpha_c^{btm} - \alpha_s^{top}\right) + A\left(\alpha_c^{top} - \alpha_c^{btm}\right) \tag{13}$$

$$\text{where } A = \min\left[1, 2.1z^{1.35\left(1-\alpha_{\hat{S}}^{top}\right)-0.1c^{top}-0.13}\right]$$

The superscripts top and btm are for the upper and lower layers respectively. $\alpha_{\hat{S}}^{top}$ and α_c^{top} are determined for the overlying snow layer using Equations 7 and 8. This equation compares very favorably (R^2 =0.985, S_e = 0.01, M_e = 0.07) to a wide range of full model results for snow of varying depth overlying an ice layer of semi-infinite depth. Table C.2 in Appendix C provides details of the full model runs to which the parameterization was fit. Equation (13) is only valid for snow overlying ice or old snow. Expanding the equation to account for finite snow depth over other surfaces, such as bare soil or vegetation, should be achievable by modeling the subsurface as an optically equivalent layer of dirty ice. Also note that equations (7) – (13) are only valid over the range of snow, ice and atmospheric conditions for which they have been developed (see Appendix C).

Discussion

We have not yet had the opportunity to conduct a field campaign to collect measurements of the spectral albedo of snow and ice, solar spectral irradiance and snow properties to compare with our model results, therefore, we look to previous studies which have compared snow albedo measurements to results produced with multi-layer plane-parallel radiative transfer models similar to the one employed in this study. Three such studies (Grenfell et al. 1994 Aoki et al. 2000 Painter et al. 2007) all show very good agreement between theoretically modeled and observed snow spectral albedos when the snow stratigraphy is well known and the instrumentation is not left unattended. In addition, Grenfell and Perovich (2008) show exceptional agreement between incident solar spectral irradiance modeled using SBDART and observed values obtained over Arctic Ocean sea ice for a wide variety of atmospheric conditions using the same sub-Arctic atmospheric profile used in this study.

The parameterization presented here accurately reproduces theoretical results under a wide range of snow and ice conditions, is computationally simple and requires, at most, five input parameters; snow/ice specific surface area, concentration of light-absorbing carbon, solar zenith angle, cloud optical thickness, and snow depth. Inputs can be determined from measurements and/or numerical model output. Snow specific surface areas can be measured directly using contact spectroscopy (Painter et al. 2007), methane adsorption (Dominé et al. 2001; Legagneux et al. 2002), photographic methods (Matzl and Schneebeli

2006), image analysis (Sergent et al. 1993; Sergent et al. 1998) and stereological techniques (Davis and Dozier 1989), or estimated from measurements of snow density and grain type (Dominé et al. 2007). Specific surface area can also be modeled using dry (Marbouty 1980; Legagneux et al. 2003; Flanner and Zender 2006; Taillandier et al. 2007) and wet (Brun 1989) snow metamorphism models that are forced with the vertical temperature gradient, snow density and liquid water content, quantities that are often modeled within snow and climate models. Carbon concentrations can be determined from field measurements (Clarke and Noone 1985) or from climate models that resolve carbon aerosol transport (Flanner et al. 2007). The solar zenith angle can be calculated from the latitude, solar declination angle, and time of day, and cloud optical thickness can be determined by comparing theoretical clear sky to observed solar irradiance, from satellite observations (Platnick et al. 2003), statistically applied climatology (Curry and Ebert 1992), or climate model output.

Physically based parameterizations of snow and ice albedo offer the opportunity to better assess the impacts of changing environmental conditions on the energy budget of snow and ice. These will not be as easy to evaluate using empirical albedo parameterizations based on measurements of site specific snow, ice and atmospheric conditions. The new broadband albedo parameterization proposed here reproduces theoretical results very well when the exact snow, ice and atmosphere properties are known. However, for use in energy balance, melt or climate models this parameterization will, at a minimum, require input of snow grain radii from a snow grain growth model. In practical terms, the proposed albedo parameterization will only be as accurate as the snow grain growth model with which it is forced. Recently there has been a renewed effort towards the improvement of such models (Legagneux et al., 2003; Flanner and Zender, 2006; Taillandier et al., 2007) but much work is still needed to confirm their validity over a wide range of environmental conditions.

Summary

The spectral albedo of snow and ice is the net result of many reflections and refraction of shortwave radiation at air-ice boundaries, and its absorption as it passes though ice and comes into contact with light-absorbing impurities. The relative number of air-ice boundaries per unit mass of ice is dependent on the specific surface area of the medium. A smaller specific surface area will, on average, result in a lower number of scattering events and longer travel paths of shortwave radiation within snow and ice, leading to lower surface albedos. Addition of light-absorbing impurities increases the probability of absorption, further reducing albedo. It is not only the characteristics of the snow/ice that govern its albedo, but also the angle of incidence (solar zenith angle and diffuse fraction of incident radiation) and, in the case of broadband albedo, the spectral distribution of the incident shortwave radiation.

The responses of broadband albedo to changes in specific surface area, impurity loading, angle of incidence, or spectral distribution and diffuse fraction of incident shortwave radiation are highly interdependent. Multiple reflections between the surface and clouds generate an interdependence between surface albedo and the spectral distribution of incident radiation. This necessitates the use of a coupled snow and ice – atmosphere radiative transfer models to model broadband albedos. However, such models can be computationally expensive and difficult to implement in existing energy mass balance and climate models.

Comparisons between selected preexisting parameterizations of snow albedo and a coupled snow and ice – atmosphere radiative transfer model show varying degrees of disagreement. In response, we have developed a new parameterization of broadband albedo that accurately reproduces theoretical results under a wide range of snow and ice conditions. It is computationally simple and requires between one and five input parameters, depending on its application. These parameters are: specific surface area of snow/ice, concentration of light-absorbing carbon, solar zenith angle, cloud optical thickness, and snow depth. More work is needed to assess the performance of existing snow grain growth models which are required to provide input to such an albedo parameterization in energy balance and climate models.

References

Ackermann, M., J. Ahrens, X. Bai, M. Bartelt, S. W. Barwick, R. C. Bay, T. Becka, J. K. Becker, et al., 2006: Optical properties of deep glacial ice at the South Pole. *Journal of Geophysical Research*, **111,** doi:10.1029/2005JD006687.

Aoki, T., T. Aoki, M. Fukabori, A. Hachikubo, Y. Tachibana, and F. Nishio, 2000: Effects of snow physical parameters on spectral albedo and bidirectional reflectance of snow surface. *Journal of Geophysical Research-Atmospheres*, **105,** 10219-10236.

Askebjer, P., S. W. Barwick, L. Bergström, A. Bouchta, S. Carius, E. Dalberg, K. Engel, B. Erlandsson, et al., 1997: Optical properties of deep ice at the South Pole: Absorption. *Applied Optics*, **36,** 4168-4180.

Bassford, R. P., M. J. Siegert, J. A. Dowdeswell, J. Oerlemans, A. F. Glazovsky, and Y. Y. Macheret, 2006: Quantifying the mass balance of ice caps on Severnaya Zemlya, Russian High Arctic. I: Climate and mass balance of the Vavilov Ice Cap. *Arctic Antarctic and Alpine Research*, **38,** 1-12.

Bohren, C. F., 1983: Colors of snow, frozen waterfalls, and icebergs. *Journal of the Optical Society of America*, **73,** 1646-&.

______, 1986: Applicability of effective-medium theories to problems of scattering and absorption by nonhomogeneous atmospheric particles. *Journal of the Atmospheric Sciences*, **43,** 468-475.

Bohren, C. F. and D. R. Huffman, 1998: *Absorption and scattering of light by small particles*. Wiley-Interscience, 544 pp.

Bond, T. C. and R. W. Bergstrom, 2006: Light absorption by carbonaceous particles: An investigative review. *Aerosol Science and Technology*, **40,** 27-67.

Bougamont, M. and J. L. Bamber, 2005: A surface mass balance model for the Greenland Ice Sheet. *Journal of Geophysical Research-Earth Surface*, **110,** doi:10.1029/2005JF000348.

Brock, B. W., I. C. Willis, and M. J. Sharp, 2000: Measurement and parameterization of albedo variations at Haut Glacier d'Arolla, Switzerland. *Journal of Glaciology*, **46,** 675-688.

Brun, E., 1989: Investigation on wet-snow metamorphism in respect of liquid-water content. *Annals of Glaciology*, **13,** 22-26.

Brun, E., P. David, M. Sudul, and G. Brunot, 1992: A numerical model to simulate snow-cover stratigraphy for operational avalanche forecasting. *Journal of Glaciology*, **38,** 13-22.

Brun, E., E. Martin, V. Simon, C. Gendre, and C. Coleou, 1989: An energy and mass model of snow cover suitable for operational avalanche forecasting. *Journal of Glaciology*, **35,** 333-342.

Brun, E., E. Martin, and V. Spiridonov, 1997: Coupling a multi-layered snow model with a GCM. *Annals of Glaciology*, **25,** 66-72.

Carroll, J. J. and B. W. Fitch, 1981: Effects of solar elevation and cloudiness on snow albedo at the South Pole. *Journal of Geophysical Research-Oceans and Atmospheres*, **86,** 5271-5276.

Cess, R. D., G. L. Potter, M. H. Zhang, J. P. Blanchet, S. Chalita, R. Colman, D. A. Dazlich, A. D. Delgenio, et al., 1991: Interpretation of snow-climate feedback as produced by 17 general-circulation models. *Science*, **253,** 888-892.

Chýlek, P., V. Ramaswamy, and V. Srivastava, 1983: Albedo of soot-contaminated snow. *Journal of Geophysical Research-Oceans and Atmospheres*, **88,** 837-843.

Clarke, A. D. and K. J. Noone, 1985: Soot in the Arctic snowpack: A cause for perturbations in radiative-transfer. *Atmospheric Environment*, **19,** 2045-2053.

Colbeck, S. C., 1979: Grain clusters in wet snow. *Journal of Colloid and Interface Science*, **72,** 371-384.

Curry, J. A. and E. E. Ebert, 1992: Annual cycle of radiation fluxes over the Arctic Ocean: Sensitivity to cloud optical properties. *Journal of Climate*, **5,** 1267-1280.

Curry, J. A., W. B. Rossow, D. Randall, and J. L. Schramm, 1996: Overview of Arctic cloud and radiation characteristics. *Journal of Climate*, **9,** 1731-1764.

Davis, R. and J. Dozier, 1989: Stereological characterization of dry alpine snow for microwave remote sensing. *Advances in Space Research*, **9,** 245-251.

Dickinson, R. E., A. Henderson-Sellers, P. J. Kennedy, and M. F. Wilson, 1986: Biosphere-Atmosphere Transfer Scheme (BATS) for the NCAR Community Climate Model. *NCAR Technical Note*, **275**.

Dominé, F., A. Cabanes, A.-S. Taillandier, and L. Legagneux, 2001: Specific surface area of snow samples determined by CH4 adsorption at 77 K and estimated by optical microscopy and scanning electron microscopy. *Environmental Science and Technology*, **35,** 771-780.

Dominé, F., A. S. Taillandier, and W. R. Simpson, 2007: A parameterization of the specific surface area of seasonal snow for field use and for models of snowpack evolution. *Journal of Geophysical Research-Earth Surface*, **112,** doi:10.1029/2006JF000512.

Dozier, J., 1989: Spectral signature of alpine snow cover from the Landsat Thematic Mapper. *Remote Sensing of Environment*, **28,** 9-22.

Durand, Y., G. Giraud, E. Brun, L. Merindol, and E. Martin, 1999: A computer-based system simulating snowpack structures as a tool for regional avalanche forecasting. *Journal of Glaciology*, **45,** 469-484.

Fitzpatrick, M. F., R. E. Brandt, and S. G. Warren, 2004: Transmission of solar radiation by clouds over snow and ice surfaces: A parameterization in terms of optical depth, solar zenith angle, and surface albedo. *Journal of Climate*, **17,** 266-275.

Flanner, M. G. and C. S. Zender, 2006: Linking snowpack microphysics and albedo evolution. *Journal of Geophysical Research-Atmospheres*, **111,** doi:10.1029/2005JD006834.

Flanner, M. G., C. S. Zender, J. T. Randerson, and P. J. Rasch, 2007: Present-day climate forcing and response from black carbon in snow. *Journal of Geophysical Research-Atmospheres*, **112,** doi:10.1029/2006JD008003.

Green, R. O., J. Dozier, D. Roberts, and T. Painter, 2002: Spectral snow-reflectance models for grain-size and liquid-water fraction in melting snow for the solar-reflected spectrum. *Annals of Glaciology*, **34,** 71-73.

Grenfell, T. C., 1991: A radiative transfer model for sea ice with vertical structure variations. *Journal of Geophysical Research-Oceans*, **96,** 16991-17001.

Grenfell, T. C., B. Light, and M. Sturm, 2002: Spatial distribution and radiative effects of soot in the snow and sea ice during the SHEBA experiment. *Journal of Geophysical Research-Oceans*, **107,** doi:10.1029/2000JC000414.

Grenfell, T. C. and G. A. Maykut, 1977: The optical properties of ice and snow in the Arctic Basin. *Journal of Glaciology*, **18,** 445-463.

Grenfell, T. C., S. P. Neshyba, and S. G. Warren, 2005: Representation of a nonspherical ice particle by a collection of independent spheres for scattering and absorption of radiation: 3. Hollow columns and plates. *Journal of Geophysical Research-Atmospheres*, **110,** doi:10.1029/2005JD005811.

Grenfell, T. C. and D. K. Perovich, 1984: Spectral albedos of sea ice and incident solar irradiance in the southern Beaufort Sea. *Journal of Geophysical Research-Oceans*, **89,** 3573-3580.

______, 2008: Incident spectral irradiance in the Arctic Basin during the summer and fall. *Journal of Geophysical Research-Atmospheres*, **113,** doi:10.1029/2007JD009418.

Grenfell, T. C., D. K. Perovich, and J. A. Ogren, 1981: Spectral Albedos of an Alpine Snowpack. *Cold Regions Science and Technology*, **4,** 121-127.

Grenfell, T. C. and S. G. Warren, 1999: Representation of a nonspherical ice particle by a collection of independent spheres for scattering and absorption of radiation. *Journal of Geophysical Research-Atmospheres*, **104,** 31697-31709.

Grenfell, T. C., S. G. Warren, and P. C. Mullen, 1994: Reflection of solar-radiation by the Antarctic snow surface at ultraviolet, visible, and near-infrared wavelengths. *Journal of Geophysical Research-Atmospheres*, **99,** 18669-18684.

Greuell, W., 2000: Melt-water accumulation on the surface of the Greenland Ice Sheet: Effect on albedo and mass balance. *Geografiska Annaler: Series A - Physical Geography*, **82A,** 489-498.

Greuell, W. and T. Konzelmann, 1994: Numerical modeling of the energy balance and the englacial temperature of the Greenland Ice Sheet: Calculations for the ETH-Camp Location (West Greenland, 1155 m a.s.l.). *Global and Planetary Change*, **9,** 91-114.

Greuell, W., C. H. Reijmer, and J. Oerlemans, 2002: Narrowband-to-broadband albedo conversion for glacier ice and snow based on aircraft and near-surface measurements. *Remote Sensing of Environment*, **82,** 48-63.

Hansen, J. and L. Nazarenko, 2004: Soot climate forcing via snow and ice albedos. *Proceedings of the National Academy of Sciences of the United States of America*, **101,** 423-428.

Hansen, J. E. and L. D. Travis, 1974: Light-scattering in planetary atmospheres. *Space Science Reviews*, **16,** 527-610.

Hanson, A. M., 1965: Studies of the mass budget of Arctic pack ice floes. *Journal of Glaciology*, **5,** 701-709.

Horvath, H., 1993: Atmospheric light absorption: A review. *Atmospheric Environment. Part A*, **27,** 293-317.

Hudson, S. R., S. G. Warren, R. E. Brandt, T. C. Grenfell, and D. Six, 2006: Spectral bidirectional reflectance of Antarctic snow: Measurements and parameterization. *Journal of Geophysical Research-Atmospheres*, **111,** doi:10.1029/2006JD007290.

Jonsell, U., R. Hock, and B. Holmgren, 2003: Spatial and temporal variations in albedo on Storglaciaren, Sweden. *Journal of Glaciology*, **49,** 59-68.

Jordan, R., 1991: A one-dimensional temperature model for a snow cover: Technical documentation for SNTHERM 89, 49 pp.

Klok, E. J., W. Greuell, and J. Oerlemans, 2003: Temporal and spatial variation of the surface albedo of Morteratschgletscher, Switzerland, as derived from 12 Landsat images. *Journal of Glaciology*, **49,** 491-502.

Klok, E. J. and J. Oerlemans, 2004: Modelled climate sensitivity of the mass balance of Morteratschgletscher and its dependence on albedo parameterization. *International Journal of Climatology*, **24,** 231-245.

Konzelmann, T., R. S. W. Vandewal, W. Greuell, R. Bintanja, E. A. C. Henneken, and A. Abeouchi, 1994: Parameterization of global and longwave incoming radiation for the Greenland Ice Sheet. *Global and Planetary Change*, **9,** 143-164.

Lefebre, F., H. Gallee, J. P. van Ypersele, and W. Greuell, 2003: Modeling of snow and ice melt at ETH Camp (West Greenland): A study of surface albedo. *Journal of Geophysical Research-Atmospheres*, **108,** doi:10.1029/2001JD001160.

Legagneux, L., A. Cabanes, and F. Dominé, 2002: Measurement of the specific surface area of 176 snow samples using methane adsorption at 77 K. *Journal of Geophysical Research*, **107**.

Legagneux, L., T. Lauzier, F. Dominé, W. F. Kuhs, T. Heinrichs, and K. Techmer, 2003: Rate of decay of specific surface area of snow during isothermal experiments and morphological changes studied by scanning electron microscopy. *Canadian Journal of Physics*, **81,** 459-468.

Legagneux, L., A.-S. Taillandier, and F. Dominé, 2004: Grain growth theories and the isothermal evolution of the specific surface area of snow. *Journal of Applied Physics*, **95,** 6175-6184.

Light, B., T. C. Grenfell, and D. K. Perovich, 2008: Transmission and absorption of solar radiation by Arctic sea ice during the melt season. *Journal of Geophysical Research-Oceans*, **113,** doi:10.1029/2006JC003977.

Light, B., G. A. Maykut, and T. C. Grenfell, 2003: Effects of temperature on the microstructure of first-year Arctic sea ice. *Journal of Geophysical Research-Oceans*, **108**.

Lüthje, M., L. T. Pedersen, N. Reeh, and W. Greuell, 2006: Modelling the evolution of supraglacial lakes on the West Greenland ice-sheet margin. *Journal of Glaciology*, **52,** 608-618.

Male, D. H. and R. J. Granger, 1981: Snow surface energy exchange. *Water Resources Research*, **17,** 609-627.

Marbouty, D., 1980: An experimental study of temperature-gradient metamorphism. *Journal of Glaciology*, **26,** 303-312.

Marshall, S. and R. J. Oglesby, 1994: An improved snow hydrology for GCMs. Part 1: Snow cover fraction, albedo, grain size, and age. *Climate Dynamics*, **10,** 21-37.

Marshall, S., R. J. Oglesby, K. A. Maasch, and G. T. Bates, 1999: Improving climate model representations of snow hydrology. *Environmental Modelling & Software*, **14,** 327-334.

Marshall, S., R. J. Oglesby, and A. W. Nolin, 2003: The predictability of winter snow cover over the western United States. *Journal of Climate*, **16,** 1062-1073.

Marshall, S. E., 1989: A physical parameterization of snow albedo for use in climate models. NCAR Cooperative Thesis no. 123. Boulder, CO.

Martin, E., B. Timbal, and E. Brun, 1996: Downscaling of general circulation model outputs: Simulation of the snow climatology of the French Alps and sensitivity to climate change. *Climate Dynamics*, **13,** 45-56.

Matzl, M. and M. Schneebeli, 2006: Measuring specific surface area of snow by near-infrared photography. *Journal of Glaciology*, **52,** 558-564.

Mätzler, C., 2002: MATLAB functions for Mie scattering and absorption, Version 2. Institut für Angewandte Physik Report No. 2002-11, 20 pp.

McClatchey, R. A., R. W. Fenn, J. E. A. Selby, F. E. Volz, and J. S. Garing, 1972: Optical Properties of the Atmosphere (3rd ed.)No. 411, 103 pp.

Mullen, P. C. and S. G. Warren, 1988: Theory of the optical properties of lake ice. *Journal of Geophysical Research-Atmospheres*, **93,** 8403-8414.

Neshyba, S. P., T. C. Grenfell, and S. G. Warren, 2003: Representation of a nonspherical ice particle by a collection of independent spheres for scattering and absorption of radiation: 2. Hexagonal columns and plates. *Journal of Geophysical Research-Atmospheres*, **108,** doi:10.1029/2002JD003302.

Painter, T. H., N. P. Molotch, M. Cassidy, M. Flanner, and K. Steffen, 2007: Instruments and methods: Contact spectroscopy for determination of stratigraphy of snow optical grain size. *Journal of Glaciology*, **53,** 121-127.

Paterson, W. S. B., 2000: *Physics of Glaciers*. 3 ed. Butterworth-Heinemann, 481 pp.

Pedersen, C. A. and J. G. Winther, 2005: Intercomparison and validation of snow albedo parameterization schemes in climate models. *Climate Dynamics*, **25,** 351-362.

Perovich, D. K., T. C. Grenfell, B. Light, and P. V. Hobbs, 2002: Seasonal evolution of the albedo of multiyear Arctic sea ice. *Journal of Geophysical Research-Oceans*, **107,** doi:10.1029/2000JC000438.

Platnick, S., M. D. King, S. A. Ackerman, W. P. Menzel, B. A. Baum, J. C. Riedi, and R. A. Frey, 2003: The MODIS cloud products: Algorithms and examples from Terra. *IEEE Transactions on Geoscience and Remote Sensing*, **41,** 459-473.

Ranzi, R. and R. Rossi, 1991: A physically based approach to modelling distributed snowmelt in a small alpine catchment. *IAHS Publ. no. 205*, 141-150.

Ricchiazzi, P., S. R. Yang, C. Gautier, and D. Sowle, 1998: SBDART: A research and teaching software tool for plane-parallell radiative transfer in the Earth's atmosphere. *Bulletin of the American Meteorological Society*, **79,** 2101-2114.

Segal, M., J. R. Garratt, R. A. Pielke, and Z. Ye, 1991: Scaling and numerical-model evaluation of snow-cover effects on the generation and modification of daytime mesoscale circulations. *Journal of the Atmospheric Sciences*, **48,** 1024-1042.

Sergent, C., C. Leroux, E. Pougatch, and F. Guirado, 1998: Hemispherical-directional reflectance measurements of natural snow in the 0.9-1.45 μm spectral range: comparison with adding-doubling modeling. *Annals of Glaciology*, **26,** 59-63.

Sergent, C., E. Pougatch, M. Sudul, and B. Bourdelles, 1993: Experimental investigation of optical snow properties. *Annals of Glaciology*, **17,** 281-287.

Serreze, M. C. and R. G. Barry, 2005: *The Arctic Climate System*. 1st ed. *Cambridge Atmospheric and Space Science Series*, Cambridge University Press, 385 pp.

Spencer, M. K., R. B. Alley, and J. J. Fitzpatrick, 2006: Developing a bubble number-density paleoclimatic indicator for glacier ice. *Journal of Glaciology*, **52,** 358-364.

Stamnes, K., S. C. Tsay, W. Wiscombe, and K. Jayaweera, 1988: Numerically stable algorithm for discrete-ordinate-method radiative transfer in multiple scattering and emitting layered media. *Applied Optics*, **27,** 2502-2509.

Stroeve, J., A. Nolin, and K. Steffen, 1997: Comparison of AVHRR-derived and in situ surface albedo over the Greenland Ice Sheet. *Remote Sensing of Environment*, **62,** 262-276.

Taillandier, A.-S., F. Dominé, W. R. Simpson, M. Sturm, and T. A. Douglas, 2007: Rate of decrease of the specific surface area of dry snow: Isothermal and temperature gradient conditions. *Journal of Geophysical Research*, **112**.

van den Broeke, M., D. van As, C. Reijmer, and R. van de Wal, 2004: Assessing and improving the quality of unattended radiation observations in Antarctica. *Journal of Atmospheric and Oceanic Technology*, **21,** 1417-1431.

Warren, S. G., 1982: Optical properties of snow. *Reviews of Geophysics and Space Physics*, **20,** 67-89.

______, 1984: Impurities in snow: Effects on albedo and snowmelt (review). *Annals of Glaciology*, **5,** 177-179.

Warren, S. G. and R. E. Brandt, 2008: Optical constants of ice from the ultraviolet to the microwave: A revised compilation. *Journal of Geophysical Research*, **113,** doi:10.1029/2007JD009744.

Warren, S. G., R. E. Brandt, T. C. Grenfell, and C. P. McKay, 2002: Snowball Earth: Ice thickness on the tropical ocean. *Journal of Geophysical Research-Oceans*, **107**.

Warren, S. G., R. E. Brandt, and P. O. Hinton, 1998: Effect of surface roughness on bidirectional reflectance of Antarctic snow. *Journal of Geophysical Research-Planets*, **103,** 25789-25807.

Warren, S. G. and A. D. Clarke, 1990: Soot in the atmosphere and snow surface of Antarctica. *Journal of Geophysical Research-Atmospheres*, **95,** 1811-1816.

Warren, S. G. and W. J. Wiscombe, 1980: A Model for the spectral albedo of snow. II: Snow containing atmospheric aerosols. *Journal of the Atmospheric Sciences*, **37,** 2734-2745.

Winther, J. G., 1993: Short-term and long-term variability of snow albedo. *Nordic Hydrology*, **24,** 199-212.

Wiscombe, W. J. and S. G. Warren, 1980: A model for the spectral albedo of snow. I: Pure snow. *Journal of the Atmospheric Sciences*, **37,** 2712-2733.

Wright, A., J. Wadham, M. Siegert, A. Luckman, and J. Kohler, 2005: Modelling the impact of superimposed ice on the mass balance of an Arctic glacier under scenarios of future climate change. *Annals of Glaciology*, **42,** 277-283.

Wright, A. P., J. L. Wadham, M. J. Siegert, A. Luckman, J. Kohler, and A. M. Nuttall, 2007: Modeling the refreezing of meltwater as superimposed ice on a high Arctic glacier: A comparison of approaches. *Journal of Geophysical Research-Earth Surface*, **112,** doi:10.1029/2007JF000818.

Zuo, Z. and J. Oerlemans, 1996: Modelling albedo and specific balance of the Greenland Ice Sheet: Calculations for the Sondre Stromfjord transect. *Journal of Glaciology*, **42,** 305-317.

Figures

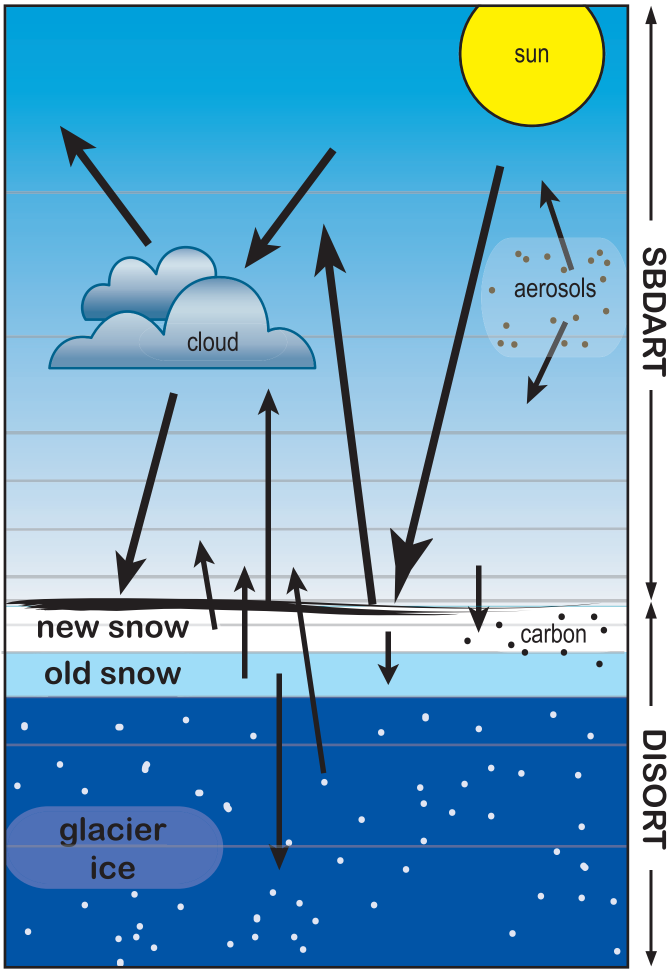

Figure 5.1: Schematic diagram showing the coupled snow and ice – atmosphere radiative transfer model.

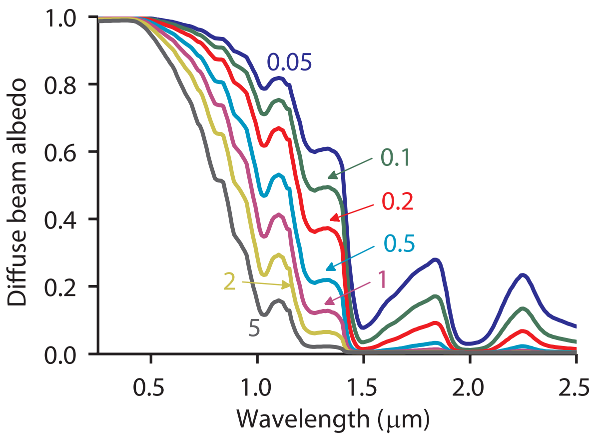

Figure 5.2: Semi-infinite diffuse beam pure snow albedo as a function of the effective grain radius r_e (mm).

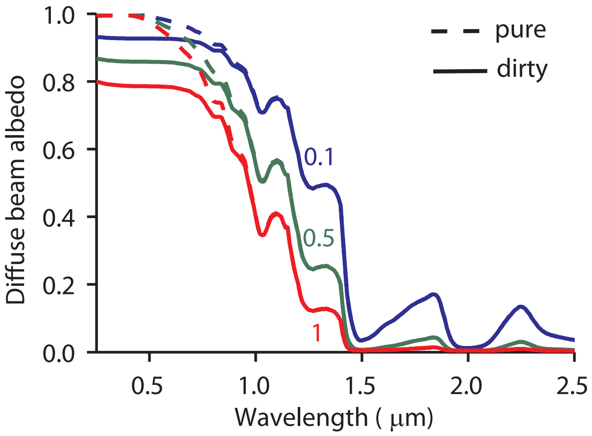

Figure 5.3 Semi-infinite diffuse beam albedo of pure (dashed) and dirty (solid) snow for three effective grain radii r_e (mm). The dirty snow contains 0.3 ppmw of light-absorbing carbon.

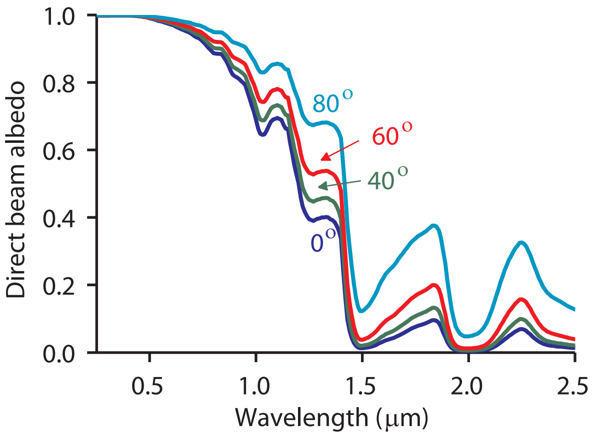

Figure 5.4: Semi-infinite direct beam albedo of pure snow ($r_e = 0.1$ mm) as a function of solar zenith angle.

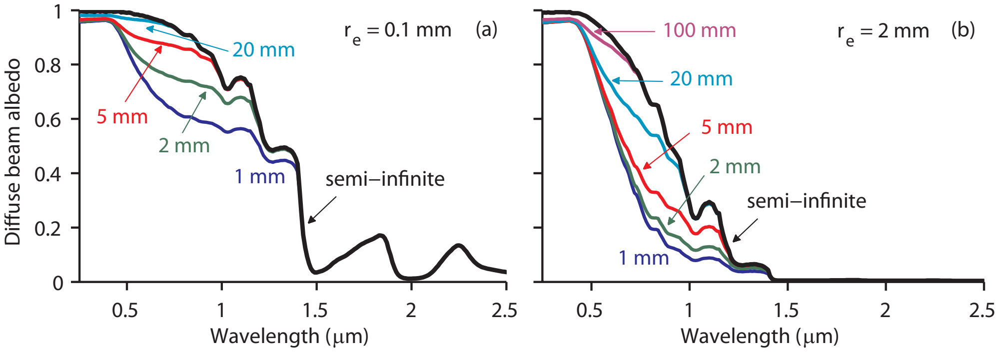

Figure 5.5: Semi-infinite diffuse beam albedo of pure white ice (contains air bubbles and has a clear sky broadband albedo of 0.40) overlain by a homogenous fine (a) and coarse (b) grained snow layer of varying thickness (mm w.e.).

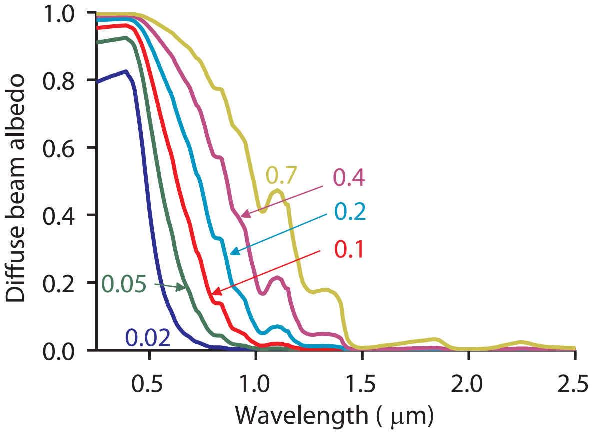

Figure 5.6: Semi-infinite diffuse beam albedo of pure ice as a function effective air bubble radius (mm) with a constant effective bubble concentration $n'_e = 0.3$ mm^{-3}. 0.3 mm^{-3} is the mean bubble concentration determined from 28 Greenland and Antarctica ice core samples (Spencer et al., 2006).

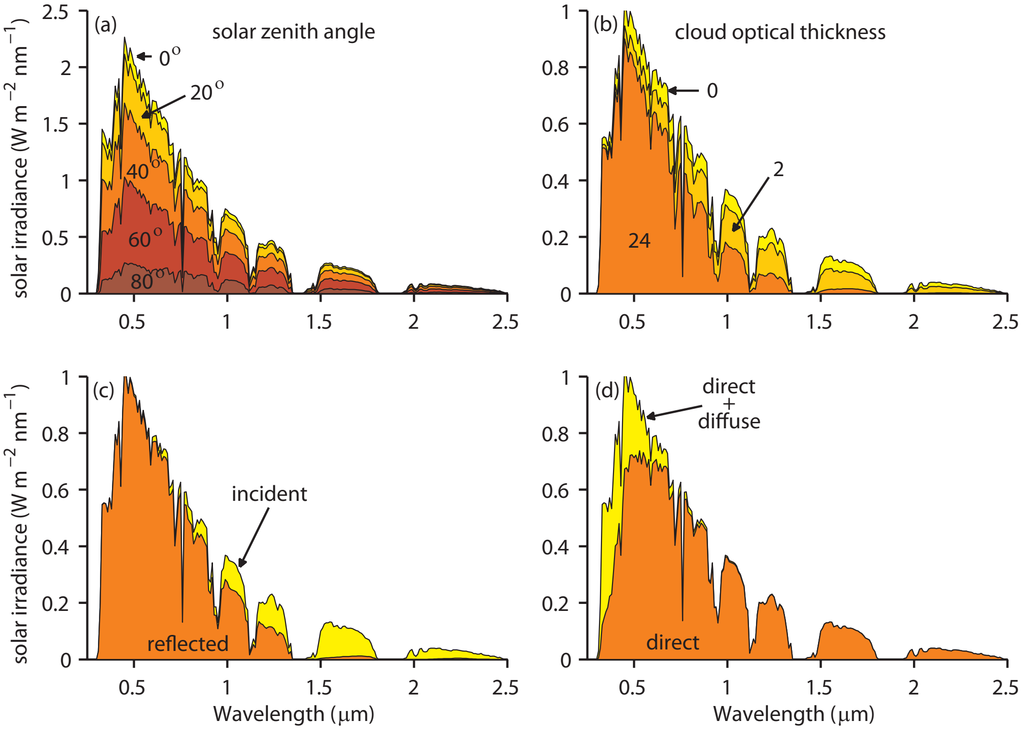

Figure 5.7: (a) Solar spectral irradiance for solar zenith angles between 0-80˚, (b) cloud optical thicknesses of 0, 2, and 24 (this range in arctic cloud optical thickness was taken from Curry et al., 1996), (c) incoming and reflected irradiance over a fresh snow surface, and (d) direct and diffuse spectral irradiance components. Figures 7a, 7c and 7d are for clear sky conditions, and Figures 7b–7d are for a solar zenith angle of 60°. See text for details.

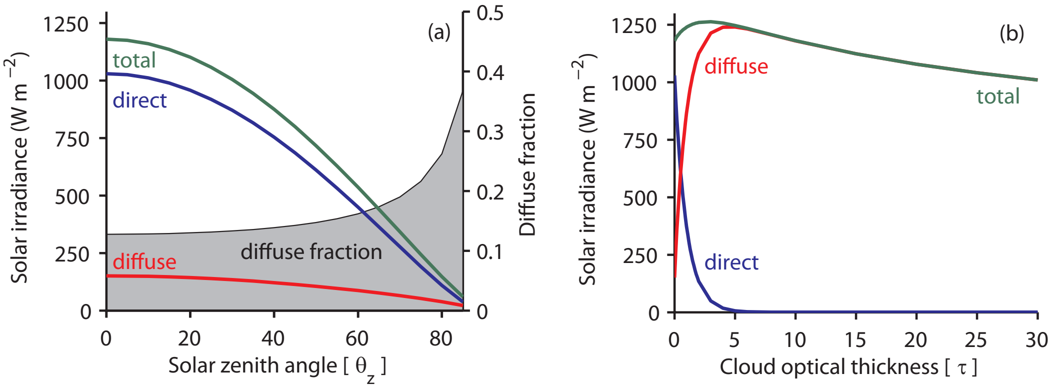

Figure 5.8: Total, direct and diffuse solar irradiance. (a) Clear sky values as a function of solar zenith angle and (b) cloud sky values for a solar zenith angle of 0° as a function of cloud optical thickness. See text for details.

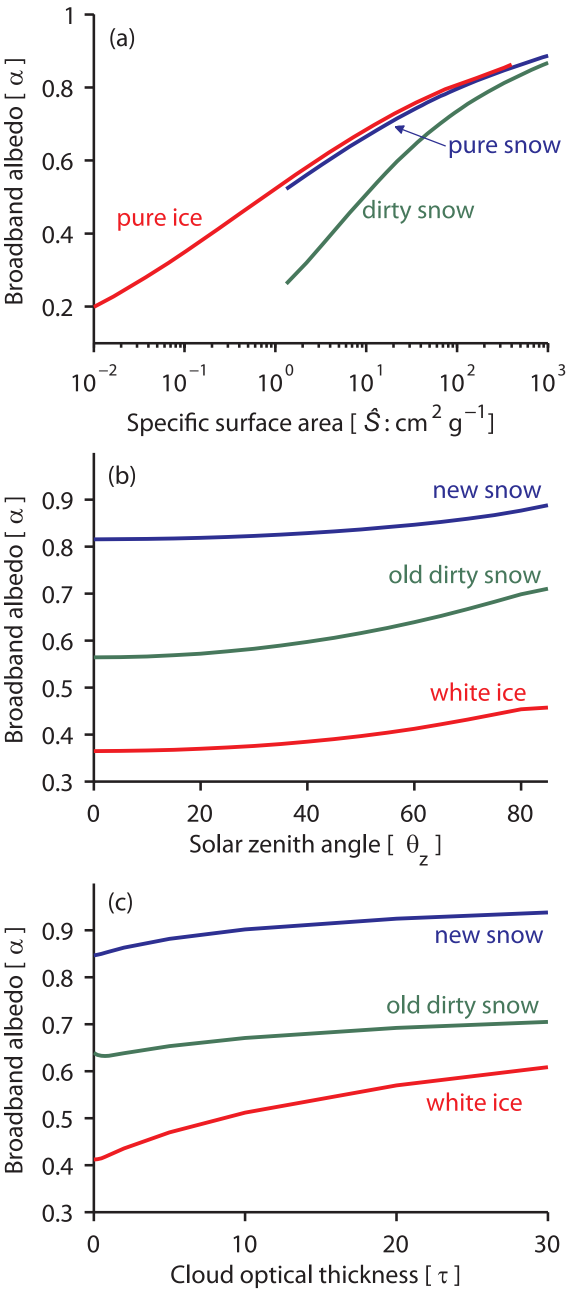

Figure 5.9: Semi-infinite broadband albedo of snow and ice as a function of (a) specific surface area ($\hat{S}$), (b) solar zenith angle and (c) cloud optical thickness. "Dirty snow" contains 0.3 ppmw of light-absorbing carbon and "old dirty snow" contains the same amount of light-absorbing carbon and has an effective grain size r_e = 1 mm. "New snow" values are for pure snow with $r_e = 0.1$ mm. "White ice" values are for pure ice that has an effective bubble radius of $r'_e = 0.075$ mm and an effective bubble concentration of $n'_e = 0.3$ mm^{-3}.

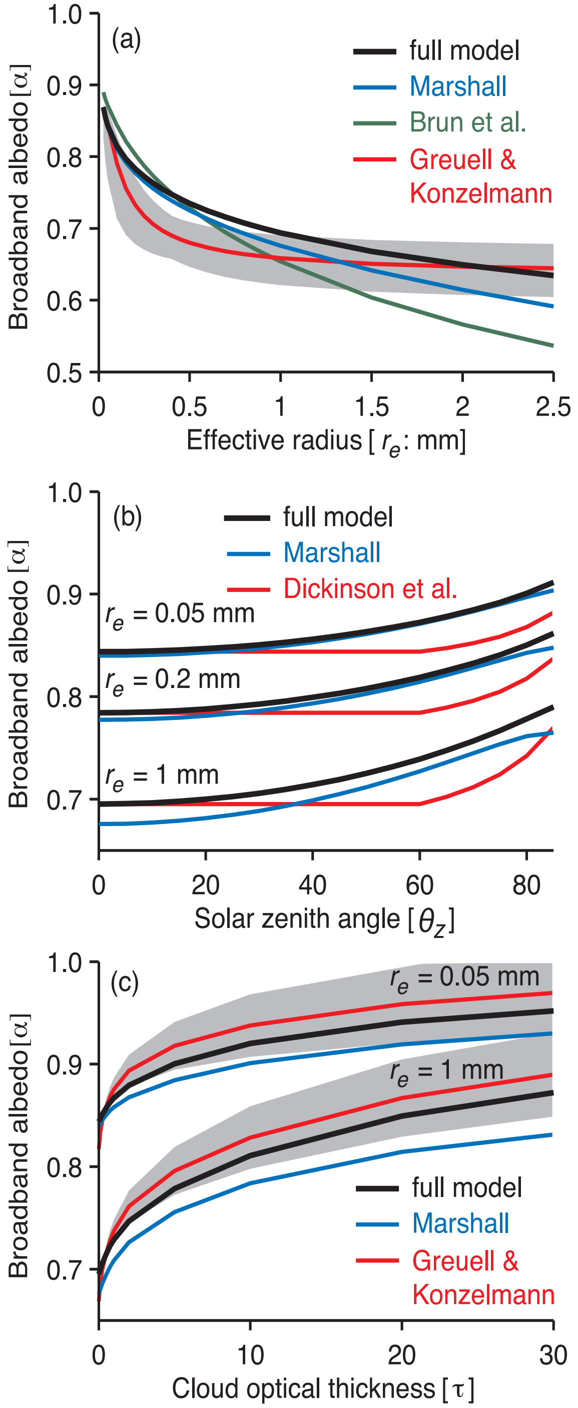

Figure 5.10: Results from five selected albedo parameterizations compared with those from the snow and ice – atmosphere radiative transfer model (full model): (a) Comparison between the Marshall (1989), Brun et al. (1992) and Greuell and Konzelmann (1994) parameterizations and full model results for varying effective grain radii (r_e) under clear sky conditions with $\theta_Z = 0°$. (b) Comparison between the Marshall (1989) and Dickinson et al. (1986) parameterization and full model results for clear sky conditions of varying θ_Z. (c) Comparison between the Marshall (1989) and Greuell and Konzelmann (1994) albedo parameterizations and full model results for varying cloud optical thicknesses (τ) with θ_Z = 0°. Shaded grey areas give the σ1 error in estimated broadband albedos resulting from; (1) the use of estimated snow densities derived from known specific surface areas as input into the Greuell and Konzelmann (1994) density based albedo parameterization and (2) the use of estimated cloud amounts derived from known cloud optical thicknesses as input into the Greuell and Konzelmann (1994) parameterization of the influence of cloud on the albedo of snow. See text for details.

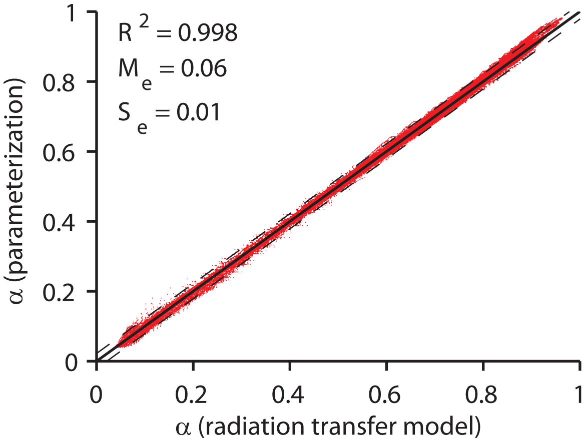

Figure 5.11: Broadband albedo of snow and ice (α) determined from the snow and ice – atmosphere radiative transfer model compared with results from the newly proposed parameterization of snow and ice albedo (Equations 7 though 12). The solid black line shows the one-to-one relationship and the dashed lines gives the 95% confidence levels.

CHAPTER 6 : CONCLUDING REMARKS

Improving the estimation of glacier surface mass balance

At around the time work first began on this dissertation, observations were showing that sea level was rising at a rate of ~3.1 mm a^{-1} (1993-2003), ~40% of which could be attributed to mass loss from the world's land ice, and the rest to thermal expansion of the oceans (Bindoff et al. 2007). Since this time thermal expansion has slowed (Cazenave et al. 2009), while mass loss from ice sheets and glaciers has accelerated (Meier et al. 2007; Chen et al. 2009; Hock et al. 2009; van den Broeke et al. 2009). Recent estimates of sea level change rates (2003-2008: ~2.5 mm a^{-1}) suggest that mass loss from land ice now accounts for ~80% of the observed rate of sea level rise (Cazenave et al. 2009). Glaciers, ice caps, and icefields outside of the major ice sheets account for less than 1% of the world's land ice volume (Radić et al. 2010) but are estimated to contribute ~50% of the current mass loss from all land ice (Kaser et al. 2006; Hock et al. 2009). These smaller ice masses are expected to continue to be significant contributors to sea level rise throughout the next century and beyond (Meier et al. 2007).

Over the past two decades, assessments of the global response of glaciers to changes in climate have improved significantly thanks to the compilation of all available surface mass balance measurements into publicly available datasets (Cogley and Adams 1998; Dyurgerov 2002; Dyurgerov and Meier 2005), and continued improvement in numerical mass balance models. That being said, current global estimates rely heavily on the statistical extrapolation of a small number of temporally discontinuous and spatially sparse measurements, often into regions which lack local measurements and are not well represented by mass balance records from other regions (Meier 1984; Dyurgerov and Meier 1997; Kaser et al. 2006; Raper and Braithwaite 2006; Hock et al. 2009). To improve upon these estimates, future assessments need to come from climate models that resolve the processes governing glacier surface mass balance and account for feedbacks between the atmosphere and the glacier surface (e.g. the albedo-temperature feedback). This is now being realized for the large ice sheets, which have small spatial gradients in surface mass balance that can be adequately modeled with lower resolution climate models (Fettweis et al. 2005; Box et al. 2006; Ettema et al. 2009; Vizcaino et al. 2010).

Glaciers, however, have steep spatial gradients in melt rates and precipitation that are associated with high relief and complex terrain. Running regional and global climate models at sufficient spatial resolution to reproduce these gradients (~1km by 1 km) is computationally challenging. For this reason, less computationally intensive approaches to modeling the surface mass balance of these complex regions are required, at least until the computational limits to high resolution climate modeling are overcome. One such approach, which is less physically realistic than the fully coupled approach, involves downscaling meteorological variables generated by climate reanalyses or climate models to higher resolutions to generate forcings for surface mass balance models (Glover 1999; Bugnion and Stone 2002; Hanna et al. 2005; Mernild et al. 2010). Although attempts have recently been made to include sub-grid downscaling within climate models (Vizcaino et al. 2010), the communication between the atmosphere and the sub-grid glacier energy balance is still only unidirectional. The next logical step is to implement two-way communication between the higher-resolution sub-grid surface energy fluxes and the coarser resolution atmospheric model.

Smoothing of the surface topography in coarse resolution climate models is responsible for a large portion of the disagreement between coarse and high resolution simulations of glacier surface mass balance (e.g. Glover 1999). It is therefore useful to develop downscaling techniques to bridge the difference in resolution between climate models and surface mss balance models. Chapters 3 and 4 contribute toward this goal though the development and validation of a method for downscaling coarse resolution air temperature fields over higher resolution glacier surfaces. This method uses a high-resolution digital elevation model and a regression model to estimate near-surface air temperature lapse rates during the ablation season from lower tropospheric air temperatures. This approach differs from the widespread approach that uses a constant free-air moist adiabatic lapse rate and a digital elevation model to predict near surface air temperatures as a function of elevation because the lapse rate used for temperature downscaling is temporally variable. There is a negative relationship between the lapse rate and the lower tropospheric air temperature during the ablation season because temperatures near the glacier surface are more sensitive to changes in free-air temperatures at higher elevations than at lower elevations. Thus, the change in near-surface air temperature associated with a 1ºC change in free-air temperature might be 0.9ºC at the glacier summit but only 0.5ºC at its terminus. This implies that lapse rates are less steep when conditions are warmer (a result of the modification of the sensible heat flux between the atmosphere and the glacier surface when the surface is melting).

When this approach is used to generate air temperature fields for input into glacier surface mass balance models it tends to reduce the sensitivity of the ablation rate to increases in lower tropospheric air temperature, i.e. a warming of the troposphere results in less warming at the glacier surface then would be predicted by temperature fields generated by downscaling using a constant lapse rate. Since the lapse rate model is solely a function of lower troposphere free-air temperatures, it provides a suitable method with which to assess the sensitivity of glacier surface mass balance to projected climate warming. Using this method to downscale coarse resolution temperatures for input into a mass balance model for a large Arctic ice cap produced mass balance estimates that fit observations much better than results produced using either the mean measured ablation season lapse rate or a free-air moist adiabatic lapse rate (Chapter 4). The general conclusions that can be drawn from this are that a free-air moist adiabatic lapse rate is not a good approximation of the near-surface lapse rate over melting glacier surfaces, and that using such a lapse rate for downscaling near-surface temperatures can result in large errors in both the downscaled temperatures and the results of glacier melt models that use those temperatures as input.

Developing appropriate methods for downscaling meteorological variables to facilitate running gridded one-way (downscaling meteorological input) and two-way (both downscaling and upscaling meteorological variables to allow for subgrid simulations within climate models) atmosphere-glacier mass balance models at higher spatial resolutions should lead to improved estimates of glacier mass balance. Additional improvements will come from the inclusion of more physically explicit representations of snow and ice processes within such models. Since absorption of shortwave radiation is often the single largest source of energy for melt (Male and Granger 1981; Paterson 2000), one of the most important parameters to model correctly is surface albedo. Sophisticated radiation transfer models do a very good job at producing estimates of snow and ice albedo that closely match observations (Grenfell et al. 1994; Aoki et al. 2000; Painter et al. 2007), but they are computationally demanding and require many inputs that are not routinely measured or modeled within climate and/or surface mass balance models. Thus, physically explicit models of the energy balance of snow and ice typically employ computationally simple, empirically derived albedo parameterizations that require minimal inputs. These parameterizations often provide a reasonable approximation of the surface albedo, whilst requiring minimal knowledge of the physical characteristics of the snow, ice and atmosphere (e.g. Brock et al. 2000; Pedersen and Winther 2005). They are, however, somewhat limited in their applicability as they are based on statistical fits to albedo measurements that are only representative of the snow, ice, and atmosphere conditions that applied at the time and place of measurement.

To move beyond the limitations of empirical snow and ice albedo parameterizations, new parameterizations based on more explicit physics must be developed. These new parameterizations need to be able to account separately for changes in albedo resulting from changes in the specific surface area of snow/ice (the surface area of air-ice interfaces per unit mass, which is dependent on the size and distribution of snow grains, ice bubbles and cracks), solar zenith angle, snow/ice impurity content, and spectral distribution of the incident solar radiation. This was the focus of Chapter 5, which outlined the development of a theoretically based parameterization of the broadband albedo of snow and ice that can accurately reproduce albedo under a wide range of snow, ice, and atmospheric conditions. This new parameterization is the first to provide a single set of equations for the estimation of the broadband albedo of both snow and ice, and it is easily implementable in climate and glacier energy mass-balance models. It was developed specifically for application to glacier surfaces but would require little adjustment for use in sea ice and seasonal snow cover models.

This parameterization is most sensitive to values of snow specific surface area. The temporal variability of snow specific surface is primarily governed by snow grain metamorphism, a process that is significantly accelerated under wet snow conditions. There is a renewed effort to improve dry snow metamorphism models (Legagneux et al., 2003; Flanner and Zender, 2006; Taillandier et al., 2007) but little effort has been put towards improving models for wet snow conditions (Brun 1989). Much work is still needed to develop physically explicit wet snow metamorphism models and to confirm the validity of dry snow models over a wide range of environmental conditions. There will be little additional improvement in the representation of snow and ice albedo in energy balance models without significant improvements in existing snow metamorphism models.

Surface mass balance of glaciers and ice caps in the Canadian High Arctic

The glaciers, ice caps and icefields of the Canadian High Arctic contain the largest volume of land ice in the world outside of the Antarctic and Greenland Ice Sheets (Radić et al. 2010) and have the potential to contribute significantly to changes in sea level. Looking at the period 1963-2003, direct measurements of surface mass balance for this region show an increase in mass loss rates after1986/1987 with concurrent increases in July temperatures (Chapter 2). In agreement with previous research by Alt (1987), the shifts in July temperatures and regional glacier mass balance are linked to changes in the characteristics of the summer mid-troposphere circumpolar vortex, the leading summertime atmospheric circulatory feature in the Arctic (Maxwell 1980). Analysis of the strength and position of the vortex (Chapter 2) shows that when the July vortex is strong, and its center is located in the Western Hemisphere, positive mass balance anomalies occur. When the July vortex is either weak, or strong without elongation over the Canadian High Arctic, and the vortex center is located in the Eastern Hemisphere, highly negative mass balance anomalies prevail. An increase in the occurrence of easterly positioned July vortices after 1987 was associated with an increased frequency of tropospheric ridging over the Canadian High Arctic, higher surface air temperatures, and more negative glacier mass balance.

The characterization of July High Arctic synoptic climate and its relation to the surface mass balance of Canadian High Arctic glaciers provides a broad and long-term perspective on changes in the glacier mass balance of this region and allows for the identification of the climatic influences that have contributed to its variability over the past 50 years. This qualitative characterization, however, does not allow for quantification of the ice volume that is being lost as a result of the observed decrease in surface mass balance. Outside of the crude statistical approximations used to estimate the global mass balance of glaciers (Meier 1984; Dyurgerov and Meier 1997; Zuo and Oerlemans 1997; Walsh et al. 2005; Kaser et al. 2006; Raper and Braithwaite 2006; Hock et al. 2009), only two studies have attempted to quantify the entire mass balance of this region. Sharp and others (2003) measured regional changes in glacier coverage between 1959 and 1999. Using a volume-area scaling relationship they estimated that the Canadian High Arctic lost ice at an average rate of ~16 km^3 a^{-1} over the 40 year period. In 1995 and again in 2000 Abdalati and others (2004) measured transects of elevations across major ice masses throughout the region using airborne laser altimetry and estimated the average volume loss of the region to be ~13 km^3 a^{-1}. Considering the significant differences between study periods and methods, these regional volume change estimates agree fairly well. This good agreement can be misleading in that it might imply that the mass balance for this region is somewhat constant. This could not be further from the truth. Direct measurements of surface mass balance for glaciers in this region display large inter-annual variability and high sensitivity to changes in lower troposphere temperature (Chapters 2 and 4). Quantitative assessment of the regional response of Canadian High Arctic glaciers to changes in climate will require temporally resolved estimates of regional mass balance. Long-term regional estimates and future projection will require the use of numerical models designed to simulate the surface mass balance for this region. Simulations will need to be run at a sufficient spatial resolution (~1km by ~1km) to resolve steep horizontal gradients in surface mass balance that result from the high relief and complex topography of this region. For the foreseeable future this will require some form of meteorological downscaling, whether simulations are conducted using a one-way forced mass balance model or a coupled ice-atmosphere climate model. To adequately represent feedbacks between troposphere and near-surface temperatures when downscaling ablation season temperatures over glacier surfaces, near-surface temperature lapse rates should be modeled as a function of lower troposphere temperature (Chapter 3). Not doing so can have a significant impact on model melt estimates (Chapter 4). If the energy balance approach is used to simulate the surface mass balance, a physically based albedo parameterization should be used (Chapter 5) to better represent the climate-albedo feedback within model simulations.

References

Abdalati, W., W. Krabill, E. Frederick, S. Manizade, C. Martin, J. Sonntag, R. Swift, R. Thomas, et al., 2004: Elevation changes of ice caps in the Canadian Arctic Archipelago. *Journal of Geophysical Research-Earth Surface*, **109,** doi:10.1029/2003JF000045.

Alt, B. T., 1987: Developing synoptic analogs for extreme mass balance conditions on Queen Elizabeth Island ice caps. *Journal of Climate and Applied Meteorology*, **26,** 1605-1623.

Aoki, T., T. Aoki, M. Fukabori, A. Hachikubo, Y. Tachibana, and F. Nishio, 2000: Effects of snow physical parameters on spectral albedo and bidirectional reflectance of snow surface. *Journal of Geophysical Research-Atmospheres*, **105,** 10219-10236.

Bindoff, N. L., J. Willebrand, V. Artale, A. Cazenave, J. Gregory, S. Gulev, K. Hanawa, C. Le Quéré, et al., 2007: Observations: Oceanic climate change and sea level. *Climate Change 2007: The Physical Science Basis. Contribution of Working Group I to the Fourth Assessment Report of the Intergovernmental Panel on Climate Change*, Cambridge University Press, 384-432.

Box, J. E., D. H. Bromwich, B. A. Veenhuis, L.-S. Bai, J. C. Stroeve, J. C. Rogers, K. Steffen, T. Haran, et al., 2006: Greenland Ice Sheet surface mass balance variability (1988-2004) from calibrated Polar MM5 output. *Journal of Climate*, **19,** 2783-2800.

Brock, B. W., I. C. Willis, and M. J. Sharp, 2000: Measurement and parameterization of albedo variations at Haut Glacier d'Arolla, Switzerland. *Journal of Glaciology*, **46,** 675-688.

Brun, E., 1989: Investigation on wet-snow metamorphism in respect of liquid-water content. *Annals of Glaciology*, **13,** 22-26.

Bugnion, V. and P. H. Stone, 2002: Snowpack model estimates of the mass balance of the Greenland Ice Sheet and its changes over the twentyfirst century. *Climate Dynamics*, **20,** 87-106.

Cazenave, A., K. Dominh, S. Guinehut, E. Berthier, W. Llovel, G. Ramillien, M. Ablain, and G. Larnicol, 2009: Sea level budget over 2003-2008: A reevaluation from GRACE space gravimetry, satellite altimetry and Argo. *Global and Planetary Change*, **65,** 83-88.

Chen, J. L., C. R. Wilson, D. Blankenship, and B. D. Tapley, 2009: Accelerated Antarctic ice loss from satellite gravity measurements. *Nature Geoscience*, **2,** 859-862.

Cogley, J. G. and W. P. Adams, 1998: Mass balance of glaciers other than the ice sheets. *Journal of Glaciology*, **44,** 315-325.

Dyurgerov, M. and M. F. Meier, 1997: Year-to-year fluctuations of global mass balance of small glaciers and their contribution to sea-level changes. *Arctic and Alpine Research*, **29,** 392-402.

______, 2005: Glaciers and the changing earth system: A 2004 snapshot. Institute of Arctic and Alpine Research, University of Colorado, 268.

Dyurgerov, M. B., 2002: Glacier mass balance and regime: Data of measurements and analysis. INSTAAR, University of Colorado Occasional Paper 55, 268 pp.

Ettema, J., M. R. van den Broeke, E. van Meijgaard, W. J. van de Berg, J. L. Bamber, J. E. Box, and R. C. Bales, 2009: Higher surface mass balance of the Greenland ice sheet revealed by high-resolution climate modeling. *Geophysical Research Letters*, **36**.

Fettweis, X., H. Gallee, F. Lefebre, and J. P. van Ypersele, 2005: Greenland surface mass balance simulated by a regional climate model and comparison with satellite-derived data in 1990-1991. *Climate Dynamics*, **24,** 623-640.

Glover, R. W., 1999: Influence of spatial resolution and treatment of orography on GCM estimates of the surface mass balance of the Greenland Ice Sheet. *Journal of Climate*, **12,** 551-563.

Grenfell, T. C., S. G. Warren, and P. C. Mullen, 1994: Reflection of solar-radiation by the Antarctic snow surface at ultraviolet, visible, and near-infrared wavelengths. *Journal of Geophysical Research-Atmospheres*, **99,** 18669-18684.

Hanna, E., P. Huybrechts, I. Janssens, J. Cappelen, K. Steffen, and A. Stephens, 2005: Runoff and mass balance of the Greenland Ice Sheet: 1958-2003. *Journal of Geophysical Research-Atmospheres*, **110,** doi:10.1029/2004JD005641.

Hock, R., M. de Woul, Radi, Valentina, and M. Dyurgerov, 2009: Mountain glaciers and ice caps around Antarctica make a large sea level rise contribution. *Geophysical Research Letters*, **36,** L07501.

Kaser, G., J. G. Cogley, M. B. Dyurgerov, M. F. Meier, and A. Ohmura, 2006: Mass balance of glaciers and ice caps: Consensus estimates for 1961-2004. *Geophysical Research Letters*, **33,** doi:10.1029/2006GL027511.

Male, D. H. and R. J. Granger, 1981: Snow surface energy exchange. *Water Resources Research*, **17,** 609-627.

Maxwell, J. B., 1980: *The Climate of the Canadian Arctic Islands and Adjacent Waters* Vol. 1, *Climatological Studies*, Environment Canada, Department of supply services, 532 pp.

Meier, M. F., 1984: Contribution of small glaciers to global sea-level. *Science*, **226,** 1418-1421.

Meier, M. F., M. B. Dyurgerov, U. K. Rick, S. O'Neel, W. T. Pfeffer, R. S. Anderson, S. P. Anderson, and A. F. Glazovsky, 2007: Glaciers dominate eustatic sea-level rise in the 21st century. *Science*, **317,** 1064-1067.

Mernild, S. H., G. E. Liston, C. A. Hiemstra, and J. H. Christensen, 2010: Greenland Ice Sheet Surface Mass-Balance Modeling in a 131-Yr Perspective, 1950-2080. *Journal of Hydrometeorology*, **11,** 3-25.

Painter, T. H., N. P. Molotch, M. Cassidy, M. Flanner, and K. Steffen, 2007: Instruments and methods: Contact spectroscopy for determination of stratigraphy of snow optical grain size. *Journal of Glaciology*, **53,** 121-127.

Paterson, W. S. B., 2000: *Physics of Glaciers*. 3 ed. Butterworth-Heinemann, 481 pp.

Pedersen, C. A. and J. G. Winther, 2005: Intercomparison and validation of snow albedo parameterization schemes in climate models. *Climate Dynamics*, **25,** 351-362.

Radić, Valentina, and R. Hock, 2010: Regional and global volumes of glaciers derived from statistical upscaling of glacier inventory data. *Journal of Geophysical Research*, **115,** F01010.

Raper, S. C. B. and R. J. Braithwaite, 2006: Low sea level rise projections from mountain glaciers and icecaps under global warming. *Nature*, **439,** 311-313.

Sharp, M., L. Copland, K. Filbert, D. Burgess, and S. Williamson, 2003: Recent changes in the extent and volume of Canadian Arctic glaciers. *Glaciological Data Report GD-32, Papers and Recommendations: Snow Watch 2002 Workshop and Workshop on Assessing Global Glacier Recession*, National Snow and Ice Data Center, Boulder, USA, 73-75.

van den Broeke, M., J. Bamber, J. Ettema, E. Rignot, E. Schrama, W. J. van de Berg, E. van Meijgaard, I. Velicogna, et al., 2009: Partitioning recent Greenland mass loss. *Science*, **326,** 984-986.

Vizcaino, M., U. Mikolajewicz, J. Jungclaus, and G. Schurgers, 2010: Climate modification by future ice sheet changes and consequences for ice sheet mass balance. *Climate Dynamics*, **34,** 301-324.

Walsh, J. E., O. Anisimov, J. O. M. Hagen, T. Jakobsson, J. Oerlemans, T. D. Prowse, V. Romanovsky, N. Savelieva, et al., 2005: Cryosphere and hydrology. *Arctic climate impact assessment*, L. A. Carolyn Symon, Bill Heal, Ed., Cambridge University Press, 183-242.

Zuo, Z. and J. Oerlemans, 1997: Contribution of glacier melt to sea-level rise since AD 1865: A regionally differentiated calculation. *Climate Dynamics*, **13,** 835-845.

APPENDIX A: TEMPERATURE SENSORS USED IN STUDY

Transect temperature sensor details (Table A.1) and sensor accuracies (Table A.2) are provided in the following tables. All quality-controlled daily average temperature measurements for each transect are available as supplementary material on the University of Alberta Arctic and Alpine Research Group's website: arctic.eas.ualberta.ca.

---

* Previously published material: Gardner, A. S., M. J. Sharp, R. M. Koerner, C. Labine, S. Boon, S. J. Marshall, D. O. Burgess, and D. Lewis, 2009: Near-surface temperature lapse rates over Arctic glaciers and their implications for temperature downscaling. *Journal of Climate*, **22,** 4281-4298.

Table A.1: Temperature sensor ID, sensor type, location and periods of operation.

Transect ID	Station ID	Sensor type	Lat (°N)	Lon (°W)	Elevation (m a.s.l.)	First month of record	Last month of record
Agassiz	A_1	107F	80.80	72.90	1736	Jun-88	Apr-06
	A_2	107F	80.83	71.90	1314	Jun-91	Apr-06
	A_3	107F	80.87	71.28	878	Apr-94	Apr-06
Devon_N	D1_N	107F	75.34	82.10	1880	Apr-97	May-05
	D2_N	107F	75.37	82.67	1780	Mar-92	Mar-95
	D3_N	107F	75.39	82.76	1768	Apr-00	May-05
	D4_N	107F	75.42	82.95	1628	May-99	Aug-03
	D5_N	107F	75.49	83.28	1339	May-98	May-05
	D6_N	107F	75.69	83.26	330	Apr-97	May-05
Devon_S	D1_S	107F	75.34	82.68	1802	May-05	Jan-07
	D2_S	107F	75.18	82.78	1415	Jun-04	May-07
	D3_S	107F	75.01	82.88	994	May-05	May-07
	Km0	HOBO	75.34	82.68	1802	May-04	Sep-04
	Km4.7	HOBO	75.30	82.70	1744	Apr-04	May-07
	Km8	HOBO	75.27	82.72	1676	Sep-04	Feb-05
	Km9.1	HOBO	75.26	82.73	1636	Apr-04	Mar-07
	Km13.6	HOBO	75.22	82.75	1502	Apr-04	Dec-06
	Km21.4	HOBO	75.15	82.79	1328	Apr-04	May-07
	Km24.6	HOBO	75.12	82.81	1255	Apr-04	May-07
	km27.9	HOBO	75.09	82.83	1194	Apr-04	Aug-04
	km30.2	HOBO	75.07	82.84	1146	May-05	Apr-06
	km31.4	HOBO	75.06	82.85	1104	Apr-06	Feb-07
	Km34.6	HOBO	75.03	82.86	1036	Apr-06	Dec-06
	Km36.8	HOBO	75.01	82.88	994	Apr-04	Feb-07
	Km39.2	HOBO	74.99	82.89	966	Apr-04	Aug-04
	Km41.7	HOBO	74.97	82.90	874	Apr-04	Feb-07
	Km43.7	HOBO	74.95	82.92	786	Apr-04	Sep-05
	km45.7	HOBO	74.94	82.93	677	Apr-04	Dec-06
	Km47.7	HOBO	74.92	82.94	478	Apr-04	Nov-06
JEG	UWS	35CF	79.71	74.56	1183	Jun-96	Jul-02
	MWS	35CF	79.67	74.35	824	Jun-96	Jul-02
	LWS	35CF	79.63	74.08	261	Jun-96	Jul-02
	1500m	HOBO	79.72	74.50	1470	May-01	Jun-03
	1300m-W	HOBO	79.70	74.55	1320	Jun-02	May-03
	1300m-E	HOBO	79.71	74.49	1324	May-01	Jun-03
	1250m	HOBO	79.72	74.55	1245	May-01	Jun-02
	1200m	HOBO	79.71	74.56	1185	May-02	Jun-03
	1100m	HOBO	79.70	74.53	1110	May-01	Jun-03
	1000m	HOBO	79.69	74.50	1026	May-01	Jun-03
	900m	HOBO	79.68	74.44	915	May-01	Jun-03
	800m	HOBO	79.67	74.35	825	May-02	May-03
	700m	HOBO	79.67	74.30	705	May-01	Jun-03
	600m	HOBO	79.65	74.30	630	May-01	May-03
	500m	HOBO	79.64	74.19	510	May-01	May-03
	400m	HOBO	79.65	74.11	400	May-01	Jun-03
	300m	HOBO	79.64	74.08	300	May-01	Jun-03
	250m	HOBO	79.63	74.08	235	Jun-02	May-03
	200m	HOBO	79.63	74.08	209	May-01	May-03
	140m	HOBO	79.62	74.07	140	Jun-01	May-03

POW_N	P_AWS	107	78.49	79.43	1727	Jun-01	Sep-02
	WL1300	HOBO	78.50	80.23	1300	May-01	May-03
	WL1100	HOBO	78.64	81.20	1094	May-01	May-03
	SL1060	HOBO	78.60	79.86	1060	May-01	Jun-02
	SL850	HOBO	78.64	79.53	850	May-01	May-03
	WL750	HOBO	78.71	81.23	747	May-01	May-03
	WL610	SP-2000	78.68	79.10	660	Apr-02	May-03
	LL1500	HOBO	78.55	79.07	1500	Apr-02	May-03
	LL1300	HOBO	78.61	78.67	1308	May-01	May-03
	LL1100	HOBO	78.63	78.47	1105	May-01	May-03
	LL800	HOBO	78.71	76.36	799	May-01	Apr-02
	LL600	HOBO	78.72	75.98	602	May-01	May-03
	LL400	HOBO	78.70	75.47	395	May-01	May-03
	LL130	HOBO	78.68	74.97	129	May-01	Jan-03
POW_S	P_STH	SP-2000	77.87	80.81	1350	May-02	May-03
	HM1050	HOBO	78.03	81.25	1056	May-02	May-03
	HM740	HOBO	78.05	81.65	740	May-02	Oct-02
	KR960	HOBO	77.71	80.25	945	May-02	May-03
	KR750	HOBO	77.64	80.00	750	May-02	Jan-03
	KR550	SP-2000	77.53	79.54	550	May-02	May-03

Table A.2: Temperature sensor measurement range and accuracy.

Sensor Type	Manufacturer	Temperature range	Accuracy (worst case)	Accuracy (@ 0°C)
107F	Campbell Scientific Ltd.	-53 to +48°C	±0.5°C	±0.2°C
107	Campbell Scientific Ltd.	-35 to +50°C	±0.9°C	±0.3°C
HMP 35CF	Vaisala	-53 to +48°C	±0.5°C	±0.2°C
HOBO H8-PRO	Onset Scientific Ltd.	-30 to +50°C	±1.0°C	±0.2°C
SP-2000	Veriteq Instruments Inc.	-35 to +85°C	±1.0°C	±0.2°C

APPENDIX B: COMPARISON BETWEEN THEORETICAL RESULTS AND SELECTED PARAMETERIZATIONS: NUMERICAL DETAILS

The parameterizations of Brun et al. (1992) and Marshall (1989) both model albedo in more than one spectral band. To determine broadband albedos, these parameterizations require weightings of the solar irradiance incident in each of the spectral bands. In addition, the Marshall (1989) parameterization requires values of the diffuse fraction and atmospheric transmittance. To provide an objective comparison with full model results, irradiance weightings, diffuse fractions and atmospheric transmittance values for each spectral band were taken directly from the full model.

Uncertainties associated with using the Dominé et al.'s [2007, equation(1)] approximation to estimate density from specific surface area for use by the Greuell and Konzelmann (1994) parameterization were determined by adjusting the known specific surface areas by ±62% (the 1σ error: Dominé et al. 2007) and setting a minimum error of ±50 cm^2g^{-1} for specific surface areas smaller than 80 cm^2g^{-1} (approximated from Dominé et al.'s (2007) Figure 1). The tunable parameters for the Greuell and Konzelmann parameterization (Equation 1) of new snow albedo ($\alpha_S = 0.84$) and density ($\rho_s = 0.01$ g cm^{-3}) were assigned values determined by the full model for snow with an effective radius of $r_e = 0.05$ mm. As with most other applications of the Dickinson et al. (1986) parameterization (Equation 5), the coefficient *b* is set equal to 2.

Parameterizations were only compared with full model results for 0.05 mm ≤ r_e ≤ 2.5 mm. This is the range of effective radii for which the Brun et al. (1992) and Marshall (1989) parameterizations were developed and is

---

* Previously published material: Gardner, A. S. and M. J. Sharp, 2010: A review of snow and ice albedo and the development of a new physically based broadband albedo parameterization. *Journal of Geophysical Research*, **115,** F01009.

approximately the range over which the density-specific surface area approximation [Dominé et al. 2007, equation (1)] is valid which was used to derive densities for input into the Greuell and Konzelmann (1994) parameterization.

References

Brun, E., P. David, M. Sudul, and G. Brunot, 1992: A numerical model to simulate snow-cover stratigraphy for operational avalanche forecasting. *Journal of Glaciology*, **38,** 13-22.

Dickinson, R. E., A. Henderson-Sellers, P. J. Kennedy, and M. F. Wilson, 1986: Biosphere-Atmosphere Transfer Scheme (BATS) for the NCAR Community Climate Model. *NCAR Technical Note*, **275**.

Dominé, F., A. S. Taillandier, and W. R. Simpson, 2007: A parameterization of the specific surface area of seasonal snow for field use and for models of snowpack evolution. *Journal of Geophysical Research-Earth Surface*, **112,** doi:10.1029/2006JF000512.

Marshall, S. E., 1989: A physical parameterization of snow albedo for use in climate models. NCAR Cooperative Thesis no. 123. Boulder, CO.

APPENDIX C: MODEL RUN SPECIFICATIONS*

This appendix provides the atmospheric, snow and ice properties assigned to the coupled snow and ice–atmosphere radiative transfer model for the determination of broadband snow and ice albedos. Table C.1 provides the properties of the 108 thousand homogenous semi-infinite depth snow and ice broadband albedos to which Equations 7-11 were fit. Table C.2 provides the specifications of the 24 thousand broadband albedos to which Equation 13 was fit. These broadband albedo values are for a homogenous finite depth snow layer overlying a homogenous semi-infinite depth ice layer.

---

* Previously published material: Gardner, A. S. and M. J. Sharp, 2010: A review of snow and ice albedo and the development of a new physically based broadband albedo parameterization. *Journal of Geophysical Research*, **115,** F01009.

Table C.1: Specifications of the 108 thousand model runs for semi-infinite snow and ice depth.

	Property	values	units
atmosphere	θ_Z	0, 5, 10, 15, 20, 25, 30, 35, 40, 45, 50, 55, 60, 65, 70, 75, 80, 85	degrees
	τ	0, 0.1, 0.25, 0.5, 0.75, 1, 2, 5, 10, 20, 30	no units
snow	r_e	0.025, 0.0375, 0.05,0.1, 0.15, 0.2, 0.25, 0.3, 0.35, 0.4, 0.45, 0.5, 0.6, 0.7, 0.8, 0.9, 1, 1.5, 2, 2.5, 5	mm
	c	0, 0.002, 0.004, 0.006, 0.01, 0.015, 0.02, 0.04, 0.06, 0.08, 0.1, 0.2, 0.3, 0.5, 1, 2	ppmw
ice	n'_e	0.3	mm^{-3}
	r'_e	0.04, 0.05, 0.075, 0.1, 0.2, 0.3, 0.4, 0.5, 0.6, 0.7, 0.8, 0.9	mm
	c	0, 0.002, 0.004, 0.006, 0.01, 0.015, 0.02, 0.04, 0.06, 0.08, 0.1, 0.2, 0.3, 0.5, 1, 2	ppmw

Table C.2: Specifications of the 24 thousand model runs for a single snow layer of depth z overlying a semi-infinite ice layer.

	property	values	units
atmosphere	θ_Z	0, 35, 75	degrees
	τ	0, 1, 2, 5, 10, 20	no units
snow	r_e	0.05, 0.15, 0.45, 1	mm
	c	0, 0.2, 0.1, 0.3	ppmw
	z	0.01, 0.03, 0.05, 0.09, 0.25, 0.5, 5	m w.e.
ice	n'_e	0.3	mm^{-3}
	r'_e	0.05, 0.3, 0.7	mm
	c	0, 0.2, 0.1, 0.3	ppmw